NASA

# The Detection of Climate Change Due to the Enhanced GREENHOUSE EFFECT



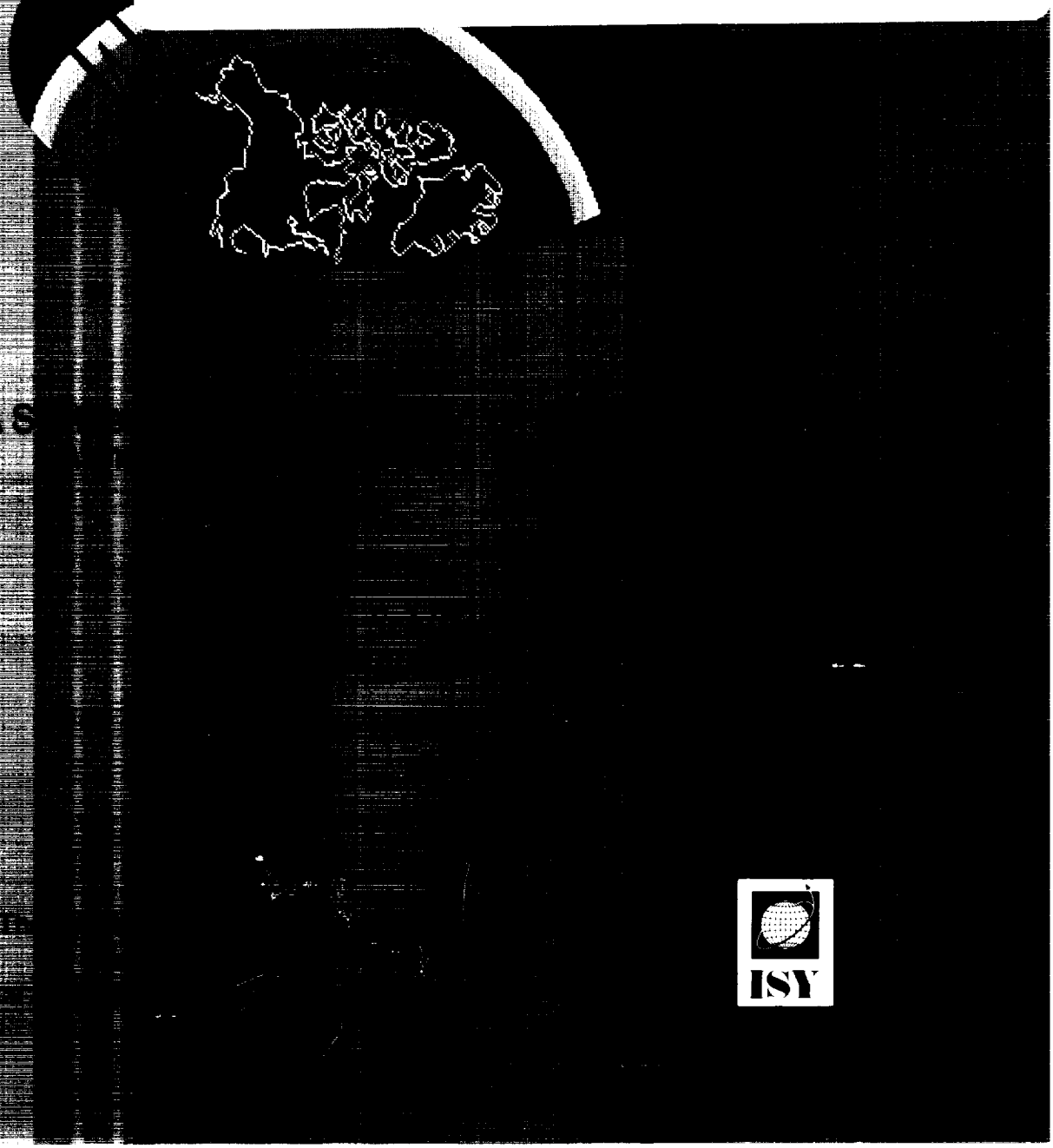

AS

Spac

ISY

# THE DETECTION OF CLIMATE CHANGE DUE TO THE ENHANCED GREENHOUSE EFFECT

*A Synthesis of Findings Based on the GEDEX Atmospheric Temperature Workshop*

Columbia, Maryland
9-11 July 1991

# *Table of Contents*

## *Table of Contents (continued)*

# *Foreword*

In May 1989, the Enhanced Greenhouse Effect Detection Project was proposed as a NASA-sponsored initiative in support of the Space Agency Forum on the International Space Year (SAFISY: 1992). Project objectives included the determination of specific signatures of an enhanced greenhouse effect; the verification of the signatures in historical data sets of conventional climate data and space-based measurements; the development and improvement of processing methods and algorithms for detecting the greenhouse effect from space observations; and the development of proposals for an international enhanced Greenhouse Effect Detection Experiment (GEDEX). In accord with the informally structured, cooperative format adopted by SAFISY, several activities and projects have been initiated since May 1989 that contribute to the broad objectives of GEDEX.

The purposes of the GEDEX Atmospheric Temperature Workshop, held in Columbia, Maryland, 9-11 July 1991, were to obtain a measure of progress in and to recommend actions required for the following:

- Consolidation and documentation of existing data sets and analysis of global climate change (emphasis on temperature);
- Assessment of ambiguities and uncertainties;
- Review of the linkages between temperature change and plausible cause-and-effect factors (e.g., greenhouse gas forcing, other climate forcing, feedback processes);
- Discussion of further research, analysis, and monitoring required; and
- Initial steps toward the development a "fingerprint" approach to the detection of climate change and enhanced greenhouse gas (GHG) effects, based on available evidence from climate models and paleoclimate reconstructions.

Temperature was selected as the focus for this first GEDEX Workshop, both because it is the most widely used measure of climate change and GHG effect and because of its ostensibly direct relationship to changes in the atmospheric and surface radiation budget. A further objective of the workshop was to assemble data sets, together with complete documentation, for the production of a compact disk (CD-ROM). It is intended to widely distribute the CD-ROM nationally and internationally to promote further research.

A list of participants and a list of presentations are contained in Appendices 1 and 2, respectively. A selected bibliography is contained in Appendix 3; names cited in parentheses in this report usually refer to the authors of presentations or specific comments at the workshop, since the report is not intended to give extensive references to the literature but rather to summarize the salient scientific points presented, raised, and discussed at the workshop. However, references are also made to selected pertinent literature in order to provide broader coverage on GEDEX-related science. A list of acronyms and abbreviations is given in Appendix 4. Available GEDEX CD-ROM datasets are described in Appendix 5.

# *Executive Summary*

The "greenhouse effect" is accepted as an undisputed fact from both theoretical and observational considerations. Solar radiation reaches the top of the atmosphere in the form of shortwave electromagnetic radiation; the solar energy flux is about 1368 $W/m^2$. Because of its spherical shape, at any instant the Earth receives, on average, half the incident solar flux (i.e., 684 $W/m^{2)}$. Because of the Earth's rotation, the average radiative flux received over a day-night cycle is half of this value, i.e, about 342 $W/m^2$. Approximately a third is reflected by the atmosphere and the Earth; the rest is absorbed. The energy absorbed by the Earth must be balanced by outgoing radiation from the Earth (terrestrial radiation) in the form of longwave invisible infrared energy.

Computations indicate that the Earth's average surface temperature (~15°C) would be -18°C were it not for greenhouse gases (GHGs) such as water vapor ($H_2O$, ~1% of the atmosphere) and carbon dioxide ($CO_2$, ~0.04%). The validity of these calculations is further verified by the observed surface temperatures of Venus (477°C) and Mars (-47°C), whose atmospheres contain large concentrations of greenhouse gases (>90% $CO_2$ for Venus and >80% for Mars), without which their surface temperatures would be -47°C and -57°C, respectively. These numbers translate into a greenhouse heating effect of approximately 33°C for Earth, 524°C for Venus, and 10°C for Mars. There are, of course, notable differences among the three planets. For example, on Earth water can exist in three forms—vapor, liquid, and ice. This introduces more complex thermodynamic mechanisms for the distribution of heat than if there were no phase changes possible.

In the Earth's atmosphere, the dominant greenhouse gas is water vapor. The atmospheric water vapor content is in equilibrium between evaporation (and evapotranspiration) and precipitation. For any given surface temperature, the latter is determined by kinematic, thermodynamic, and convective (clouds/precipitation) processes. Clouds are simultaneously strong infrared warming and shortwave cooling agents.

Both water vapor and clouds are variables that respond to changes in surface temperature that are "forced" by other means, such as the increasing concentrations of anthropogenically injected greenhouse gases: $CO_2$ (from fossil fuel burning), $CH_4$ (from agriculture and livestock), CFCs (from industry), etc. These considerations have resulted in the notion of an "enhanced" greenhouse effect, over and above that due to such naturally occurring greenhouse gases as water vapor.

The specific concern today is that the exponentially increasing concentrations of anthropogenically introduced greenhouse gases will, sooner or later, irreversibly alter the climate of the Earth, and thereby disrupt global weather distribution, agricultural production, water supplies, and other economic and social activities. Over the last five years, substantial worldwide efforts have been directed, toward (a) determining whether the climate has changed from preindustrial times, when anthropogenic greenhouse gas concentrations were only about half of the present concentrations; (b) searching for the enhanced greenhouse effect; and (c) developing sophisticated mathematical models to predict future global climate changes in order to guide national and international policy decisions.

Detecting climate change has been complicated by uncertainties in historical observational measurements, even though all independent analyses conclude that the global average near-surface temperature has increased by about 0.5°C over the past 100 years. Identifying the cause of this change has been one of the primary objectives of recent research. The current hypothesis is that the observed climate change—in particular, the change in global average temperature—is due to an enhanced greenhouse effect. This contention is supported by state-of-the-art climate models run on the most powerful supercomputers available. That is, the change simulated by the models with enhanced greenhouse gas forcing is consistent with observations. This hypothesis forms the basis for accepting the possibility of future climate states predicted by climate system models for which a doubling of equivalent $CO_2$ yields an increase in global average temperature of 1.5°C to 4.5°C at equilibrium.

However, there are uncertainties arising from the various approximations and assumptions made in mathematically depicting the physical world in the current generation of climate models. At issue is the manner by which other competing (with or against GHG) forcing or feedback processes are quantified, parameterized, and incorporated in the models. In particular, there are serious questions about water vapor feedback, cloud feedback, aerosol effects, and the interactions among the atmosphere and the ocean, land surface and vegetation, and the cryosphere. At present, much of the global warming (about 70-80%) simulated and predicted by climate models is due to a positive feedback from an increase in water vapor and to a decrease in total global average cloud amount as a result of initial warming from the "direct" enhanced greenhouse effect. These effects depend on how the modeled atmosphere handles these feedback processes, and not all models agree on their magnitude—or, sometimes, even on their sign. Furthermore, the observed global warming signal is still within the range of observed (from paleoclimatic evidence) and modeled natural variability of climate.

Thus the primary question for the GEDEX project is: How can climate change and enhanced greenhouse effects be unambiguously detected and quantified? To help answer these questions, the GEDEX project was conceived to

promote observational experiments, data analysis, and modeling research to reduce uncertainties in existing assessments of climate change and enhanced greenhouse effects.

The First GEDEX Workshop (July 1991) addressed the primary issues involved in the detection of climate change and enhanced greenhouse effects, with the global atmospheric temperature record as a unifying theme. The workshop participants concluded that there were compelling needs to (a) better assess uncertainties in the observational record of climate change; (b) quantify climate sensitivity to GHG and other forcings; (c) improve observation and detection capabilities, using space-based and surface-based techniques, to monitor climate forcing and feedback processes; and (d) improve the parameterization of forcing and feedback processes in climate models.

It was noted that several international programs address various areas of the scientific objectives of GEDEX, e.g., the World Climate Research Programme (WCRP) and the International Geosphere-Biosphere Programme (IGBP). In particular, there are projects designed to scrutinize climate system processes, such as TOGA-COARE (atmosphere-ocean interaction), WOCE (world ocean circulation), ISCCP (cloud climatology), ISLSCP (atmosphere-land surface interactions), GEWEX (global energy and water cycles), and TRMM (tropical precipitation); details are provided in section 5.3. Workshop participants therefore felt that GEDEX should provide a focus to channel resources and direct research on topics relevant to the objectives of GEDEX, but should avoid duplicating existing national and international institutional structures. Examples of appropriate subject areas are climate sensitivity; climate processes, such as water vapor feedback, cloud feedback, and aerosol-radiation feedback (e.g., using Pinatubo as a case study); atmosphere-ocean coupling on long time scales; biogeochemical cycles affecting atmospheric concentrations of greenhouse gases; observational and analysis projects for the detection of climate change and enhanced greenhouse effects, including second and higher order variables; and natural climate variability.

As a first GEDEX initiative, a comprehensive data set containing a wide spectrum of climatic variables will be prepared and distributed on a CD-ROM by NASA to the climate research community in early 1992.

For convenience, the following table summarizes estimates for a wide variety of climate variables particularly relevant to the greenhouse issues. (This table should not be referenced as it is only intended to suggest orders of magnitude for the quantities cited.)

## *Estimated Values of Commonly Quoted Constants, Parameters, and Variables*

| | |
|---|---|
| Solar radiation flux | |
| Top of atmosphere | 1368 $W/m^2$ |
| At Earth's surface (avg.) | 342 $W/m^2$ |
| Absorbed by Earth (avg.) | 240 $W/m^2$ |
| Surface heating decrease caused by 0.1% dimming of the sun | 0.25 $W/m^2$ |
| Decrease in solar radiation at 60°N over past 10,000 yrs | 35 $W/m^2$ |
| Earth surface temperature (avg.) | 15°C |
| Earth surface temperature with no greenhouse effect | -18°C |
| Effective greenhouse heating (Earth) | 33°C |

Key greenhouse gas concentrations, excluding water vapor

| | Atmospheric Lifetime | Pre-Industrial (1750-1800) | Present (1991) |
|---|---|---|---|
| $CO_2$ | 50-200 yrs | 280 ppmv | 360 ppmv |
| $CH_4$ | 10 yrs | 800 ppbv | 1720 ppbv |
| $CFC_{11}$ | 65 yrs | 0 pptv | 280 pptv |
| $CFC_{12}$ | 130 yrs | 0 pptv | 485 pptv |
| $N_2O$ | 150 yrs | 300 ppbv | 310 ppbv |

| | |
|---|---|
| Observed surface air temperature change (global avg.) | 0.5°C/100 yrs |
| Regional urban warming bias (range over ~85 yrs) | 0.03 to 0.15°C |
| Global warming due to ENSO (past 15 yrs) | 0.1° C |
| Change in radiative climate forcing due to surface albedo change (deforestation, urbanization, etc.) | ±0.03 $W/m^2$ |
| Equilibrium sensitivity of climate models to 2x $CO_2$ (global mean equilibrium surface T change; i.e., $\Delta T$ 2x) (range) | 1.5°C - 4.5°C |
| Components of equilibrium climate change predicted by climate models typical for a 2x GHG Scenario | |
| Direct radiative effect of 2x GHG | 1.2° C |
| Water vapor feedback (positive) | 1.0° C |
| Cloud feedback (positive; decrease in global cloud) | 0.8° C |
| Sea ice/snow cover feedback (positive) | 0.4° C |
| **Total** | 3.4° |
| Global avg. IR greenhouse heating due to clouds | 31 $W/m^2$ |
| Global avg. SW cooling due to clouds | 48 $W/m^2$ |
| Radiative climate forcing change due to GHGs (2000-2050) | 1.3 - 3.5 $W/m^2$ |
| Radiative climate forcing change due to GHGs since 1958 | 1.1 $W/m^2$ |
| Climate forcing due to anthropogenic GHGs (past 10 yrs) | 0.6 $W/m^2$ |
| Climate forcing (cooling) due to volcanic eruptions (e.g., El Chichon, Pinatubo) | -2 to -3 $W/m^2$ |
| Average cooling due to aerosols | 0.5 to -1.5 $W/m^2$ |
| Uncertainties in climate forcing due to $O_3$ and tropospheric aerosols | 1.0 $W/m^2$ |

# 1. Climate and the Greenhouse Effect

## 1.1 Introduction

Industrial and agricultural activities over the past century have resulted in an unprecedented rate of increase in the atmospheric concentrations of radiatively active trace greenhouse gases (GHGs) including $CO_2$, $CH_4$, CFCs, $N_2O$ (see Table 1). Models of the global climate system predict a consequent increase in global average temperature of 1.5°C to 4.5°C at equilibrium for a doubling of equivalent $CO_2$. While the regional scale is not accurately resolved by the models, the temperature change is forecast to be even larger in the middle and high latitudes, but smaller in the tropical belt. Attempts to model the existing historical record of global temperature for the past century have not yet provided unambiguous proof that an enhanced GHG effect already exists. Concern about such a warming stems from its potential impact on environmental factors, such as shifting precipitation patterns, weather extremes (droughts, floods), and sea-level rise, and their consequences to agriculture, water supply, the energy and transportation industries, world trade balance, etc.

TABLE 1.—Summary of key greenhouse gases affected by human activity

| Gas | Pre-Industry (1750-1800) | Present (1990) | Rate of Change/yr | Atmospheric Lifetime (yrs) |
|---|---|---|---|---|
| $CO_2$ | 280 ppmv | 360 ppmv | 0.5% | 50-200 |
| $CH_4$ | 800 ppbv | 1720 ppbv | 0.9% | 10 |
| $CFC_{11}$ | 0 pptv | 280 pptv | 4% | 65 |
| $CFC_{12}$ | 0 pptv | 485 pptv | 4% | 130 |
| $N_2O$ | 300 ppbv | 310 ppbv | 0.25% | 150 |

*Source: Houghton et al.; 1990, p.xvi.*

## 1.2 Climate

Climate commonly refers to the "average" physical environment of any given location or region as defined by such variables as surface air temperature, precipitation, wind, humidity, sunshine, and pressure. In its simplest form, this leads to the broad zonal belts with tropical, subtropical, temperate, and polar climates. Most climate classification systems use a combination of the above variables, together with relatively more constant features such as topography and soil, to describe a set of zones and parameters that generally determine the types of vegetation that can grow and the types of life forms that may flourish. Since natural and mineral resources may be found in areas that are otherwise unsuitable for unprotected living, climate can also determine the types of technological support systems (including construction, agriculture, energy, and transportation) that are required to take advantage of these resources—thus underscoring the importance of quantifying and predicting climate change.

It is emphasized that, while climate implies "average" conditions, "average" does not refer merely to the arithmetic mean state over a sufficiently long period of time. The average must also include estimates of temporal and spatial variability and statistics of extreme values.

In recent years, the problems or complexities involved in predicting even seasonal weather has rapidly forced science and technology to deal with global scale interactions and the notion of the physically interactive climate system comprising the atmosphere, oceans, biosphere, cryosphere, and geosphere. Exponentially increasing world populations and industrial activity (largely driven by fossil fuel energy) point to the anthropogenic factor as a leading candidate for inducing rapid climate change, particularly by altering the radiative balance of the planet via the injection of radiatively active GHGs into the atmosphere.

## 1.3 The Greenhouse Effect

Figure 1 is a schematic illustration of the greenhouse effect, showing that surface climates are basically a result of the radiational balance between incoming solar radiation and outgoing net (i.e., reflected solar plus infrared) radiation. As implied in Figure 1, the final average land and ocean surface temperatures would be modulated by induced or forced changes in the emission, transmission, or reflection of incoming solar radiation or outgoing terrestrial longwave radiation. Thus, changes in solar energy flux, atmospheric aerosols, albedo change due to deforestation or desertification on a large scale, and, of course, infrared absorbing gases and clouds would affect climate. Internal processes, such as the rate of overturning of the deep ocean circulation, could also cause surface temperature change.

The fact that the greenhouse effect exists is undisputed. Computations indicate that the Earth's average surface temperature ($\simeq$15°C) would be -18°C were it not for GHGs such as water vapor ($\simeq$ 1% of the atmospheric gases) and carbon dioxide ($\simeq$ 0.04%). The validity of these theoretical calculations is verified by the observed surface temperatures of Venus (477°C) and Mars (-47°C), whose atmospheres contain large concentration of greenhouse gases (>90% $CO_2$ for Venus and >80% for Mars), without which their surface temperatures would be -46°C and -57°C, respectively.

The dominant GHG in the Earth's atmosphere is water vapor. Atmospheric water vapor content is in approximate equilibrium between evaporation and precipitation; this

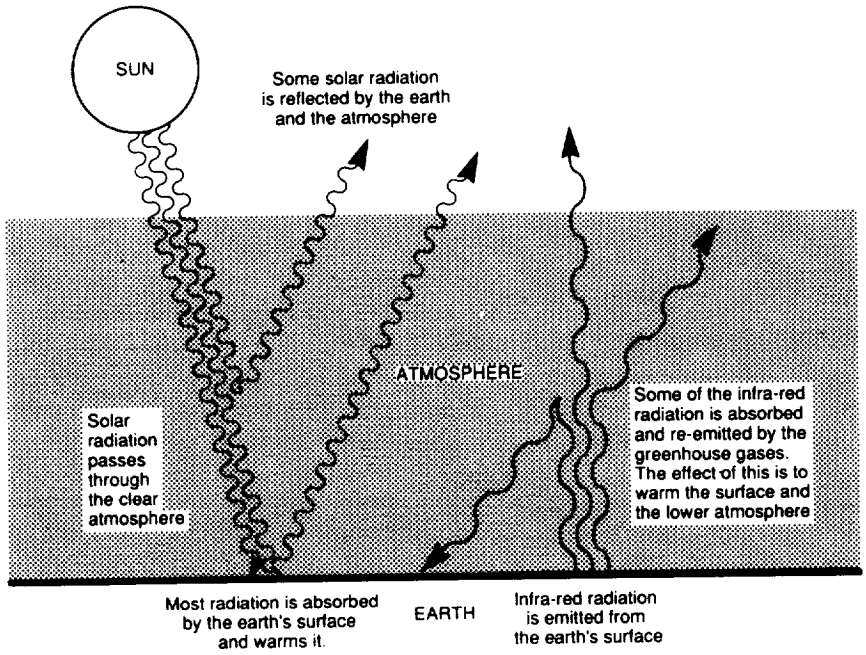


*Figure 1.–A simplified diagram illustrating the greenhouse effect. Source: Houghton et al., IPCC, 1990, p. xiv.*

equilibrium is determined by the overall radiational balance of the planet and the dynamic and thermodynamic processes that redistribute the excess solar radiation flux received in the tropics over the middle and polar latitudes. The atmospheric water vapor holding capacity is controlled by the surface temperature, vertical structure, and moisture supply (through evaporation and convective processes). Thus, the water vapor effect is considered to be a "feedback" response to an otherwise introduced temperature change. Likewise, clouds, which are simultaneously very strong infrared warming and shortwave cooling agents, are also dependent on surface temperature, vertical structure, and thermodynamic processes, and thus introduce feedback that could enhance or counter an initial surface warming induced by other forcing agents.

The notion of an "enhanced" greenhouse gas effect refers primarily to the incremental global warming caused by increasing concentrations of anthropogenically introduced radiatively active gases, such as $CO_2$, $CH_4$, CFCs, and $N_2O$, over and above the greenhouse effect caused by such naturally occurring greenhouse gases as water vapor. Though the word "enhanced" is frequently omitted, the distinction is central to the current discussion of greenhouse effects and, indeed, to the way climate models simulate future scenarios of climate change. This central thesis has also been the cause of much of the controversy about predicting future climate change in absolute terms. The controversy arises from uncertainties over the manner in which other forcings and feedbacks compete (with or against) the enhanced GHG effect.

Figure 2 shows the association of fluctuations in temperature with atmospheric concentrations of $CO_2$ and $CH_4$; the data have been derived from air bubbles trapped in Antarctic ice cores. The correlation is very high, lending credence to the hypothesis that an enhanced GHG effect would cause climate change. But GHG forcing does not operate in isolation. The atmospheric vertical and horizontal distributions of some GHGs (e.g., $O_3$) and greenhouse agents (e.g., clouds), in combination with other elements affecting the radiation balance (e.g., aerosols), would determine the net surface effect (warming or cooling) and magnitude. Also, the surface "climate" change depends on how the physical system responds to an initial change forced by GHGs—thus, feedback processes that may enhance or subdue the initial tendency change to need to be taken into account.

An entirely complete and mathematically tractable description of the climate system is probably beyond the

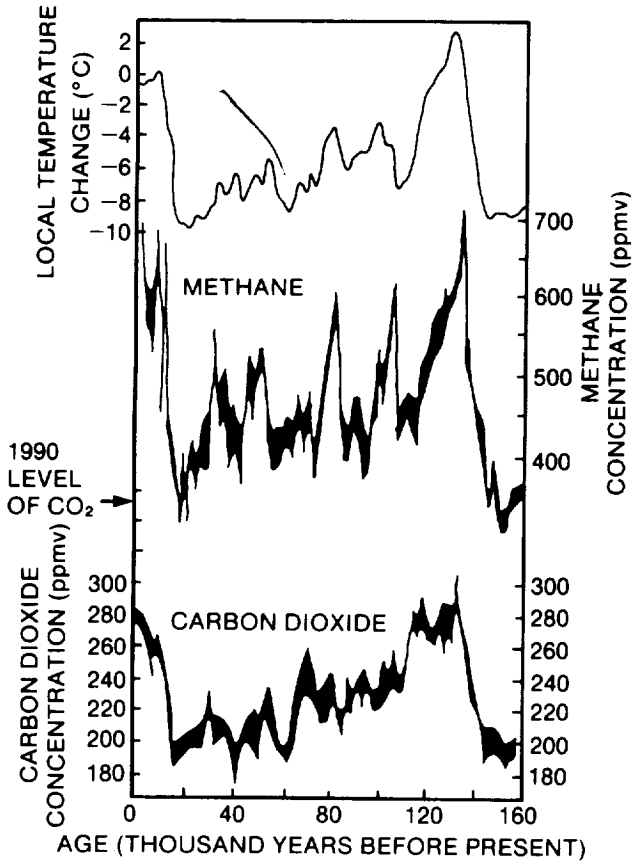


*Figure 2.–Analysis of air trapped in Antarctic ice cores showing the correspondence between local temperature and concentrations of methane and carbon dioxide over the last 160,000 years. The 1990 concentration of $CO_2$ is also indicated. Source: Houghton et al., IPCC, 1990, p. xv.*

scope of present observing and modeling technology. However, it is felt that sufficient advances have been made in recent years to capture the essentials of climate system physics and to provide projections on possible change, whether it is due to GHGs or to other causes such as natural variability (on long time scales) or aerosol injection through massive volcanic eruptions. Nevertheless, model simulations of past and present climates need to be validated and verified before model predictions can be interpreted reliably—hence the need for observations and analysis to detect climate change and GHG effect.

Precisely how to handle the entire scientific problem of the detection and prediction of GHG effect and climate change is still the subject of some discussion, even if generalities are commonly assumed to be known. The global atmospheric temperature record emerges as one of the most analyzed indices of change. Observational analyses generally show that the temperature change over the past 100 years is consistent with climate model simulations, but the change is not large enough to be beyond the range of naturally occurring possibilities. There are other means, conceivably, to detect an enhanced GHG effect, such as a change (increase) in the global average surface downward infrared radiation. But a lack of observational data precludes such an analysis; furthermore, even changes in this parameter may not be the unique result of changes in anthropogenically injected GHGs (i.e., $CO_2$, $CH_4$, CFCs, etc.). Presumably, natural biogeochemical processes could alter the moisture and cloud fields, thereby causing a surface temperature change. In order to isolate enhanced GHG effects from changes caused by other processes, all forcings and feedbacks must be quantitatively observed and modeled.

# 2. The Global Atmospheric Temperature Record

This section is somewhat arbitrarily divided into "surface temperature," "free atmosphere," and "space-based measurements." This has been done to distinguish, in part, surface-based and space-based observing technology and to provide separation between the conventional understanding of "climate" and the intricacies of the interactive forces and feedbacks that determine surface climate change, as described briefly in section 2.1 and dealt with more completely in sections 2.3 and 2.4. Thus, there is overlap and the sections are not mutually exclusive. For example, volcanic effects are described under "free atmosphere" in section 2.2.2 although the aerosol cloud would clearly also affect surface temperature. Similarly, ENSO will affect the upper atmospheric temperature although it is covered under "surface temperature" in section 2.1.2.

## 2.1 Surface Temperature

The analysis of global average temperature anomalies by centers in the United Kingdom (University of East Anglia, Climate Research Unit [CRU]); the United States (National Aeronautics and Space Administration, Goddard Institute for Space Studies [NASA/GISS]) and the Soviet Union (State Hydrological Institute [SHI]) all show a long-term warming trend of approximately 0.5°C over the past 100-plus years. The basic land surface data used in most studies comprise surface climate station data exchanged via the Global Telecommunications System (GTS) of the World Meteorological Organization (WMO), presently numbering about 1,000 stations worldwide. The synoptic station network is larger (approximately 5,000 stations), and the ensemble of regional/national stations is even more so (about 40,000); the latter, however, are not exchanged internationally. The GTS-exchanged monthly climate data have been extended and enhanced, especially for the first half of the 20th century and the latter part of the 19th century, from the archives of various meteorological services (e.g., United Kingdom, France, United States, Germany, Soviet Union) and special data collection efforts by scientists.

Over the ocean, data are primarily from ship observations (and a few island stations), exchanged by and large regionally; a subset is internationally exchanged. The currently available database is, however, a result of major efforts by the U.K. Meteorological Office (UKMO) and the US-Comprehensive Ocean-Air Data Set (COADS) Project, through which ship logs from the 1850s onward were digitized.

Most current and historical observations contain a variety of possible errors and biases due to station moves and changes in instrumentation, observing practices (e.g., the change from bucket to intake manifold for ocean water sampling), computational methods (e.g., daily mean temperature computation), etc. Substantial effort has been expended in understanding and accounting for such possible errors, for example, by CRU in selecting reliable stations and assessing urban effect by UKMO for ocean surface temperature observations from ships; and by the National Climate Data Center of NOAA (NOAA/NCDC) for urban effect. These studies have resulted in corrected global time series. Figure 3 shows the global mean, combined land air (CRU), and sea surface (UKMO) temperature anomalies from 1861 to 1989.

While there are differences between analyses due to differences in averaging techniques, station selection criteria and gridding techniques, the basic decadal warming trend are reflected in all of the independently conducted analyses. As an example, Figure 4 compares the UK (CRU), and USSR (SHI) land (only) air temperature analyses of P.D. Jones et al. (1986), J. Hansen and S. Lebedeff (1987) from

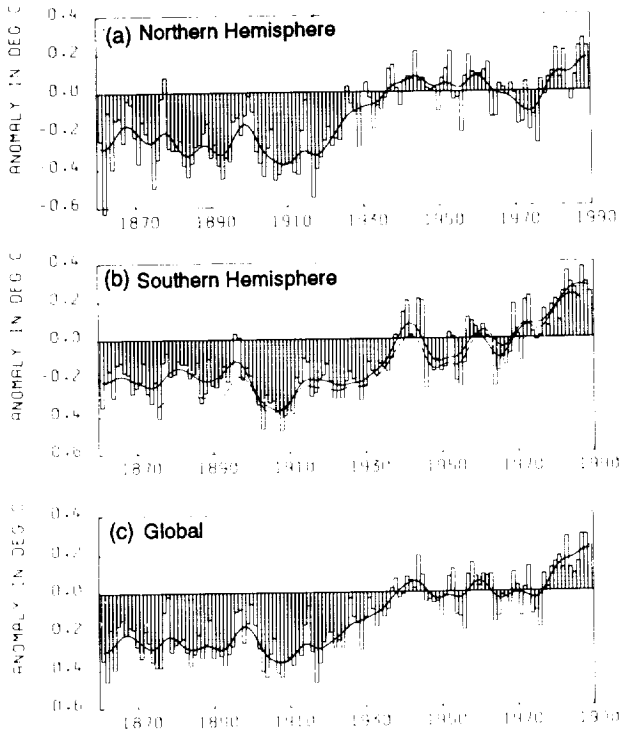


*Figure 3.–Combined land air and sea surface temperatures, 1861-1989, relative to 1951-1980. Land air temperatures are from P.D. Jones, and sea surface temperatures are from the U.K. Meteorological Office and Farmer et al. (average of the two data sets). (a) Northern Hemisphere, (b) Southern Hemisphere, (c) globe. Source: Houghton et al., IPCC, 1990, p. 213.*

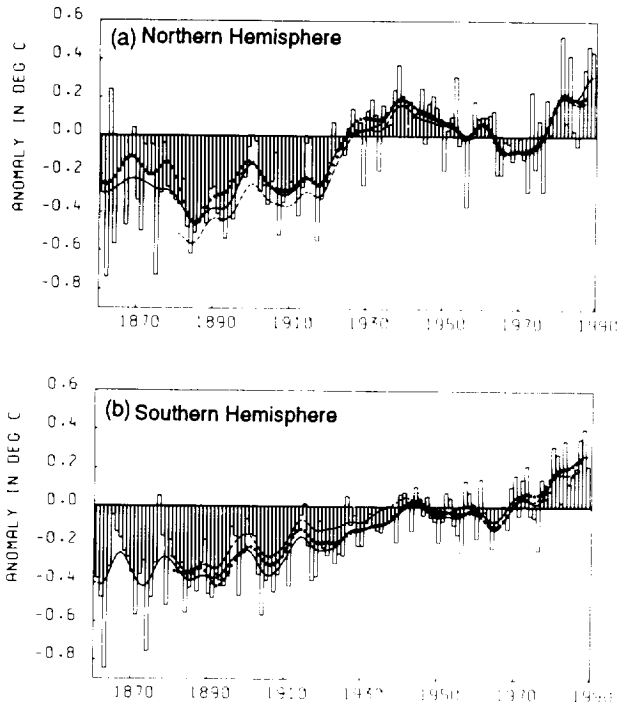


*Figure 4.–Land air temperatures expressed as anomalies relative to 1951-1980. Annual values from P.D. Jones; smoothed curves of values from P.D. Jones (1861-1989) (solid lines), Hansen and Lebedeff (1880-1987) (dashed lines), and Vinnikov et al. (1861-1987 for Northern Hemisphere and 1881-1987 for Southern Hemisphere) (dots), (a) Northern Hemisphere, (b) Southern Hemisphere. Source: Houghton et al., IPCC, 1990, p. 206.*

NASA/GISS and K. Vinnikov et al. (1987) from SHI. General agreement is clear, even if the values for individual years sometimes differ.

### 2.1.1 Urban Effect

A major controversy regarding the observed climate (temperature) trend over the past century relates to the so-called urban effect. This arises from the fact that many climate stations are in urban locations (airports, cities) and that, with population growth, airports and cities have expanded. Such an expansion or urbanization could lead to an apparent increase in global average temperature, because urbanized areas are still only a small section of the global surface area.

In order to assess urban effects more thoroughly, an analysis has been carried out by the CRU (P.D. Jones) jointly with NOAA/NCDC (T. Karl), BMRC (N. Plummer, M. Coughlan), State University of New York at Albany (Wei-Chyung Wang), and SHI (Groisman). For urbanized regions of the world, regional time series based on rural station temperature data were compared with regional averages derived from the global gridded data set of Jones et al. The results are summarized below in Table 2.

TABLE 2.—Comparison of regional temperature trends: Rural station vs. gridded data of Jones et al. (units °C over the period of record)

| Region | Period | Rural/Grid | Trend |
|---|---|---|---|
| Contiguous United States | 1901-84 | Rural | 0.16 |
| | | Grid | 0.31 |
| Western USSR | 1901-87 | Rural | 0.38 |
| | | Grid | 0.35 |
| Eastern Australia | 1930-88 | Rural | 0.56* |
| | | Grid | 0.60* |
| Eastern China | 1954-83 | Rural | 0.23 |
| | | Grid | 0.19 |

**Significant at 5%.*
*Source: P.D. Jones, 1991, personal communication.*

The urban bias of about 0.15°C per 85 years is largest in the United States and is attributed to the rapid expansion of cities over the past century, compared with the stabler and older urban areas in other parts of the world. The urban bias for the western USSR is -0.03°C, for eastern Australia 0.04°C, and for eastern China -0.04°C. It is considered unlikely that the remaining unsampled regions of the developing tropics and western Europe could significantly increase the urban bias above 0.05°C per 100 years, an order of magnitude smaller than the observed warming over the last 100 years.

### 2.1.2 ENSO Effect

The El Niño/Southern Oscillation (ENSO) is a major tropical ocean-global atmosphere interaction event with a recurrence frequency of about 2-7 years. During an ENSO, large portions of the central and eastern Pacific are warmer (2-5°C) than normal, as is the tropical (belt) atmosphere. The term La Niña has been used to described periods of colder than normal central and eastern Pacific ocean temperatures.

To address speculation that the observed warming could be due to more frequent and intense ENSO events, and to assess the warming trend unperturbed by unusually warm or cold El Niño/La Niña cycles, regression analysis methods have been applied to statistically remove their influence on the global average temperature trend. Figure 5 shows the tropical belt (20°N - 20°S) temperature anomalies from 1961 to 1989. With the mean ENSO signal removed, the warming of the globe in the last 15 years is reduced by about 0.1°C, i.e., by about half.

The impact of a major El Niño on the global average temperature is about +0.5°C and that of La Niña about -0.5°C. The effects persists for about 1-3 years after each episode, injecting a change in variability but not, apparently, in the observable long-term trend. However, the frequency of major El Niños could alter the short-term (i.e., 1- to 10-year) trend and needs to be distinguished from 50-

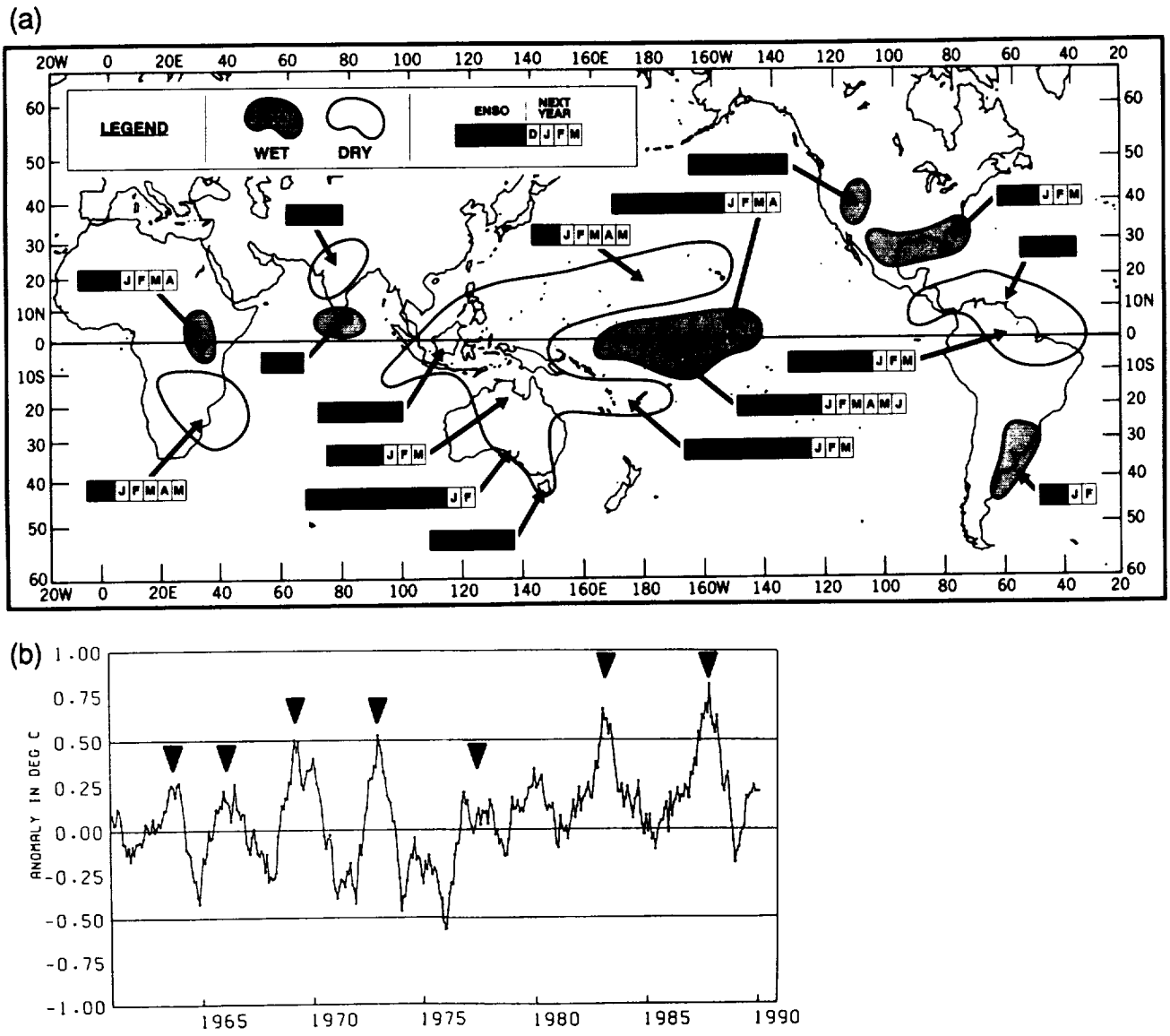


*Figure 5.–(a) Schematic diagram of areas and times of the year with a consistent ENSO precipitation signal (adapted from Ropelewski and Halpert, 1989). (b) Monthly tropical (20°N-20°S) sea surface and land air temperature anomalies, 1961-1989; land data from P.D. Jones and sea surface temperature data from UKMO; arrows mark maximum ENSO warmth in the tropics. Source: Houghton et al., IPCC, 1990, p. 227.*

to 100-year trends. Insufficient historical data precludes a more thorough analysis of the impact of ENSO variability on decadal and >100-year trends.

### 2.1.3 Sampling Network Considerations

At issue is the sampling, or rather the de facto sampling, of the "true" field as determined by available observations in data sets. For land areas, the general consensus is that although there were fewer stations in the early part of the 20th century, the number of stations used seems to have made little difference in the analyses, at least as far as the time series for global average temperature anomaly is concerned. Thus, using a degraded or undersampled "modern" network to match that of 50 years ago did not substantially alter the observed decadal temperature trend, as illustrated in Figure 6.

Note that all global average surface temperature analyses deal with temperature anomalies. Because there are large data-sparse areas, particularly in the oceans, it is not possible to compute or derive a representative absolute global mean temperature time series. It is felt that this does not invalidate the various techniques used to determine global averages for temperature anomalies, because the anomalies at each station or grid-box are more amenable to extrapolation than are the absolute values. However, the inability to obtain absolute temperature values for the planet (as well as absolute average surface radiative temperature)

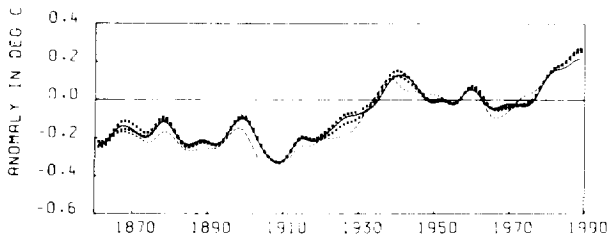


*Figure 6.–"Frozen grid" analyses for 1861-1989 for the globe, using land data shown as in Figure 3, and UKMO SST data: 1861-70 coverage (dashed), 1901-10 coverage (dotted), 1921-30 coverage (crosses), and all data (solid line). Source: Houghton et al., IPCC, 1990, p. 213.*

renders the problem of detecting an enhanced GHG effect more complicated because the dynamic and thermodynamic responses to an initial GHG-induced warming could vary according to absolute temperature changes and the location of such "changes," especially in a nonlinear interactive system.

Over ocean areas, a sampling experiment (C. Ropelewski) indicated that the undersampling forced by the nature of commercial shipping over time could lead to a fairly significant difference in the resulting global mean temperature anomaly—as much as about 0.3°C. The study used a present day sea-surface temperature field at 2.5° spatial resolution produced by the NOAA Climate Analysis Center (CAC) blended analysis method (Reynolds) as the "truth" field (Figure 7) and undersampled the field based on ship-track observational locations from the COADS data set for the years 1880, 1920, and 1970. The corresponding observational locations are shown in Figure 8 a, b, and c.

The results of the NOAA/CAC Study are summarized below in Table 3, using February and August to represent winter and summer, respectively. Note that there are fairly substantial differences between the "true" global SST anomaly—and the 1880 and 1920 fields—about 0.3°C. The difference decreases in 1970 to about 0.05-0.15°C, presumably because of the substantially improved sampling array in 1970 compared with 1880 and 1920.

Interpreting the results in Table 3 is not necessarily straightforward. Note in particular:

- In data-sparse areas, an observation receives a disproportionately large weight and sphere of influence. Thus, if a point happened to be located in a region of large but local anomalous SST, it would erroneously influence the global average.

- Results comparing the undersampled array of observations with the hypothetical "truth" field would differ with each month, year and distribution of anomalies in the "truth" field, because the precise accidental juxtapositioning of the "truth" field values and ship-track location could completely change the grid field values and the computed global average—perhaps even in sign.

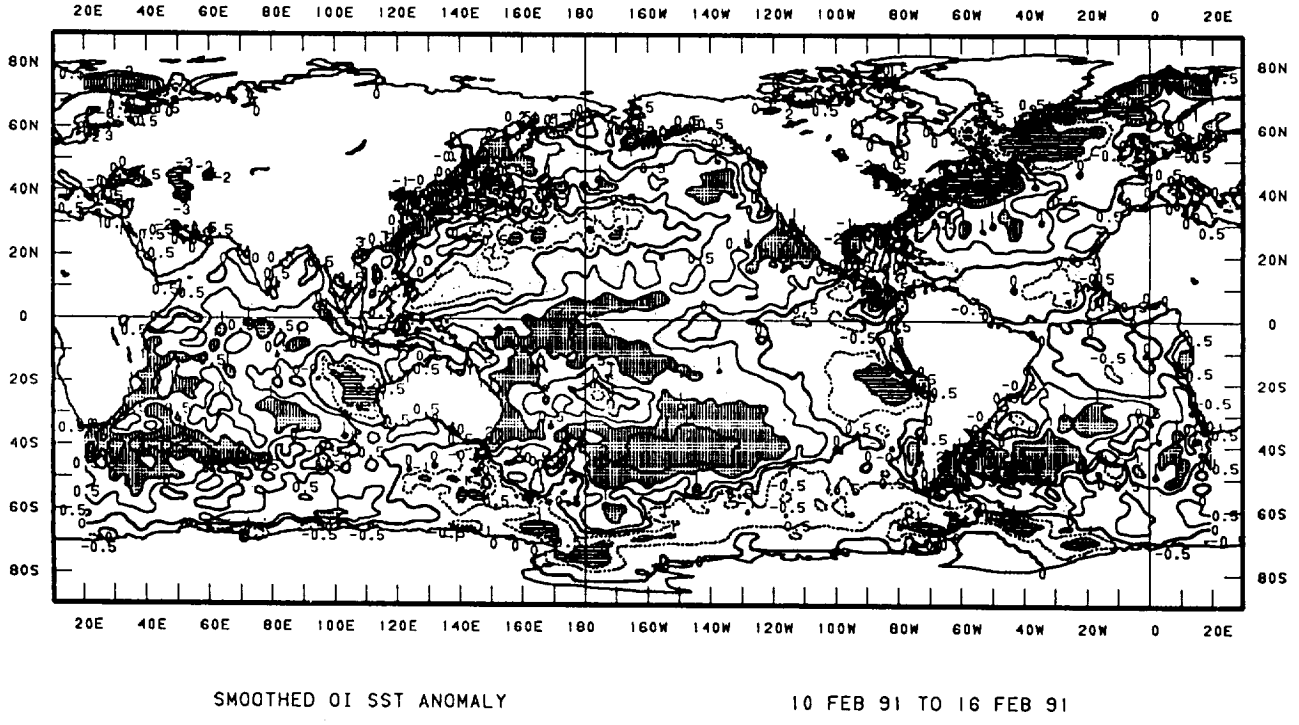


*Figure 7.–The SST "truth" field chosen arbitrarily for the period 10-16 February 1991 to assess the impact of undersampling. Source: C. Ropelewski, NOAA/CAC.*

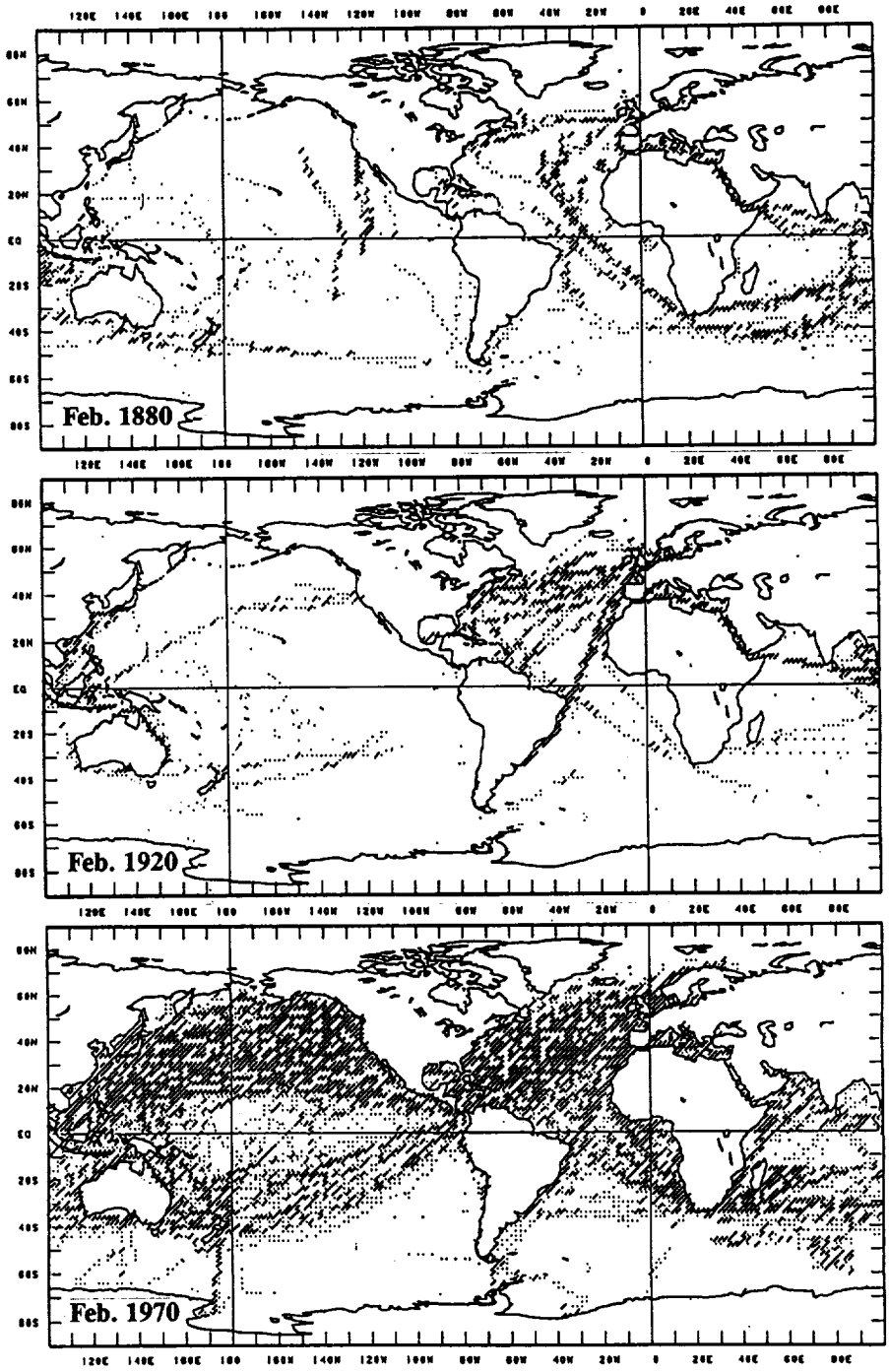


*Figure 8.–Ship track positions from the NOAA/COADS data set for (a) February 1880, (b) February 1920, and (c) February 1970. Source: C. Ropelewski, NOAA/CAC.*

TABLE 3.—Reanalysis of the mean SST anomaly for winter February and summer August using COADS/ Ice climatology data*

| Zone | Truth | Field 1880 | 1920 | 1970 |
|---|---|---|---|---|
| | | February | | |
| 60N - 60S | 0.37 | 0.09 | 0.10 | 0.30 |
| 60N - 30N | 0.20 | -0.04 | 0.09 | 0.23 |
| 30N - EQ | 0.29 | 0.09 | 0.07 | 0.25 |
| EQ - 30S | 0.35 | 0.06 | 0.07 | 0.30 |
| 30S - 60S | 0.58 | 0.21 | 0.17 | 0.40 |
| | | August | | |
| 60N - 60S | 0.30 | 0.11 | 0.10 | 0.20 |
| 60N - 30N | 0.42 | 0.14 | 0.23 | 0.43 |
| 30N - EQ | 0.19 | 0.04 | 0.07 | 0.16 |
| EQ - 30S | 0.22 | 0.07 | 0.08 | 0.18 |
| 30S - 60S | 0.42 | 0.20 | 0.07 | 0.14 |

**Latitude cosine weighted; values over land excluded.*
*Source: C. Ropelewski, 1991, personal communication.*

A large number of sampling experiments would need to be carried out with variations in the "truth" field to cover all seasons, years, and episodic events such as ENSO, La Niñas, and extratropical fluctuations. The significance of the one-experiment case study (C. Ropelewski) presented however, is to point out the potential magnitude of the impact of changes in the sampling array and to emphasize the need to quantify and document the uncertainties arising from changes in the temporal and spatial distribution of networks or arrays as well as to account for errors or biases introduced by instrumentation, urban effect, etc. From the example chosen, it is clear that the magnitude of possible error is of the same order as that of the climate change signal.

The study also raises questions about the interpretation of data from current and future observing systems, particularly space-based systems; i.e., "over sampling" with respect to ground-based measurements could alter global estimates and lead to the appearance of climate change.

### 2.1.4 "Change" Signal

To determine the region responsible for most of the global temperature change observed, the CRU (P.D. Jones) computed the correlation between individual grid-point data and the global average for the periods 1901-1945 and 1946-1990, reproduced in Figures 9 and 10. Stipled areas are data sparse. It appears that the correspondence is uniform and positive over large areas of the Northern and Southern Hemispheres for the first half of the century—indicating a relative warming over almost the entire globe. In contrast, the last 45 years (Figure 10) shows large areas of positive correlation in the tropics but areas of positive and negative

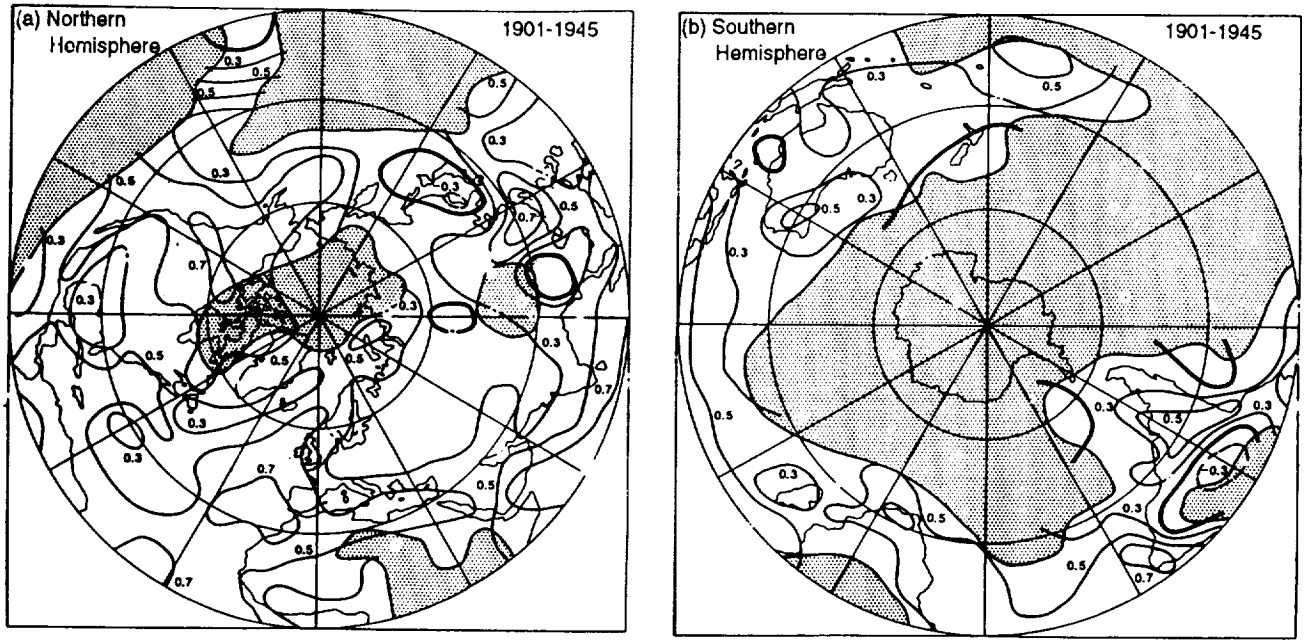


*Figure 9.–Correlation between grid-point data and global average annual temperature anomalies for the period 1901-1945 (combined land air and sea surface temperatures). Data set details are as described in Figure 3; shaded areas are data sparse. (a) Northern Hemisphere, (b) Southern Hemisphere. Source: P.D. Jones, 1991.*

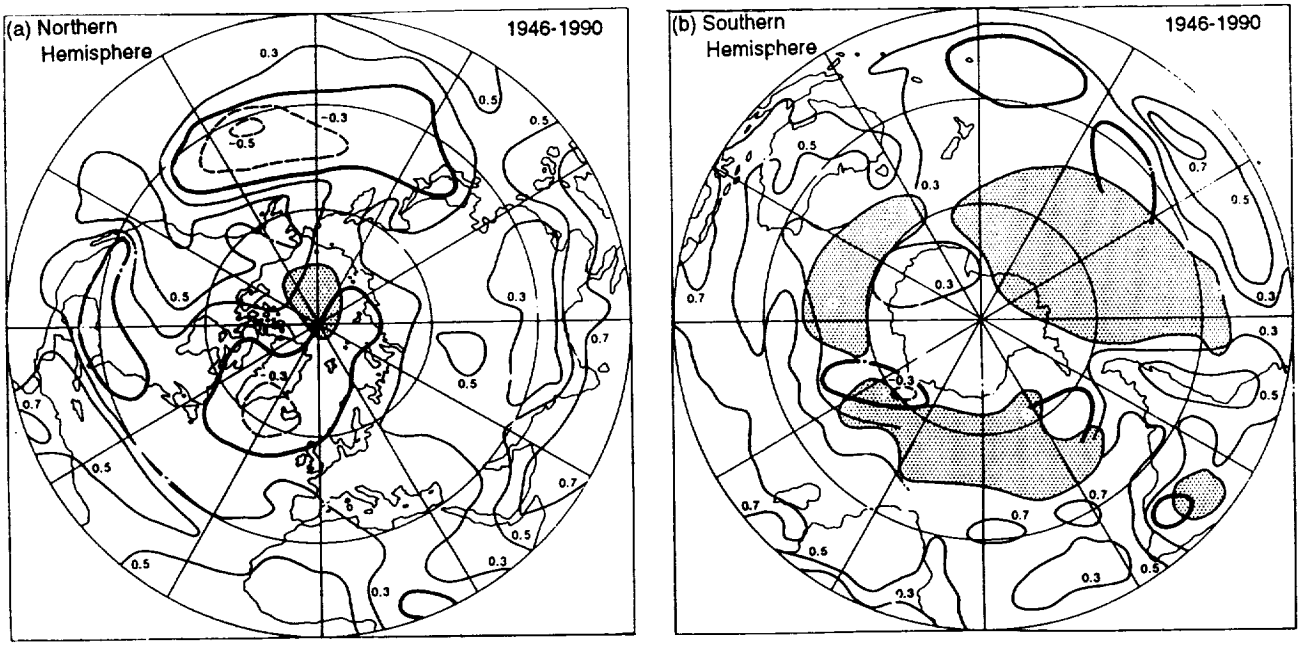


*Figure 10.–Correlation between grid-point data and global average annual temperature anomalies, for the period 1946-1990 (combined land air and sea surface temperatures). Data set details are as described in Figure 3; shaded areas are data sparse. (a) Northern Hemisphere, (b) Southern Hemisphere. Source: P.D. Jones, 1991.*

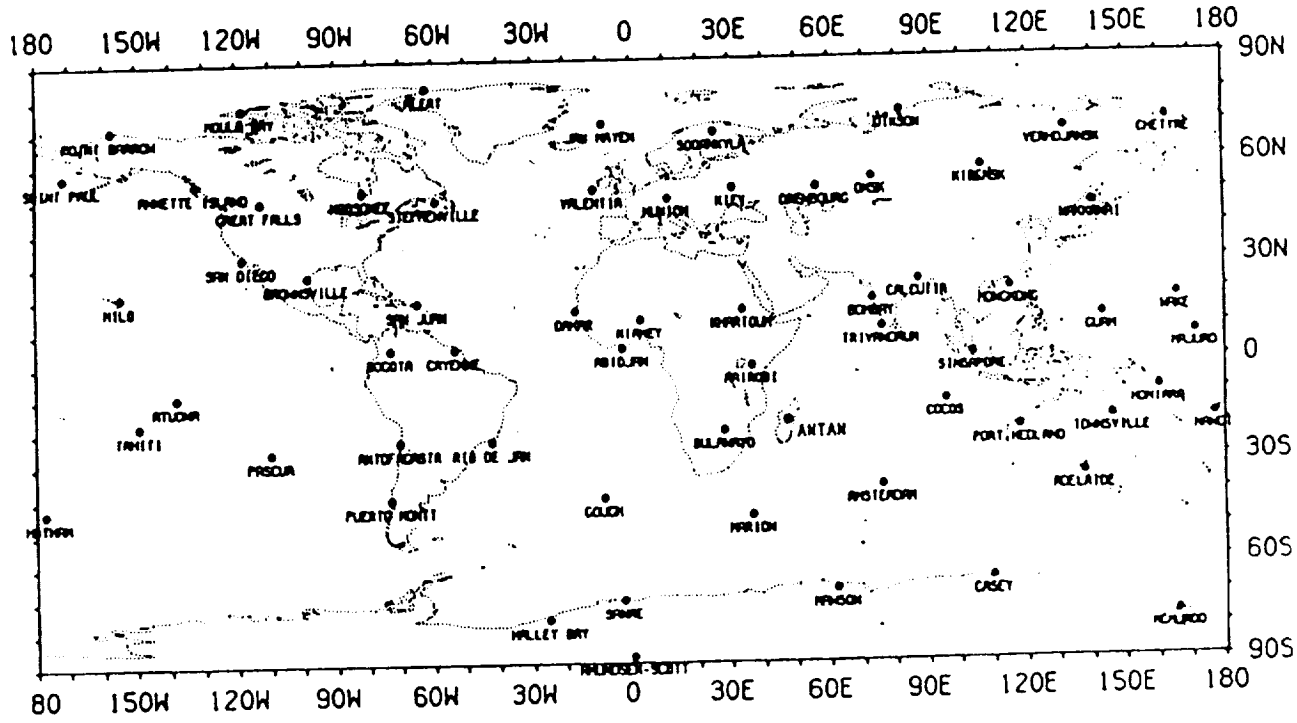


*Figure 11.–Distribution of the fixed set of upper air radiosonde stations used in the analysis of layer mean atmospheric temperature anomalies. Source: J. Angell, 1991.*

correlation over the middle and higher latitudes. The implication is that most of the global warming is attributable to the tropical belt, while the middle and higher latitudes exhibited some regions that cooled as much as others warmed. This may explain why the belt at 60°-90° did not show significant warming in the SHI analysis (K. Vinnikov et al.), which computed latitudinal zonal averages with available land station data instead of grid-point fields.

## 2.2 The Free Atmosphere (850 mb and above)

### 2.2.1 Temperature

Using a fixed set of 63 evenly distributed radiosonde land stations (Figure 11), the NOAA Environmental Research Laboratory (ERL) (J. Angell) analyzed the global layer mean temperature changes in the atmosphere. The data set extends from 1958 through spring 1991 and consists of mean temperatures for the following layers: 850-300 mb (lower troposphere), 300-100 mb (upper troposphere/tropopause), 100-50 mb (lower stratosphere), the surface, surface-100 mb, and 100-30 mb. A weighting of polar, temperate, subtropical, and equatorial climatic zones at 1:2:2:1 (approximating their areal extent) yields a hemispheric-average seasonal temperature deviation and an average for the two hemispheres, the global average.

Figure 12 shows the temperature deviation observed over the past 35 years. While the interannual variability is substantial, the decadal tendencies show a warming of the lower troposphere and a cooling of the upper troposphere and lower stratosphere. The finding of cooling of the upper troposphere is in contradiction to the effects of GHG-induced warming suggested by climate models, and it requires further model analysis. The problem involves the large temperature decrease found (J. Angell) in the 100-50 mb layer. Schmidlin suggested that this might be due to a transition to Vaisala radiosondes. This now appears not to be the case. It is noteworthy, however, that international radiosonde intercomparison by WMO identified a large number of manufacturers (17) and types (31) of radiosondes that have significant differences among them. Even within the United States, new stations using radiosondes in Arizona and California, for example, are 1-2°C warmer than older stations using similar VIZ radiosondes (F. Schmidlin).

Thus is the case as with surface stations and sea surface temperature measurements, upper atmospheric radiosonde-derived measurements of temperature change require the complete documentation of changes in sensors, observing practices, observing times, calibration constant, and intercomparison results in order to take into account artifacts due to extraneous causes. Nevertheless, it is considered unlikely that the structure of long-term trends—as evident in the upper atmospheric temperature record—will be altered since there has been a consistent and evenly distributed set of stations over the entire analysis period (J. Angell).

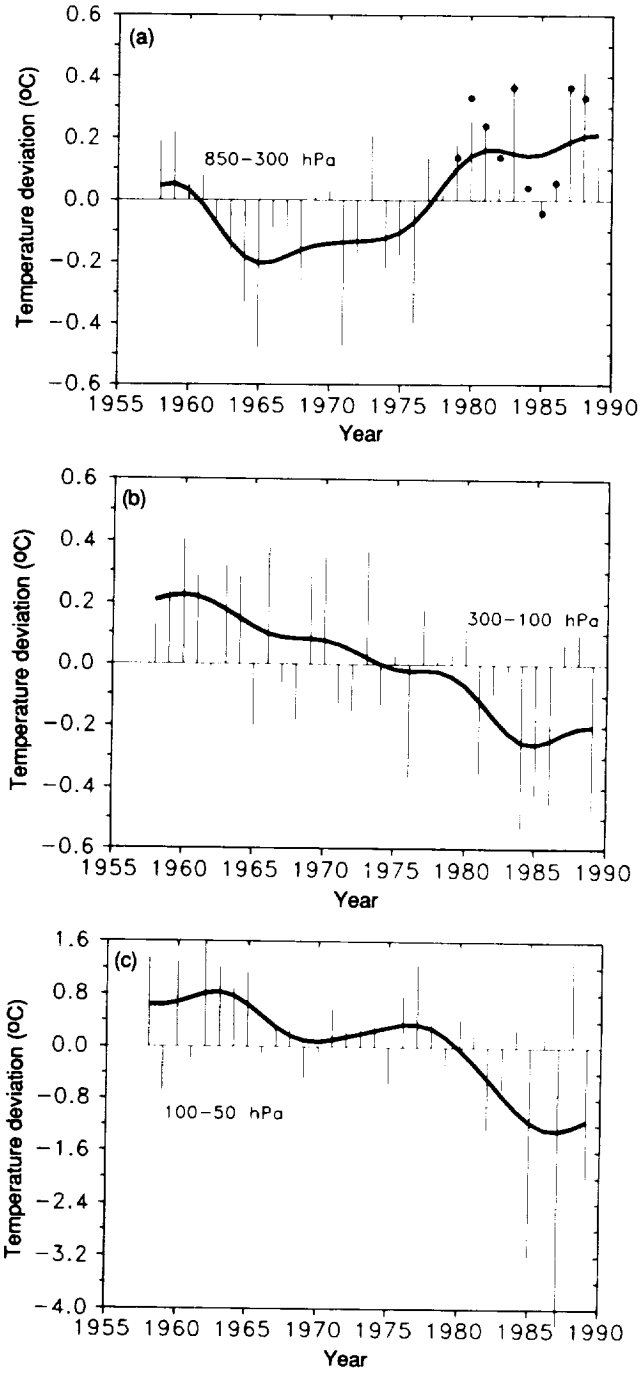


*Figure 12.–Temperature anomalies in the troposphere and lower stratosphere for 1958-1989, based on Angell (1988). (a) Annual global values for 850-300 mb. Dots are values from satellite MSU; Spencer and Christy, 1990). (b) 300-100 mb. (c) Annual Antarctic (60°S-90°S) for 100-50 mb. Source: Houghton et al., IPCC, 1990, p. 221.*

### 2.2.2 Volcanic Effects

The effects of volcanic eruptions are somewhat difficult to detect, since the signal is buried by the interannual variability that is dominated by ENSO.

However, with the adjustment for El Niño an El Chichon-induced cooling of about 0.3°C in the 850-300 mb layer becomes apparent, and the warmest year is 1990, followed by 1989. In 1990, the surface was relatively warmer than the troposphere, with a record cold in the low stratosphere. This may explain the depressed (compared with radiosonde data) TIROS-N microwave sounder unit (MSU) temperature measurements in 1990 (section 2.3.1).

Preliminary data on the Pinatubo (Philippines) volcanic eruption (B. Mendonca) indicated that the injection of sulfates and aerosols into the stratosphere was much greater than that from El Chichon. At the time of the workshop, the Pinatubo cloud was rapidly spreading east over the tropics with an aerosol cloud peak around 23 km on 9 July 1991 detected by lidar at Mauna Loa, Hawaii (Figure 13). The NASA/GISS (J. Hansen et al.) climate model integration arbitrarily provided for an El Chichon-type eruption around 1995 and forecast a consequent cooling effect. Based on available information from NOAA/GMCC (B. Mendonca) during the workshop, Pinatubo is anticipated to produce a cooling effect of about 2-3 W/m$^2$. Thus the predicted GHG warming trend could be more than offset for the next 5 years or more.

It is to be noted that the climate forcing rate due to major volcanic eruptions is orders of magnitude larger than the GHG forcing rate. For example, the climate forcing (as popularly defined for a 2x GHG) is about 2 W/m$^2$. The actual change is spread over 30 to 50 years, with temperature changes of about 1.5° to 4.5°C. Thus the annual forcing change is about 0.04-0.15 W/m$^2$/year due to GHGs compared with 2-3 W/m$^2$/year for Pinatubo. Although the volcanic clouds are usually not sustained for more than about 5 years, the frequency of such major volcanic eruptions (as yet an unpredicted quantity) could have a major impact on how the future climate evolves. As is evident from Figure 13 (b), the aerosol cloud had just reached Hawaii in late June. Both the height of the cloud and its optical opacity were expected to increase substantially with time.

Very long term integration of simplified models (i.e., not general circulation models [GCMs] with 3-D grid resolution, but models that contain much of the basic physics of interactions among temperature, climate forcing, and feedback processes) shows that most of the fluctuations over the past 500 years can, in principle, be explained by prescribed volcanically injected aerosol changes, with a slight, but very gradually increasing, differential due to GHGs during the last 100 years (A. Robock); see Figure 14.

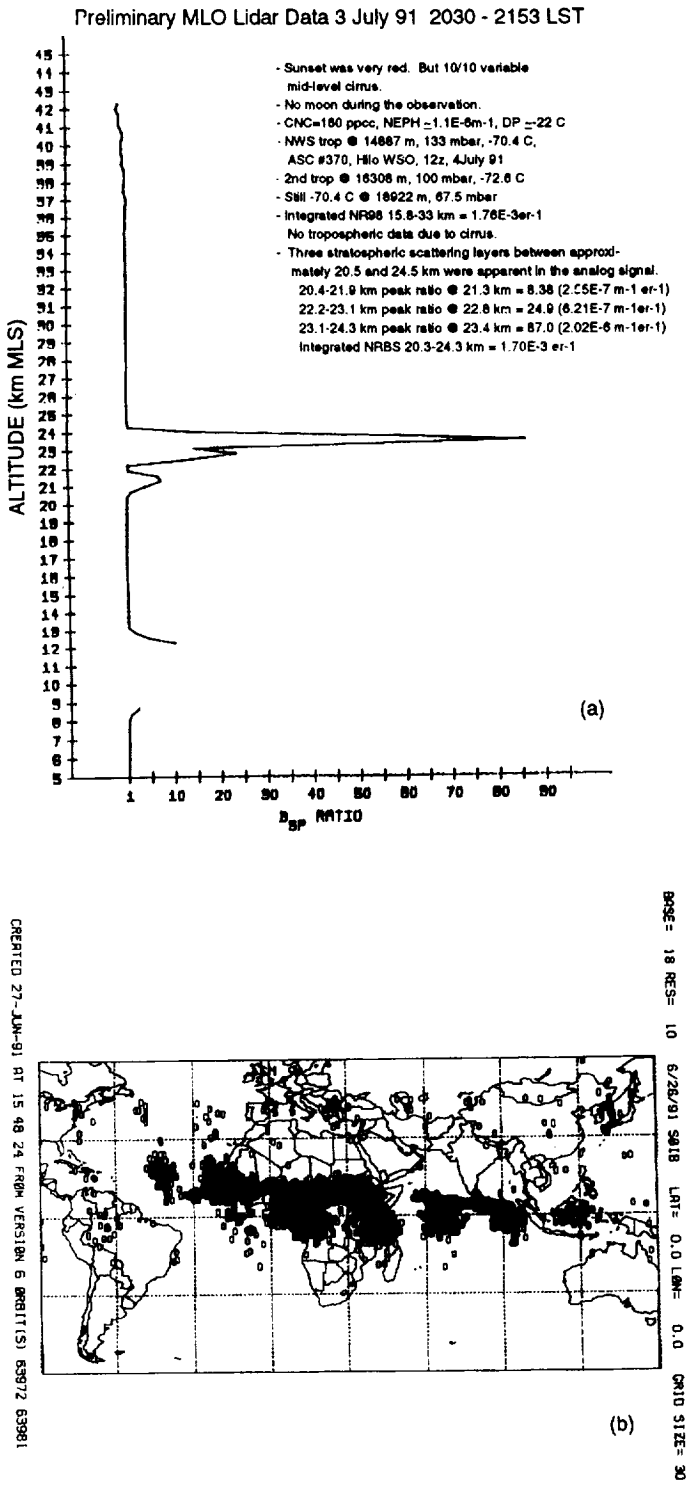


*Figure 13.–Left: (a) The Pinatubo volcanic aerosol clouds as measured by lidar at the Mauna Loa observatory in Hawaii on 9 July 1991, (b) The aerosol cloud distribution on 26 June 1991. Source: B. Mendonca, NOAA/GMCC, 1991.*

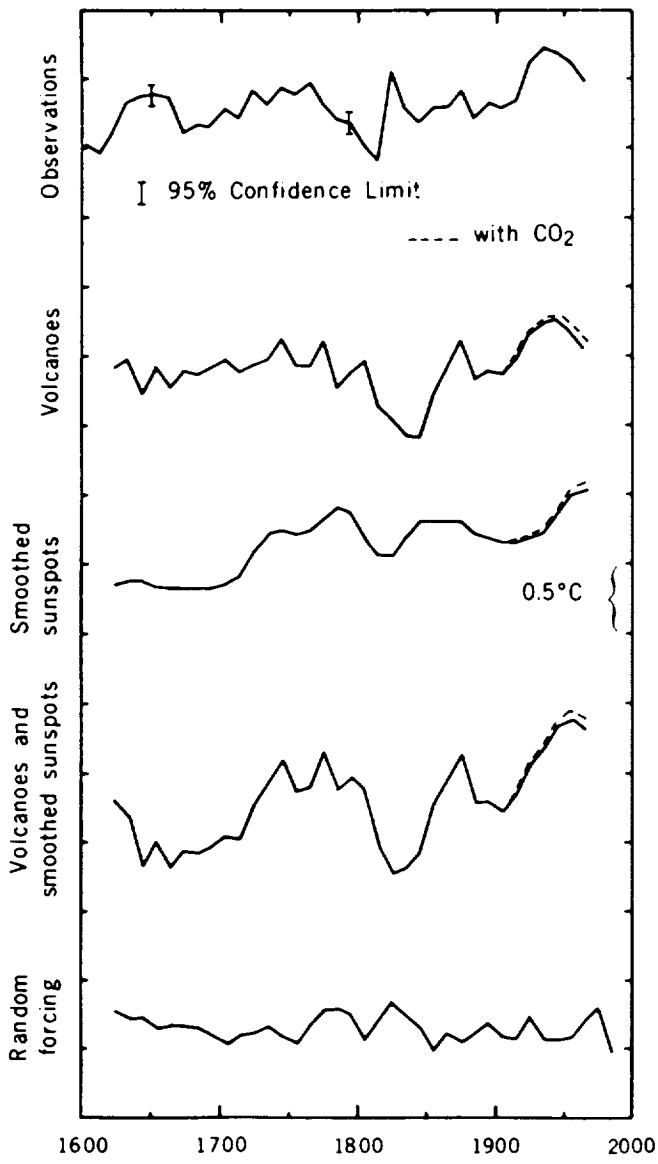


*Figure 14.–Northern Hemisphere average surface temperature observations and climate model calculations, shown as 10-year averages. The observations come from the reconstruction of Groveman and Landsberg for 1600-1880, shown with the 95 percent confidence interval, and from the data of Borzenkova et al. for 1881-1975. Source: A. Robock, 1979.*

### 2.2.3 Sunspot/Solar Correlations

US rocketsonde data suggest (J. Angell) that between 1972 and 1989 the temperature decreased by about 1.0°C, 1.5°C, and 2.0°C per decade in the 26-35, 36-45, and 46-55 km layers, respectively. In these layers, a decrease in sunspot number of 100 has been associated with a decrease in temperature of about 0.8°C.

Detailed analysis of relations between solar fluctuations and stratospheric geopotential height and temperature have been carried out by H. van Loon and K. Labitzke, using consistently analyzed radiosonde data available for the Northern Hemisphere. Figure 15 shows the correlations between a 10.7 cm solar flux at Charleston (32°N, 30°W) and geopotential heights of 30 mb and 100 mb (which correspond to the mean atmospheric column temperature). The effect of the 11-year solar cycle appears to be to raise the height of stratospheric constant-pressure surfaces and temperatures in middle and lower latitudes of the Northern Hemisphere at solar maxima and to lower them at solar minima.

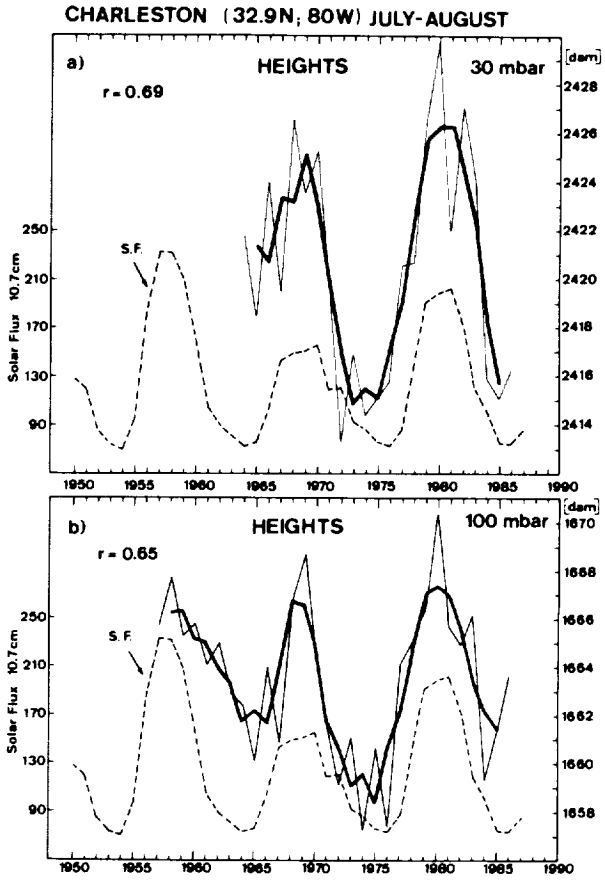


*Figure 15.–Time series in July-August at Charleston (32°N, 80°W) of observed (a) 30-mb height (dam), (b) 100-mb height, and the 10.7 cm solar flux (S.F.). The heavy line is the three-year running mean. Source: H. van Loon and K. Labitzke, 1990.*

## 2.3 Space-Based Measurements

### 2.3.1 Tropospheric Temperature

Atmospheric sea surface temperatures derived from satellite temperature soundings and imaging radiometer

measurements have been used for several years in operational meteorology and oceanography. Their utility in obtaining other information as well, such as the vegetation index, has recently been demonstrated. One clear advantage that satellites offer over conventional surface-based observing systems is their ability to provide true global coverage. Their disadvantages include random signal contamination or obstruction by clouds, water vapor, aerosols, and atmospheric particulate matter.

For the measurement of atmospheric temperature, the MSU onboard the TIROS-N series of NOAA satellites has shown considerable promise. The channels (2, 3, 4) have demonstrated long-term stability (R. Spencer and J.R. Christy) and cloud effects are reported to be relatively small. In addition, simultaneously operating satellites allow precise intercalibrations, drift checks, and estimates of measurement precision. Independent comparisons are possible with radiosonde data. Indeed, the MSU-derived temperature anomaly data for the lower troposphere (850-300 mb) compare very well with the radiosonde data of J. Angell shown in Figure 16.

It is possible that the MSU temperature retrievals can be contaminated by tropical convective clouds with high liquid water content (C. Prabhakara) as well as by ice-crystal clouds. An analysis based on the 1982-83 ENSO year, using an alternative MSU retrieval method that took this effect into account, reportedly produced a more realistic anomalous warming pattern than that obtained from the Spencer and Christy formulation referred to above. In addition, the signal from satellite data is related not only to the thermal field but is also affected by the atmosphere's dynamics. For example, during the 1982-83 ENSO, maximum tropospheric warming was hypothesized (C. Prabhakara) to be displaced away from the equator, where subsidence heating is high.

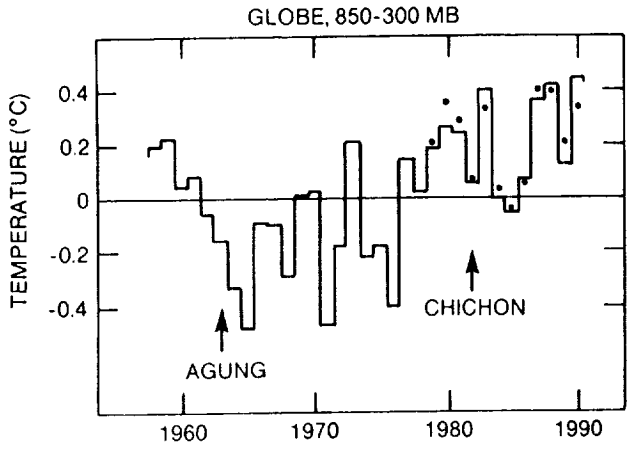


*Figure 16.–Comparison between global atmospheric temperature anomalies derived from radiosondes (solid line) (J. Angell; see Figure 12) and from microwave sounding units on board the TIROS-N series of NOAA satellites (dots). Source: J. Angell, 1991.*

### 2.3.2 Regional and Global Surface Temperature

Comparisons with surface measurements are somewhat more complicated because the satellite MSU and, for example, the surface station thermometer network measure different quantities. A further complication arises over the oceans, for which water temperatures (SSTs), not air temperatures, are taken at the surface. In this case, the correlation must overcome the discontinuities between the SST and near-surface air temperature and between the marine boundary layer and the free atmosphere (MSU).

Channel 2R removes stratospheric effects and has a weighting function that is maximized in the lower troposphere. It therefore represents the tropospheric layers predicted to have the largest GHG warming signal.

The comparison shown in Figure 17 over the well-monitored North American continent between MSU 2R and CRU data (1979-89) shows remarkable agreement in correlation (annual: .98, monthly: .95) and trends (MSU 2R: +0.38°C decade$^{-1}$; CRU: +.35°C decade$^{-1}$). When that portion of the globe subsampled by the combined UKMO and CRU data is compared with that for MSU 2R, the "global" correlations fall (.72, .61) and the disagreement in decadal trends is substantial (MSU 2R: -.04°C; UKMO-CRU: +.14°C). Comparisons with other regions that are well monitored at the surface (e.g., Eurasia, Argentina, Australia, eastern tropical Pacific) all show very strong agreement. The disagreement in "global" correlation and trend is due to disagreements in those parts of the globe that have considerably fewer observations at the surface (e.g., most oceans); MSU is completely systematic in its spatial and temporal global sampling. As a final note, the MSU 2R full global mean anomaly for 1990 was cooler than those for 1987, 1988, and 1980, unlike the anomaly derived from the various surface networks, which indicated that 1990 was by far the warmest ever.

### 2.3.3 MSU and Grid-Point Temperature Comparisons

Grid-point-based comparisons with, for example, the NASA/GISS surface (land only) analysis of temperature show good correlations where actual observational stations exist. It was demonstrated (R. Spencer and J.R. Christy) that the poor correlation (often negative) between GISS and MSU 2R over oceanic areas in the middle and high latitudes was due to the GISS extrapolation of land surface air temperature anomalies over the unmonitored ocean. In these cases, the spatial scale of the actual in situ MSU temperature anomalies is such that land and off-shore values are often negatively correlated at a distance of 1000 km. Therefore, in situ surface data are required for proper comparison with the (already in situ) satellite data. [Note that correlations between in situ SSTs and MSU 2R data in well-monitored mid-latitude oceans are generally .5 to .9, and they are never negative.]

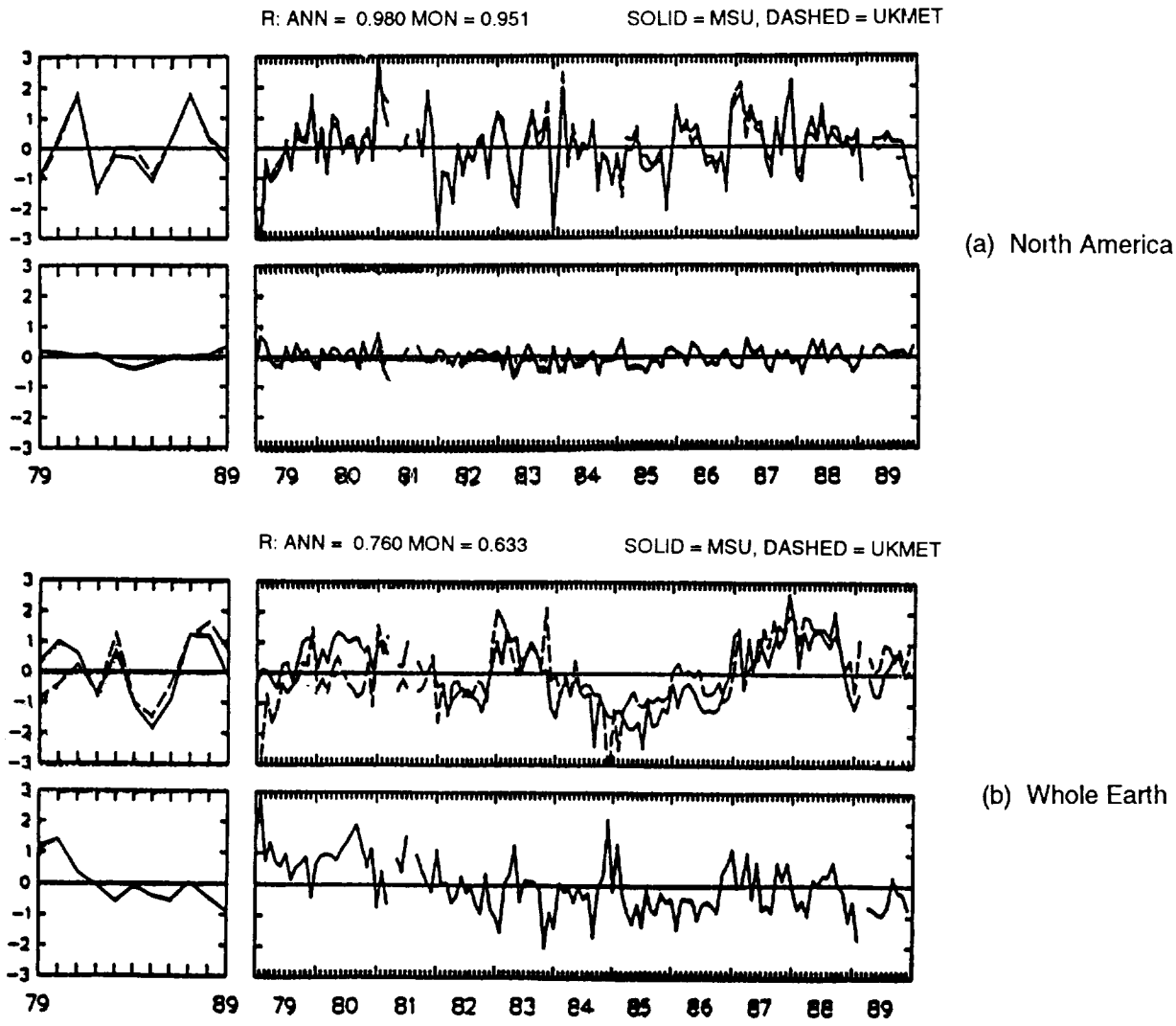


*Figure 17.–Comparison between MSU channel 2R and thermometer-derived temperature anomalies for (a) North America and (b) whole Earth. Lower right panels of each set show difference between MSU and thermometer values. Over North America during 1979-1989, there is no trend in the difference, but over the whole Earth the thermometers show a trend +0.18°C warmer than the MSU data. Source: R. Spencer and J.R. Christy, 1991, personal communication.*

The NASA/GISS analysis scheme applies the concept of zones of influence (approximately 500 km) around each station, the dimensions of the zones being obtained from statistical structure functions derived from observational data (H. Wilson). Thus, the surface area covered by the Hansen/Lebedeff global temperature analysis extends over water, at the boundaries of continental land masses. A case study (H. Wilson) showed that the 700 mb anomalous air flow corresponded with the structure of grid-point temperatures obtained from the data set, which somewhat supports, the concept of extended influence zones. More direct verification with independent measurements may be required if this controversy is crucial.

### 2.3.4 MSU and GCM Comparisons

A comparison (J. Hurrell) of monthly mean temperature anomalies derived from MSU retrievals over the past decade with both weighted and pressure level monthly means from the European Centre for Medium-Range Weather Forecasting (ECMWF) showed good agreement over most of the globe. The worst agreement found was in the tropics and portions of the Southern Hemisphere, where changes introduced to the assimilation and analysis system had significant effects, e.g., apparent changes of 1-2°C throughout the troposphere. This type of intercomparison is directly relevant to the use of model output data fields over long periods of time, i.e., changes in operational data assimilation and forecast schemes need

to be well documented. In addition, the impact of such operational changes on the resulting gridded data set needs to be understood before the gridded data sets are suitable for climate change research.

With the recent advances made in forecast models, particularly the introduction of 4-D assimilation techniques, the output from these models is rapidly becoming an excellent source of data with global coverage. Comparisons with temperatures obtained from radiosonde stations in the tropics show that the ECMWF analyses have clearly improved with time. Since the observational network contains large data-sparse areas (J. Hurrell, J. Susskind) and the conventional observational record also suffers from various inconsistencies, a strong case emerges for the reanalysis of all data using a state-of-the-art assimilation system. Further, models provide computer estimates of many important parameters that are not directly observed.

## 2.4 *Measurement Uncertainties*

### 2.4.1 Sea Surface Temperature

Surface observations particularly sea surface temperatures, are prone to a large number of errors. Estimates of the noise and errors in monthly mean sea surface temperatures (K. Trenberth, J.R. Christy, J. Hurrell) are as follows:

| | |
|---|---|
| (1) Errors in individual observations (conservative estimates) | $1.00°C^2$ |
| (2) Insufficient sampling of the diurnal cycle | $0.01°C^2$ |
| 3) Insufficient sampling of within-month variance | $0.10°C^2$ |
| (4) Insufficient sampling of mean annual cycle within the month (some mid-latitude areas have mean differences from first to last day of over 3°C) | $0.28°C^2$ |
| (5) Insufficient sampling of gradients within boxes | ? |
| Total (1-4) estimated error variance for 5° grid box | $1.39°C^2$ |

Areal stratification indicates that, for a single observation to estimate the monthly anomaly in a 5° grid box (in areas with minimal temperature gradients), standard errors are about 1.0°C in the tropics and 1.2°C elsewhere. For large gradient boxes, standard errors are over 3°C. These are reduced by $(N)^{-1/2}$ where N is as small as 3 in the UKMO data set. Insufficient spatial sampling of gradients within grid boxes for a uniform gradient of 2a°C across 2° latitude would lead to an expected variance within a 2° box of (1/3) $a^2°C^2$ if well sampled. [Note that this last estimate is not included in the above total expected variance.] In comparison, channel 2 (MSU) standard errors for 2.5°C grid boxes range from less than 0.05°C in the tropics to 0.2°C over interiors of mid-latitude continents (0.1° and 0.4° for MSU 2R). For SSTs to obtain the same accuracy as the MSU 2R, a minimum of 75 observations per 5° grid box is necessary. This is now achieved only in portions of the North Atlantic and North Pacific Oceans and near the Panama Canal. For climate purposes, the measurement should be consistent throughout the period of record.

While recognizing these advantages of satellite versus surface measurements, it should to be noted that the satellite data time series is relatively short; thus, there is little option but to extract maximum possible "signal" information from available observations. However, given the problems inherent in surface observations, the analysis of trends must be treated carefully.

Attempts to compare satellite-derived temperature measurements with surface measurements have also led to investigations on exactly what is being measured by each. MSU channel 2 temperatures relate best to the 500-300 mb ECMWF temperatures (J. Hurrell). Clearly, the MSUs measure physically different quantities than surface temperatures, although on monthly time scales the vertical atmospheric structure is essentially barotropic, and correlations with all pressure levels and with the weighted ECMWF anomalies are quite high. The lower correlations in the tropics (section 2.3.4) are due in part to changes in data assimilation and forecast schemes at ECMWF, but the surface also becomes decoupled from the mid-troposphere due to trade wind inversions.

Some analyses have also compared the trends obtained from the WMO "CLIMAT" land stations (the basic network of stations used by most global temperature change studies) and other available stations. In California, for example, although the WMO stations were distributed reasonably evenly over the state, they did not represent the actual temperature trend for the state (J.R.Christy). Oddly, most WMO stations displayed warming trends above the median level of about 0.07°C for the period 1910-1989, while most other stations were below; some even had cooling trends of up to -0.15°C. The zone-of-influence assumptions in the GISS data set extended the effect of the WMO sites up to about 1200 km around each site, including neighboring oceanic areas. The results show that, for accurate long-term trend assessment, a very high density of stations is required to produce any level of confidence in the calculation.

### 2.4.2 Urban Bias

Several attempts have been made to use polar orbiting satellite sounding data to study the global bias in surface temperature records due to the urban heat-island effect (G. Johnson et al.). The magnitude of the bias was

estimated by comparing urban station data with reference temperatures (maximum and minimum) derived from TIROS operational vertical sounder (TOVS) data. Although the results for daily, clear-sky cases generally agreed with those from station-based studies, the method was not applied globally because of problems with cloudy cases (and, consequently, the inability to calculate good monthly averages). Work in progress (K. Gallo et al.) is attempting to estimate the bias using urban-rural Advanced Very High Resolution Radiometer (AVHRR)-derived vegetation index differences, urban-rural DMSP visible-channel data differences, and reference temperatures derived from ECMWF model analyses. This would then permit the determination of urban bias for any given weather station, with estimates of monthly and annual bias derived from sufficiently large samples. Satellite brightness temperatures do not correspond to actual surface temperatures because of problems in accurately estimating surface emissivity; this precludes the direct use of such measurements in estimating bias.

### 2.4.3 Diurnal Cycle Sampling Time

The satellite-measured surface skin temperature is influenced strongly by the diurnal cycle (W. Rossow). Consequently, the timing of twice-a-day satellite passes with respect to local time is important. A comparison between 500-1000 mb layer mean temperatures derived by high-resolution infrared radiation sounder (HIRS)/MSU from TIROS-N and NOAA 6 with different orbital overpass times showed a difference of 0.5°C between 2:30 am and 2:30 pm equatorial crossover times (Figure 18). Differences also exist when switching to new satellite with differing equatorial crossover local times. Further the

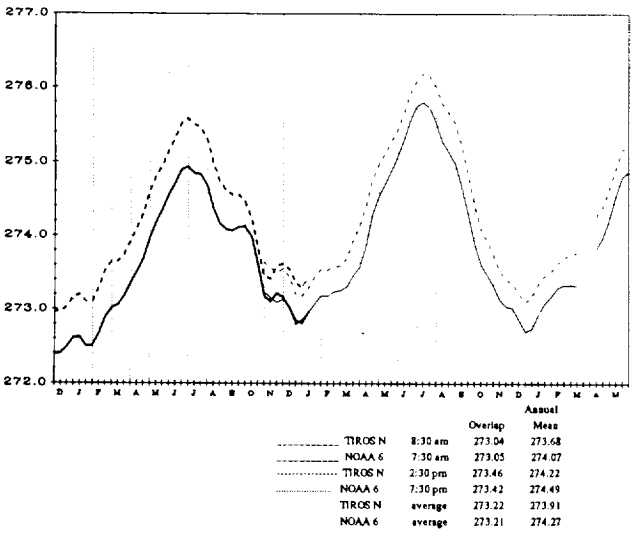


*Figure 18.–Time series of HIRS/MSU retrieved 500-1000 mb layer mean temperature from TIROS-N and NOAA 6. Source: J. Susskind, 1991.*

satellite would be sampling different geographical areas at different points on the diurnal cycle. Thus, it is important for 4-D assimilation schemes to explicitly incorporate diurnal changes and crossover between satellite observing platforms. The NASA/GLA retrieval system will re-analyze all data beginning in December 1978 as part of the EOS sponsored Pathfinder project to provide a consistent data set for research (J. Susskind). Recent analyses of Earth Radiation Budget Satellite (ERBS) data by D.L. Hartmann et al. also shows that diurnal variations in cloud type and amount in many regions are sufficient to cause substantial errors in radiation budget quantities and cloud properties estimated from observations orbit. Errors in estimated net radiation can be as large as 50 W/m$^2$ for oceanic stratus regions and for land regions, during summer.

## 2.5 *Modeling the Observed Temperature Record*

### 2.5.1 Statistical and Statistical Dynamic Models

Attempts to statistically describe, through a simplified energy-balance climate model and an autoregression model, the observed atmospheric temperature changes (K. Vinnikov) showed that 40% of the variance of the mean annual globally averaged surface air temperature anomaly (for the period 1881-1988) is related to changes in the atmospheric concentration of GHGs, 20% is due to volcanic eruptions, less than 1% is due to changes in the solar constant, and about 15% is due to the El Niño/Southern Oscillation. This empirical analysis constructs an energy-balance model of the climate system, develops a statistical analogue of the model, and estimates the statistical model's parameters by using available time series of the change in equivalent $CO^2$ (i.e., GHG) concentration, volcanic activity (Lamb's dust veil index or DVI), the ENSO index (C. Ropelewski, P.D. Jones), and temperature (J. Hansen, S. Lebedeff).

There have also been attempts to analyze the predictability problem by applying statistical processing methods to decompose the observational record to obtain model parameters and to subsequently look at, for example, the predicted response to changes in initial conditions. Such studies show that, without invoking an increasing GHG scenario, a variety of future climate evolutions are possible that have long-term decadal warming and, indeed, cooling trends (A.A. Tsonis). Similar results have been obtained by the long-term (100,000-yr) integration of simplified upwelling-diffusion climate models (T. Wigley and S.C.B. Raper), in which the model assumes a climate sensitivity of $\Delta T$ (2x GHG) = 4°C and is forced with random interannual radiative changes chosen to match observed interannual variations in global mean temperature

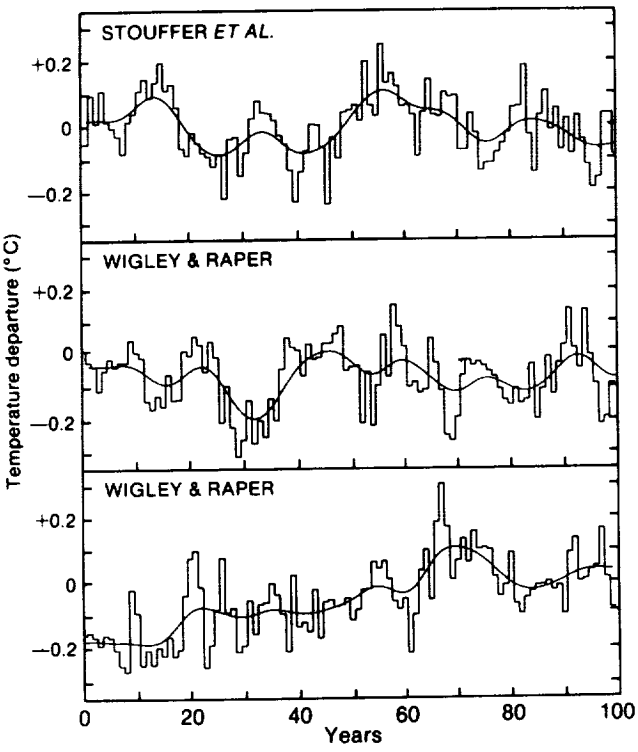


*Figure 19.–Simulated natural variability of global mean temperature. The upper panel shows results from the 100-year control run with the coupled ocean-atmosphere GCM of Stouffer et al. The lower two panels are 100-year sections from a 100,000-year simulation using an upwelling-diffusion model that has the same climate sensitivity as the model of Stouffer et al. ($\Delta T2x = 4°C$). Source: Houghton et al., IPCC, 1991, p. 247.*

(Figure 19). The low-frequency variability obtained is due to the modulating effect of oceanic thermal inertia. A significant proportion of model integrations show century time-scale trends (warming) as large as or larger than that in the bottom panel of Figure 19, indicating that a warming trend over 100 years is possible through natural variability.

In a recent study (A.H. Gordon), global and hemispheric series of surface temperature anomalies were examined in an attempt to isolate any specific features of the series structure that might contribute to the global warming of about 0.5°C that has been observed over the past 100 years. It was found that there are no significant differences between the means of the positive and negative values of the changes from one year to the next; nor do the relative frequencies of the positive and negative values differ from the frequencies that would be expected by chance with a probability near 0.5. The study concludes that the global and hemispheric temperature series are the result of a Markov process and, if interannual changes are plotted in a Cartesian frame of reference, the resulting path closely resembles the kind of random walk that occurs during a coin-tossing game.

### 2.5.2 Dynamic Models

The current, state-of-the-art generation of climate models encapsulates much of what is currently known about climate system physics. The NASA/GISS model (J. Hansen) simulation/prediction of the global temperature record displays a remarkably good correspondence with that observed (Figure 20).

Most climate models are basically sophisticated atmospheric general circulation models that interact with simplified/parameterized oceans, the cryosphere, and the land surface vegetation. A variety of interactive processes and feedbacks are incorporated, such as ice-albedo, temperature-water vapor-cloud, and cloud-radiation. Grid resolutions are typically 5° x 10° with about 10 vertical levels. Much higher resolution models are also used experimentally, but substantial supercomputer resources are required.

While simplified but sophisticated physics is invoked, parameterized, and/or modeled in all present studies, model "tuning" is dependent on information extractable from the observational record and, as available, paleo-reconstructions of prehistoric climate-forcing relationships. A simple analysis of climate fluctuations and time scales of change, along with basic "set" theory, suggests that to capture, in its entirety, the physics of change (even at a single point) may require either a near-infinite time-series of observations or a near-infinitely dimensioned model. The observational record is, in fact, relatively short (~100 years) and even somewhat ambiguous; e.g., the observed temperature change (Figure 3) showing a level shift between about 1910 and 1940 may indicate a nonergodic or nearly intransitive climate system rather than the commonly assumed linear "warming" trend (S. Unninayar). Looking at a different set of parameters, such as water vapor and clouds, a change in climatic regime was noted before and after about 1976 (M. Chahine), with mean tropical specific humidity increasing by about 10% between 1976 and 1979 and remaining stable thereafter.

The point here is to be aware of the possible pitfalls arising from analysis based on short data time series. While 100 years may appear long with respect to the human life span, and extraordinarily long compared with the human attention span, it is very short for the physics of fluctuation of many climate forcing factors and the feedback process.

A particularly important issue is "climate sensitivity" in both climate models and the physical climate system (T. Wigley). A quantifiably accurate estimate of climate sensitivity to climate forcing(s) is necessary both for the detection of climate change and enhanced GHG effects and for climate prediction. A discussion is contained in section 4.3.1.

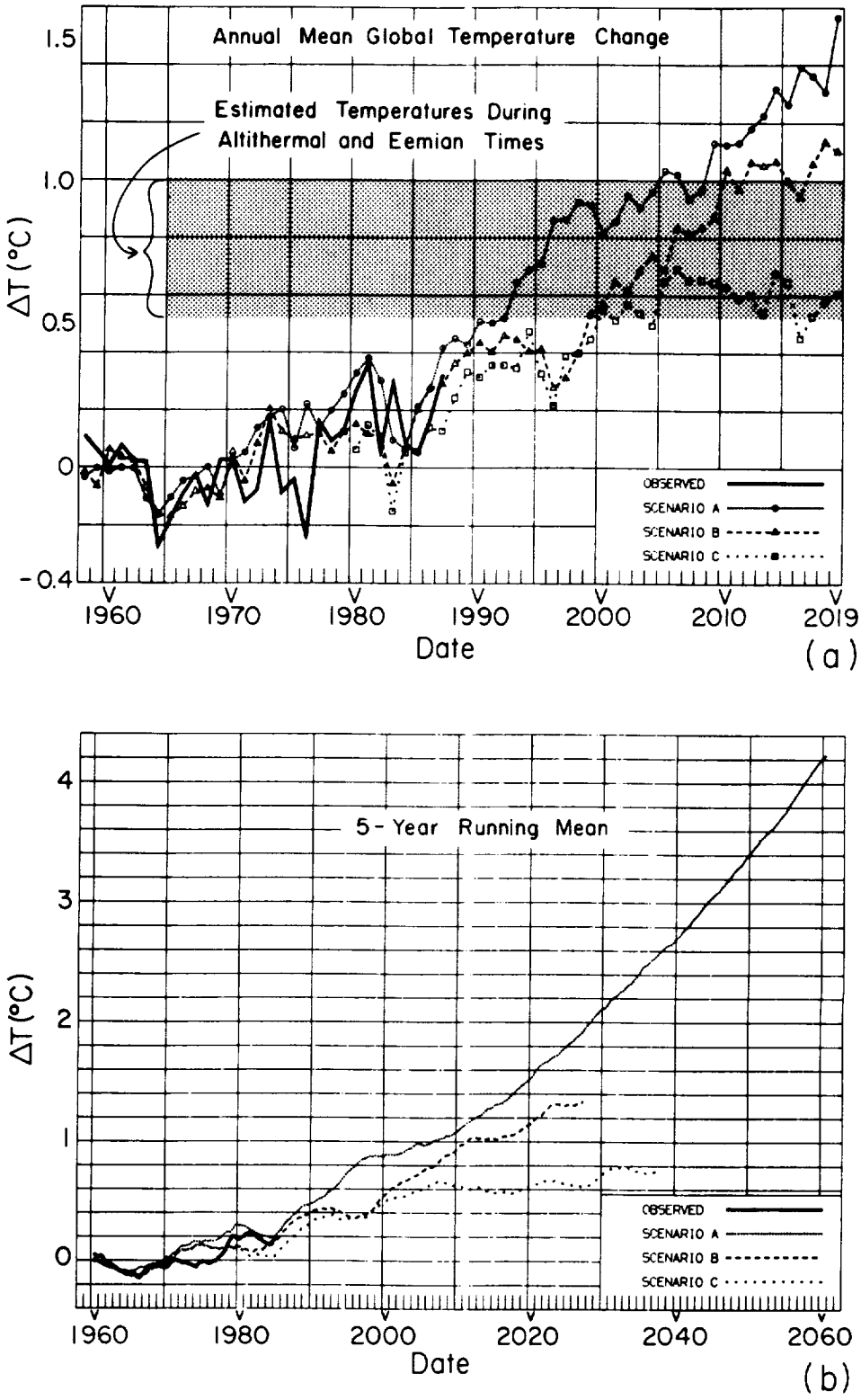


*Figure 20.–Annual mean global surface air temperature computed for scenarios A, B, and C. (a) Annual mean global temperature change, 1958-2019; (b) five-year running mean, 1960-2060. Observed data are from J. Hansen and S. Lebedeff (1987, 1988). The shaded range in part (a) is an estimate of global temperature during the peak of the current and previous interglacial periods, about 6,000 and 120,000 years before the present, respectively. The zero point for observations is the 1951-1980 mean (J. Hansen and S. Lebedeff, 1987); the zero point for the model is the control run mean. Scenaria A: Growth rate of trace gas emissions increasing at present level of about 1.5% per year; B: Decreasing trace gas growth rate such that annual increase in GHG climate forcing remains constant at present level; C: Drastically reduced trace gas growth between 1990 & 2000 such that GHG climate forcing ceases to increase after 2000. Source: J. Hansen et al., 1988.*

# 3. Climate Forcing(s) and Internal Feedback Processes

It is emphasized that all significant climate forcings must be measured or accurately computed from relevant indirect measurements to allow cause-and-effect assessments of any observed climate changes. Equally important is the role of climate feedback processes. While an accurate measure of various climate forcings would conceivably permit an evaluation of changes to the planetary (i.e., global) energy balance, climate feedbacks must be assessed accurately in order to evaluate the sensitivity of climate to forcings (J. Hansen, T. Wigley). Also, until feedback processes are rather precisely quantified and modeled, regional or subregional change (e.g., at a point) would be impossible to forecast. Ultimately, global impact is a consequence of the ensemble of regional impacts at a scale that affects agriculture, water supply, surface vegetation, etc., and, consequently, economics and populations.

Positive feedbacks amplify an initial climate change that is the result of one or more forcing factors or agents; negative feedbacks conversely would diminish it. It is currently assumed that a negative feedback cannot reverse the direction of a climate change because the feedback is driven by the climate change. Indeed, the feedback processes contained in existing climate models would not permit nonlinear, unstable amplification. However, even under the constraints of this assumption, if a negative feedback were strong enough, it could reduce the climate change to negligible proportions.

Both climate forcings and climate feedbacks need to be rather precisely quantified before an accurate assessment can be made as to whether an enhanced greenhouse effect is already the cause of the observed warming. Furthermore, the observed signal needs to be separated from possible long-term fluctuations of the climate system that are the result of internal interactive processes. Current hypothesis, supported by numerical model predictions, suggests that the global radiation budget change caused by forcings(s) such as GHGs would result in a climate change signal superimposed on top of the inherent variability of climate. Proving this hypothesis would require a continuous verification of climate model forecasts. It is not entirely clear whether the existing observational record or climate model simulations are sufficient to unambiguously attribute climate change to one or more of the known forcings or feedbacks.

## 3.1 Climate Forcing

### 3.1.1 Orbital and Solar

By far the strongest of "forcings" is the sun, whose energy influx in the form of ultraviolet and visible electromagnetic radiation (0.2 to 0.4 μm) is the driving force of weather and climate. At the top of the atmosphere the shortwave energy flux is about 1368 W/m$^2$. Because of its spherical shape, at any instant the Earth receives on average, half the incident solar flux (i.e., 684 W/m$^2$). Because of the Earth's rotation, the average radiative flux received over a day-night cycle is half of this value, i.e., about 342 W/m$^2$. Approximately a third is reflected by the atmosphere and the Earth; the rest is absorbed.

The solar energy flux is in approximate equilibrium with the energy emitted by the Earth in the form of long-wave terrestrial radiation; otherwise, the Earth would warm up or cool as a result of an imbalance in these quantities. However, small differences persisting over long periods of time could conceivably lead to climate change. [Note that, in comparison to the solar forcing of 342 W/m$^2$, the enhanced greenhouse effect is only about 2 W/m$^2$, but this is significant enough to cause climate change.] It is believed that an important cause of recurring glaciation is variations in the seasonal radiation received in the Northern Hemisphere. These variations stem from small changes in the distance of the Earth from the sun in given seasons, and slow changes in the tilt of the Earth's axis. These "Milankovitch" orbital effects appear to be correlated with the glacial-interglacial cycle, which exhibits temperature variations as great as 10°-15°C in some middle and high latitude regions of the Northern Hemisphere. On a 100-year time scale, mini-ice ages have been associated with changes in the fluctuation of the envelope of the sun-spot cycle.

To provide perspective to the magnitude of solar forcing, it is estimated that, in the past 10,000 years, the incident solar radiation at 60°N in July has decreased by about 35 W/m$^2$ (Houghton et al., IPCC, 1990); the average change in one decade is -0.035 W/m$^2$. This change is much smaller than the increased heating due to enhanced greenhouse forcing over the most recent decade, estimated at about 0.6 W/m$^2$.

Precise measurements from spacecraft show a decline in solar irradiance of 0.1% between 1979 and 1986 with a subsequent partial recovery. A 0.1% dimming represents a direct heating decrease of about 0.25 W/m$^2$. Fluctuation in reconstructed solar irradiance from 1874 to 1988 derived from the model of P. Foukal and J. Lean (1990) is shown in Figure 21a. The 11-year sunspot cycle is clear. Also evident is the approximately exponential increase in the envelope fitting irradiance maxima. Climatic effects have been attributed to the long-term decadal changes in the envelope of the 22-year sunspot cycle by J. Eddy, T. Mitchel, and others, though direct radiational effects are computed to be small. A recent comparison by Friis-Christensen and K. Lassen (1991) of sunspot cycle length and Northern Hemisphere temperature anomalies is shown in Figure 21b. The correlation is remarkably good, about

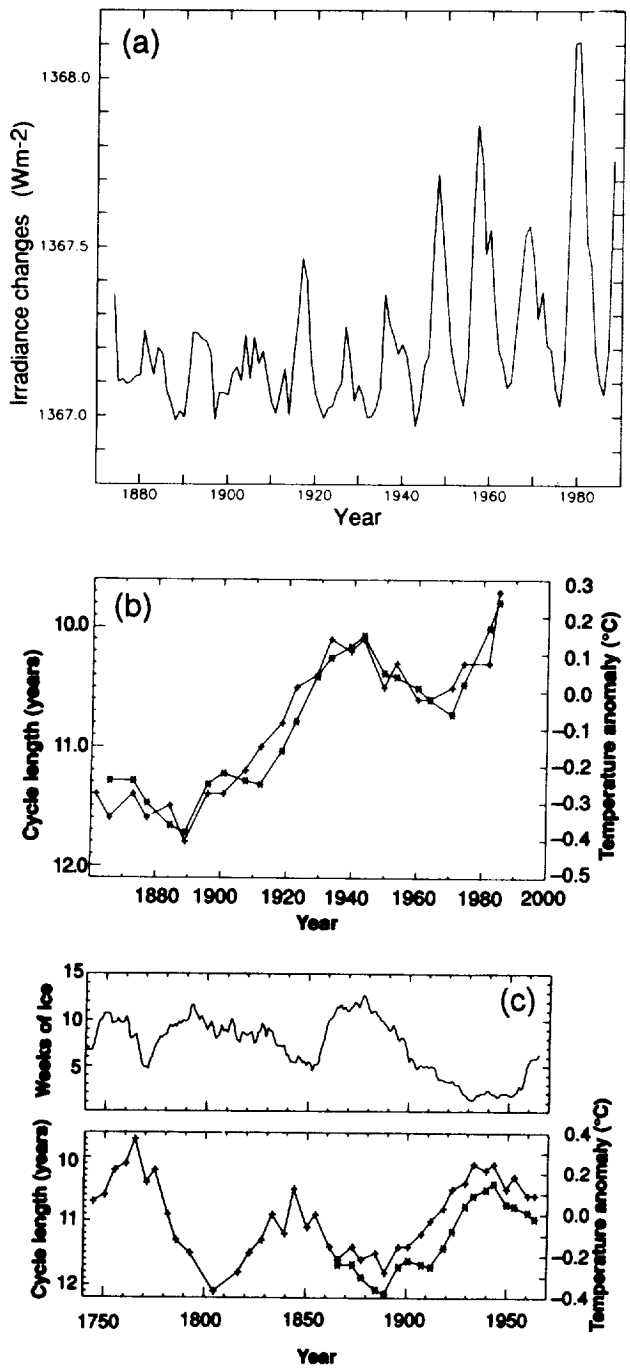


0.95. The authors suggest that this parameter based on determinations of cycle length from epochs of maximum and minimum sunspot number may be associated with a physically meaningful index of solar activity. It also removes the apparent lag of the solar activity curve relative to surface temperature as obtained from the smoothed sunspot number. Figure 21c compares the sunspot cycle length to sea-ice fluctuations around Iceland. Presently there is considerable discussion about the physics behind such a high correlation with solar activity fluctuations which were previously thought to be rather small from satellite observations. There is however some evidence that low frequency variations could be large and as yet undetected by satellites, e.g., a change of solar output of 4 $W/m^2$ between 1968 and 1978 (0.3% of the total output) has been reported by C. Frohlich (1987).

There are several other factors which contribute to climate forcing (J. Hansen) as described below.

### 3.1.2 GHGs

The primary reason for concern about increasing concentrations of GHGs is the effect on the planetary radiation balance, which could alter global surface temperatures. Climate forcing is measured by the change in the heating rate of the Earth in watts per square meter ($W/m^2$). For example, the increase in concentrations of the greenhouse gases carbon dioxide, chlorofluorocarbons, methane, and nitrous oxide since the International Geophysical year, in 1958, theoretically cause a heating change of 1.1 $W/m^2$. The accumulated increases in these greenhouse gases since the Industrial Revolution beginning in 1800, has caused a heating change of more than 2 $W/m^2$ by decreasing the infrared radiation emitted into space—an amount equivalent to increasing by 1% the solar radiation absorbed by the Earth (J. Hansen). The atmospheric abundance of the above gases have been monitored accurately over long periods, and they are relatively well mixed in the troposphere up to about 10 km. Ozone ($O_3$) in the upper troposphere and stratospheric water vapor—two very important GHGs—are, however, not measured accurately. Both need to be known to assess total GHG climate forcing.

*Figure 21a.–Reconstructed solar irradiance ($Wm^{-2}$) from 1874 to 1988 using the model of P. Foukal and J. Lean (1990). The model was calibrated using direct observations of solar irradiance from satellites between 1980 and 1988 (data from J. Lean, personal communication). Note that solar forcing is only 0.175 times the irradiance due to area and albedo effects. Source: Houghton et al., IPCC, 1990, p.62.*

*Figure 21b.–Variation of the sunspot cycle length (left-hand scale) determined as the difference between the actual smoothed sunspot extremum and the previous one. The cycle length is plotted at the central time of the actual cycle (+). The unsmoothed last values of the time series have been indicated with a different symbol (*) which represents, as in Figure 1, the Northern Hemisphere temperature anomalies. Source: E. Friis - Christiansen and K. Lassen, 1991.*

*Figure 21c.–(Top) 22-year running mean of the amount of sea ice around Iceland from 1740 to 1970 during summer months (represented by the number of weeks when ice was observed). (Bottom) Smoothed sunspot cycle lengths from 1740 to 1970 (left-hand scale) and Northern Hemisphere mean temperature (right-hand scale). Source: E. Friis - Christiansen and K. Lassen, 1991.*

### 3.1.3 Ozone

Model simulations (J. Hansen) also show that the atmospheric temperature is rather sensitive to ozone concentration changes. It is hypothesized that some, if not all, of the inconsistencies between model results for the 1980s and 1990s and observational results (e.g., J. Angell) are likely to be due to $O_3$. Because ozone absorbs ultraviolet (UV) radiation and infrared thermal radiation, a change of ozone can either increase or decrease temperature, depending on the change of the ozone profile.

When $O_3$ was removed in the upper troposphere/lower stratosphere (250-20 mb) strong cooling of the troposphere (~-1 to 4°C) was produced. When $O_3$ was removed above 10 mb, a cooling of the stratosphere (up to -80°C) resulted. Precise measurements, of $O_3$ with information on its vertical concentration distribution, is required to accurately quantify the effect of ozone changes. Uncertainties with regard to $O_3$ and tropospheric aerosols are estimated to be on the order of 1 W/m$^2$. An analysis of SAM II, SAGE I, SAGE II, and TOMS data measuring aerosol (optical depth), $O_3$, and water vapor (J. Zawodny) indicated a large (5-10%) change in $O_3$ in the 15-20 km layer.

### 3.1.4 Tropospheric Aerosols and Dust

Aerosols are increasingly seen as a direct modulator of the greenhouse effect; they interact with incoming solar radiation through scattering and absorption processes. Aerosols could modulate the greenhouse effect indirectly since they are critical as nuclei for the formation of cloud droplets, which, in turn, determine such optical properties of clouds as brightness and ability to reflect incoming solar radiation.

The dominant, tropospheric aerosols are sulfates, which form from sulfur dioxide ($SO_2$) released by the burning of coal and oil. Their overall impact would be a cooling effect due to the increased reflection of sunlight. About 25 to 50% of the aerosols in the atmosphere may be of anthropogenic origin and would correspond to a mean cooling change of between 0.5 and 1.5 W/m$^2$. Thus, the enhanced greenhouse heating due to the burning of fossil fuels could be offset by cooling due to aerosols produced by the very same anthropogenic activity. Unlike GHGs, however, sulfate aerosols are not well mixed in the atmosphere, and therefore their impact on climate is likely to be different from that of GHGs. The actual tropospheric aerosol loading is very poorly measured.

Lately, interest has also focused on dimethyl sulfide (DMS), released at the ocean surface to the atmosphere by ocean biological processes (phytoplankton?). DMS, an efficient condensation nucleus, is speculated to be capable of modifying cloud microphysical processes and, thereby, climate. The atmospheric concentration changes in DMS is relatively unknown. A variety of organic aerosols also exist in the troposphere; however, these are assumed to be in equilibrium and not increasing, as sulfates are.

Large dust clouds originating in the desert regions of the world are likely to have a cooling effect similar to that of aerosols, through the reflection of solar radiation. Satellite pictures also show (Figure 22) dust clouds originating in the Sahara region and stretching across the Atlantic to Amazonia. The causes of fluctuations in this dust cloud are unknown, but they are hypothesized to be linked to fluctuations in the African and Indian monsoon. It is speculated that the Amazonian forest is mineralized by the fall out of this Saharan dust, and, on a long-term basis, forest growth cycles fluctuate with the availability of minerals from across the Atlantic.

### 3.1.5 Stratospheric Aerosols

The stratosphere is relatively clean, since the tropopause behaves as a cap over the troposphere, containing most of the atmospheric aerosols, dust, etc. Stratospheric aerosols are primarily the result of episodic injections of $SO_2$ and dust high into the atmosphere by large volcanoes and of meteoritic sources over the longterm; global data are lacking. Model results indicate a direct cooling effect of up to 5 years and longer (>10 years) for the relaxation of secondary circulation and feedback processes (A. Robock). During this period, the aerosol cooling effect would more than offset the enhanced GHG effect. Thus, any change in the frequency of large volcanic eruptions could have a major impact on climate.

### 3.1.6 Surface Albedo

Changes in the Earth's surface reflectivity (albedo) due to large-scale deforestation or desertification and urbanization may also produce significant climate forcings. Although they are not accurately known, (estimates vary by as much as a factor of 2 or 3), deforestation and desertification rates are increasing with population pressure. Operational meteorological satellites that measure surface reflectivity are not calibrated well enough to provide long-term data, but in several countries major portions of tropical forests have disappeared. Deforestation also continues in the mid-latitude countries.

### 3.1.7 Comparative Estimates of Climate Forcings

Radiative forcing of the climate system can be specified by the global surface air temperature change ($\Delta T_o$) that would be required to maintain the energy balance with space if no climate feedbacks occurred (J. Hansen et al.). The estimates in Figure 23 are based on calculations with a one-dimensional radiative-convective (RC) model (A. Lacis et al.). The absolute accuracy of the forcings are of the order of 10% because of the uncertainties in the absorption

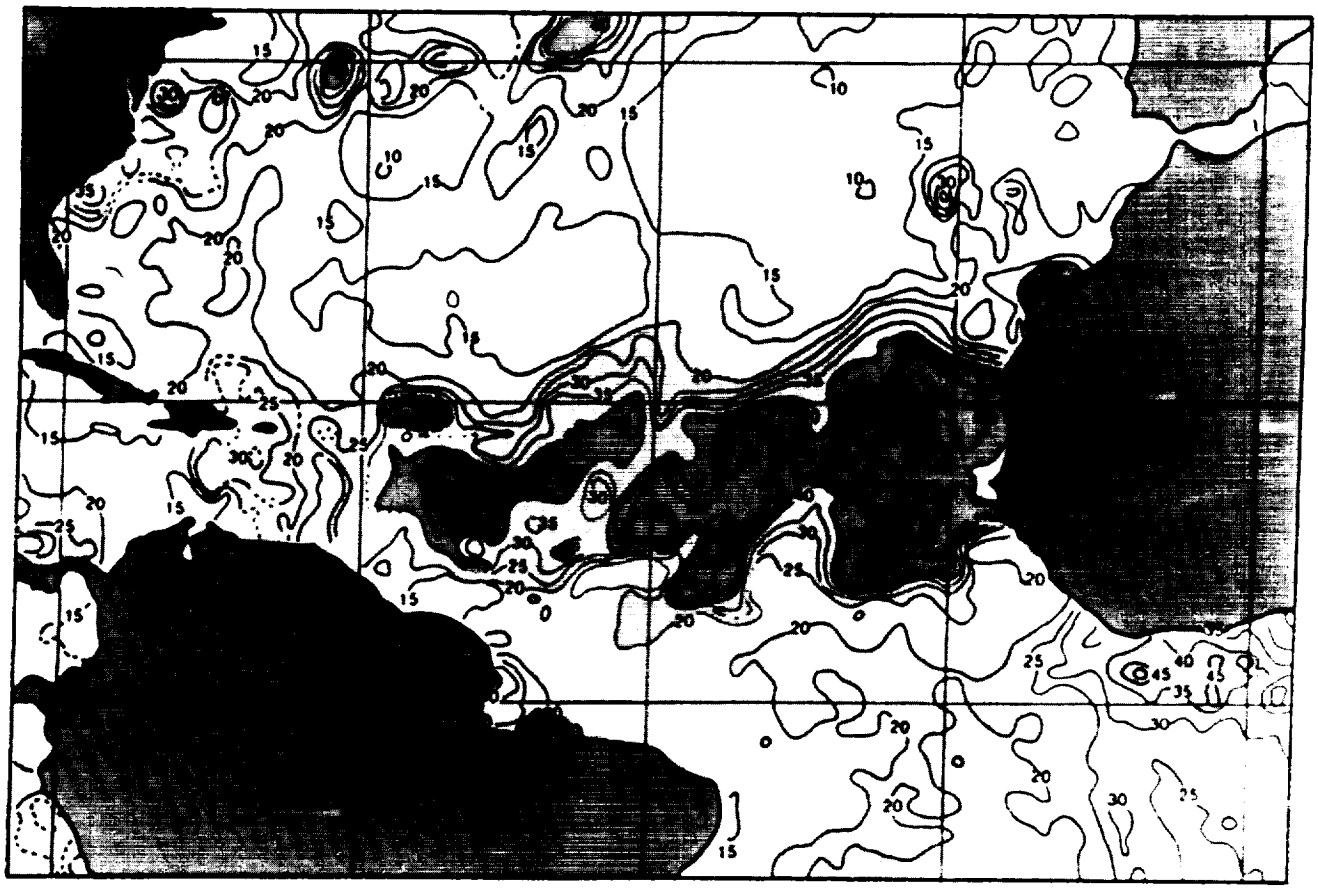

*Figure 22.–Aerosol optical depth (X100) on 18-25 June 1987, estimated from the visible channel of AVHRR. Note Sahara dust off Africa and sulfate haze off the US east coast. Source: L. Stowe, NOAA.*

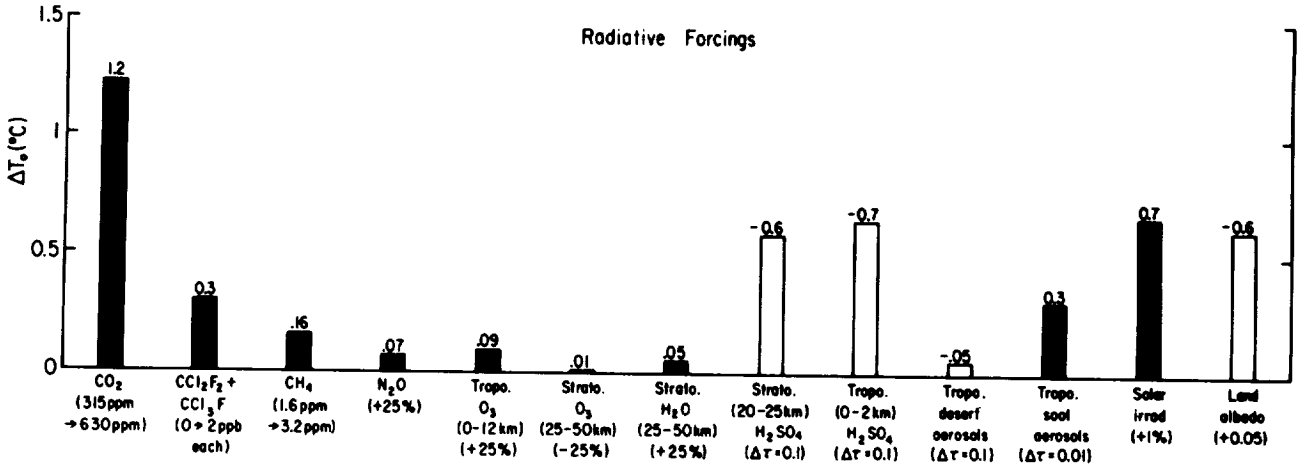


*Figure 23.–Global mean radiative forcing of the climate system for arbitrary changes of radiative parameters. Here $\Delta T_0$ is the temperature change at equilibrium ($t \rightarrow \infty$) computed with a one-dimensional RC model for the specified change in radiative forcing parameter, with no climate feedbacks included; $\Delta T_0$ must be multiplied by a feedback factor f to get the equilibrium surface temperature change including feedback effects (paper 2). Tropospheric aerosols are all placed in the lower 2 km of the atmosphere; the desert aerosols have an effective radius of $r_{eff} \approx 2$ μm and a single scattering albedo $w \approx 0.8$ at wavelength $l = 550$ nm, while the soot aerosols have $r_{eff} \approx 1$ μm and $w \approx 0.5$. The land albedo change of 0.05 is implemented via a change of 0.015 in the surface albedo, corresponding to 30% land cover. Source: J. Hansen et al., 1988.*

coefficients and approximations in the one-dimensional calculations. Figure 24 summarizes the estimated decadal increments to global greenhouse forcing. The forcings shown by dotted lines in the figure are speculative; their effect was included in Scenario A but was excluded in Scenarios B and C. The $CH_4$ forcing in the 1980s represents a 1.5% per year growth rate; recent data suggest that a 1.1% per year growth rate is probably more realistic.

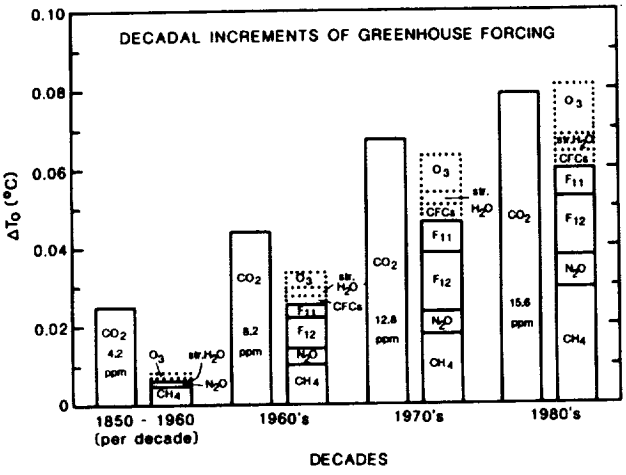


*Figure 24.–Estimated decadal additions to global mean greenhouse forcing of the climate system. The value of $\Delta T_0$ is defined in the caption of Figure 23. Forcings shown by dotted lines are highly speculative. Source: J. Hansen et al., 1988.*

## 3.2 *Climate Feedbacks*

The physical climate system is a nonlinear interactive system, and final equilibrium or average state is the result of a balance between various forces. Most climate forcings are directly related to radiational aspects, as discussed earlier. Changes in one or more forcings will lead to a re-adjustment of internal processes of the climate system until a new quasi-equilibrium state is reached. These readjustment processes or feedbacks need to be known before the effect of any forcing changes on surface temperature can be determined. The climate feedbacks treated in the following sections are considered to be very important.

### 3.2.1 Clouds

Clouds are simultaneously strong downward infrared radiators and shortwave solar radiation reflectors. How clouds are likely to change with increased greenhouse warming is essentially unknown. Higher surface temperature is expected to cause increased evaporation, which could increase cloud cover and, thereby, cooling—a negative feedback. But most climate models suggest that increased evaporation would lead to more vigorous moist convection and thunderstorms over a very small portion of the Earth's surface and increased drying by subsidence over the rest of the planet ,resulting in reduced overall cloud cover—a positive feedback. Other cloud feedback effects are possible and currently unknown as to the sign of their changes, e.g., changes in cloud microphysics such as size and phase of cloud droplet which affect reflection and

Table 4.—Estimates of the mean annual, global (except as otherwise indicated) effect of clouds on the net downward flux of total radiation energy at the top of the atmosphere (C), longwave ($C_{LW}$), and shortwave ($C_{SW}$) components in $W/m^2$. These estimates of cloud forcing are based on climatology with simple models (CLIM), satellite-based observations (SAT), and general circulation models (MOD).

| Basis | Investigation | Source | $C_{LW}$ | $C_{SW}$ | $\lvert C_{SW}/C_{LW} \rvert$ | C |
|---|---|---|---|---|---|---|
| CLIM | Schneider (1972) | Simple Model | 37.5 | -65 | 1.7 | -27.5 |
| | Cess (1976) | Empirical | 45.5 | -44.5 | 1.0 | +1 |
| SAT | Ohring et al. (1981) | NOAA AVHRR 0° - 60°N | 17.5 | -53 | 3.0 | -35.5 |
| | Ellis (1978) | Nimbus 3 MRIR 65°S - 65°N | 22 | -42 | 1.9 | -20 |
| | Ramanathan et al. (1989) | ERBE | 31 | -48 | 1.5 | -17 |
| | Ardanuy et al. (1991) | Nimbus 7 ERBE | 24 | -51 | 2.1 | -27 |
| MOD | Cess and Potter (1987) | Range of 6 GCMs January conditions | 23 to 55 | -45 to -74 | 1.0 to 2.0 | -2 to -34 |

absorption of solar and terrestrial radiation. Observing and modeling cloud feedback is critical to climate change detection and prediction because the shortwave and longwave components of cloud-radiative forcing are about ten times as large as those for a $CO_2$ doubling (V. Ramanathan et al.). ERBE data analysis, for example, shows that the global shortwave cloud forcing is about -48 $W/m^2$ due to the enhancement of planetary albedo, while the longwave cloud forcing is about 31 $W/m^2$ as a result of the greenhouse effect of clouds.

The global mean effect of clouds is therefore to cool the climate system by about -17 $W/m^2$. Some studies (P. Ardanuy) suggest that this could be as much as 27 $W/m^2$. A summary (A. Arking) of the mean annual global effect of clouds forcing, obtained from observational and modeling studies is shown in Table 4.

It should be noted that even an accurate description of net cloud forcing does not particularly address the issue of GHG-induced climate change or cloud-climate feedback. Another quantity, cloud sensitivity which represents the differential response of Earth radiation budget parameters and other variables of the climate system to changes in cloud cover parameters about their mean distribution, is a critical factor in determining the cloud feedback in climate simultations.

### 3.2.2 Water Vapor

In warm climate regimes such as the present and that of a 2x GHG scenario, the thermodynamics of $H_2O$ have a dominant influence in the radiative feedbacks (V. Ramanathan and W. Collins). The saturation humidity varies exponentially on temperature; as a result, a 1% increase in temperature from 300K, for example, increases saturation humidity by 17%. Supporting satellite observations reveal that the total atmospheric water vapor increases by ~17% per 1% increase in sea surface temperature. The latent energy of a parcel of air also grows by 17% per 1% increment in temperature (T). The surface emission increases at a rate close to 6.1 $W/m^2$ per degree K at around T = 300K, but the emitted energy cannot escape to space; instead it is trapped in the atmosphere. And the trapping increases faster than the surface emission as temperatures increase above ~300K. That is, in the tropics, the warmer tropical ocean/atmosphere system is not governed by the the fundamental negative feedback between temperature and infrared emission that expels excess heat by radiating to space.

This tropical "super-greenhouse effect" is caused by a combination of several mutually reinforcing factors, including increases in total column $H_2O$, $H_2O$ continuum absorption that scales quadratically with $H_2O$ partial pressure, higher middle- and upper-troposphere $H_2O$ concentrations; and changes in the lapse rate. When T > 300K, a parcel of moist air near the surface has sufficient latent energy that, if it is forcibly lifted until it reaches saturation, it can overcome the gravitational potential energy and rise to the upper troposphere as a cumulonimbus cloud. The system is potentially unstable unless another negative feedback exists to stabilize it. The warming continues until the clouds become thick enough to shield the ocean from solar radiation and arrest further warming. Most of this shielding is by highly reflective cirrus clouds that act like a thermostat. It is thought that the regulatory effect of these cirrus clouds may limit sea surface temperatures to less than 305K.

In the lower atmosphere, water vapor, a major if not dominant greenhouse gas, is generally expected to cause a positive climate feedback, because warmer air can hold more water vapor. Models explicitly include such a positive feedback. However, several processes within the large-scale atmospheric circulation and the injection of water by thunderstorms influence the atmospheric humidity profile in different ways. Thus the magnitude of the water vapor feedback is uncertain. Significantly better observations are also required, particularly of stratospheric water vapor. Further, water vapor changes associated with observed climate changes must be determined so that the correlation between the two can be quantified.

### 3.2.3 Ocean

The ocean can be both a climate forcing and a climate feedback component or element of the climate system. The ocean can serve as a forcing element by storing large amounts of heat in subsurface and deep ocean layers, over thousands of years, and releasing this stored heat at a later time. Temperature and salinity distributions and the thermohaline circulation, which determines horizontal and vertical heat transport (and rate), are therefore important ocean features that need to be better understood. [In 1715, Halley recommended to the Royal Society that experiments be conducted to measure the degree of saltiness of the ocean.] On shorter time scales (10-100 years), the ocean is treated as a feedback loop in climate models, particularly when addressing the response of the system to a change in climate forcing such as that caused by GHGs.

Most 2x GHG climate model simulations are obtained as an equilibrium response to a prescribed abrupt change in radiative forcing. The treatment of the oceans is relatively primitive compared with that of the atmosphere. It is important, however, that the ocean feedback, be much better quantified when GHGs are changing (increasing) continuously. The thermal holding capacity of the oceans would delay and effectively reduce the observed climatic response, because part of the heat would be stored in the stably stratified layers of the upper ocean and be only realized 100 or more years later. Detecting the enhanced greenhouse effect is thus rendered more complicated

because the signal is masked by the ocean response. Further, even without any GHG forcing, the interactions between the atmosphere and the ocean can cause interannual and interdecadal fluctuations. To properly estimate ocean feedback and ocean-atmosphere interaction, coupled atmosphere-ocean general circulation models (GCMs) are essential. Indeed, there exist complex high-resolution eddy-resolving ocean GCMs, but very few coupled numerical experiments have been conducted with them because of their prohibitively large demand on supercomputer resources. The performance of complex ocean models and coupled GCMs need to be verified through observational tracer experiments before their predictions can be reliably accepted with reliance.

In order to properly simulate and derive the ocean response, accurate boundary conditions at the ocean surface involving wind stress, net heat flux and net freshwater flux must be obtained from atmospheric and land surface/biosphere models. The latter quantities have large uncertainties associated with their treatment in atmospheric models. In recent years, several "transient" and time-dependent coupled model experiments have been run with a simplified ocean, in order to more realistically track the climate change predicted by the enhanced GHG effect with ocean feedback included.

### 3.2.4 Sea Ice

Sea ice freezes at approximately -2°C, insulates the atmosphere from the water below, and limits the rate at which the ocean loses energy. However, ice reflects much of the visible radiation that impinges on it and thus also limits the rate at which the ocean gains energy. The area-averaged heat flux from the ocean to the atmosphere is often dominated by the flux through open water "leads" (a small proportion of the sea ice field). These openings are determined by a combination of surface winds and the underlying ocean circulation.

Generally, increased temperature would tend to melt ice and result in increased absorption of solar energy by the ocean, which is darker than ice—a positive feedback. However, a decrease in sea ice would also lead to larger heat fluxes from the ocean to the atmosphere, which would tend to decreased ocean temperature—a negative feedback. Other effects must also be considered, such as the interaction between the greenhouse effect, the thermohaline circulation, and sea ice. In a warmer climate, there would be a thermal expansion of sea water. But the thermal expansion coefficient of sea water also increases with temperature; hence, smaller meridional temperature gradients do not necessarily mean smaller meridional density gradients. Owing to this effect, the intensity of the thermohaline circulation remains nearly constant over a wide range of warm climates (S. Manabe and K. Bryan).

If $CO_2$ is reduced to half of current concentrations, however, the results are dramatically different—the sea surface temperature is held at the freezing point down to 45° latitude because of the formation of sea ice, and the thermohaline circulation is weak and confined to the region between the ice edge and the equator. The poleward heat transport by the ocean is significantly lessened, as is the upward oceanic heat flux over the region covered by the sea ice. Such a reduction causes an intense cooling limited to the very stable surface layer of the atmosphere, inducing a further extension of sea ice with high albedo.

Such a positive feedback process between climate sea ice and the thermohaline circulation is thought to have induced the cold climates of past ice ages. Thus the interaction among the atmosphere, the ocean, and sea ice, the hydrologic cycle, and the sensitivity of sea ice to climate change need to be observed and quantified.

### 3.2.5 Snow

Global climate change could affect regional snow and vegetation cover, particularly when the effects of temperature and precipitation changes are considered together. In turn, changes in land surface characteristics would alter the exchange of energy, water, and trace gases with the atmosphere. Recent experiments using the NASA/GISS 3-D GCM (J. Cohen and D. Rind) indicate that the snow-climate feedback may act counter intuitively, in that increased snow cover does not necessarily cause reduced surface heating because of the higher (than bare soil) albedo of snow.

To fully comprehend the interaction between snow cover and climate and the effects of snow cover on land surface temperature and the energy balance, the influence of snow cover on all the diabatic heating terms must be taken into account. The GISS/GCM experiment suggests that there is a negative feedback built into the interaction between snow cover and climate through energy balance considerations. The energy terms can be divided into two groups according to the relationship between the individual energy term and surface temperature. The first group of energy terms is directly influenced by the physical properties of snow cover, its high albedo and its large latent heat of melting. These properties of snow cover contribute a negative gain of energy to the net heating, which would cause a significant cooling in the surface temperature; they are referred to as the "action" energy terms because they act directly on the surface temperature. The second group of energy terms is indirectly affected by snow cover; they consist of emitted longwave radiation and sensible and latent heat flux. Since they are not altered by the physical properties of snow cover but rather by the impact of snow cover on the environment, they are referred to as "reaction" terms.

The vertical transfer of energy and mass in the atmosphere is dependent on the vertical temperature profile. The increased stability caused by the cooling quickly suppresses the flux of sensible and latent heat away from the surface. The gain in the net heating is large enough to reverse the negative heating trend at the surface; instead, an overall positive heating term (not including snow melt) is produced for the remainder of the time that an anomalous snow cover remains—a negative feedback. Further modeling, observational, and empirical studies are probably required to confirm the above findings.

### 3.2.6 Vegetation

Vegetation changes caused by a climate change would affect the hydrologic cycle (through changes in evapotranspiration) and surface boundary layer convergence (through altering surface roughness). Vegetation also interacts directly with atmospheric $CO_2$, and the effect of $CO_2$ enhancement on photosynthetic productivity now appears to be as important as the greenhouse effect due to increasing concentrations of anthropogenically injected atmospheric $CO_2$ (S. Idso). In a controlled experiment with sour orange trees over a two-year period, the $CO_2$-enriched trees in an atmosphere of about 680 ppmv contained 2.8 times more above-ground and root-sequestered carbon than did the trees grown in ambient air. The annual cycle of atmospheric $CO_2$ shows sharp changes in response to the vegetation, as would be expected, but the peaks and troughs are becoming more enhanced each year. This is attributed to a more robust global plant life due to the aerial "fertilization effect" of the rising $CO_2$ content of the Earth's atmosphere. In a 2x $CO_2$ atmosphere, i.e., with an increase in $CO_2$ of approximately 300 ppmv mean productivity of the global forests is expected to increase by 182%. This number translates into an increase in the rate of carbon sequestering by 2.8 times, leaading to a reduction in atmospheric $CO_2$. That is, the vegetation-$CO_2$-climate feedback is negative if all other factors remain the same and deforestation does not decimate the planetary biomass.

# 4. Detection of Climate Change and Enhanced GHG Effects

## 4.1 Cause or Source of the Global Signal

Uncertainties no doubt exist in the currently observed decadal and longer trends in temperature over approximately the past 100 years. So far, most analyses use monthly mean data from stations that measure from eight observations per day (most surface climate stations) to one or two per day (radiosonde and upper air stations). Monthly average values are internationally exchanged. Over oceanic areas, observations are binned into Marsden squares or grid boxes and averaged. Thus, a single monthly value is constructed from several different ship measurements that differ in instrumentation, time, and space. Nevertheless, the general consensus is that the observed temperature trend of about 0.4° C per 100 years is real.

Few analyses have been carried out for other parameters, such as precipitation and climate variability. Even monthly analysis is somewhat recent; the most popular representation of climate change is the annual mean temperature record. The analysis of P.D. Jones (Figures 9 and 10) comparing the first half of the century (1901-1945) with the second (1946-1990) indicates that the character of the signal contributing to the global average temperature signal is rather different for these two periods. Analysis for the last 10 years (1981-1990) (Figure 25), categorized as the warmest decade in the observational record, appears to indicate that the largest contribution to the global warming signal was from the tropics. The middle and higher latitudes displayed substantial regional and seasonal variation with areas of strong (up to 1.0°C) warming and cooling, which possibly affected regional weather but had little impact on the hemispheric or global average.

It is tempting to speculate that the 1981-1990 decadal warming was dominated by the ENSO. Other signs of regime shifts have been noted earlier. The precise cause of the global warming signal is thus unclear. If it were indeed a GHG effect, then the manner in which radiative climate forcing is expressed is clearly not a simple globally uniform increase in surface temperature. Rather, the actual temperature is a consequence of a combination of forcing, feedback, and other internal dynamic and thermodynamic adjustments.

## 4.2 Detecting Climate Change

In examining the subject of climate change several points emerge. Detecting climate change and determining its precise cause presents subtle problems. So far, the thrust of analysis has been driven by the enhanced greenhouse effect and its consequent surface warming, postulated by Arrenhius in 1896 with approximately the same range of predicted global temperature change as now.

The temperature change signal is defined as an average of the deviation at each point, be it station or ocean grid box. There are relatively few analyses of regional change or comparisons of interdecadal variation. Some analyses indicate

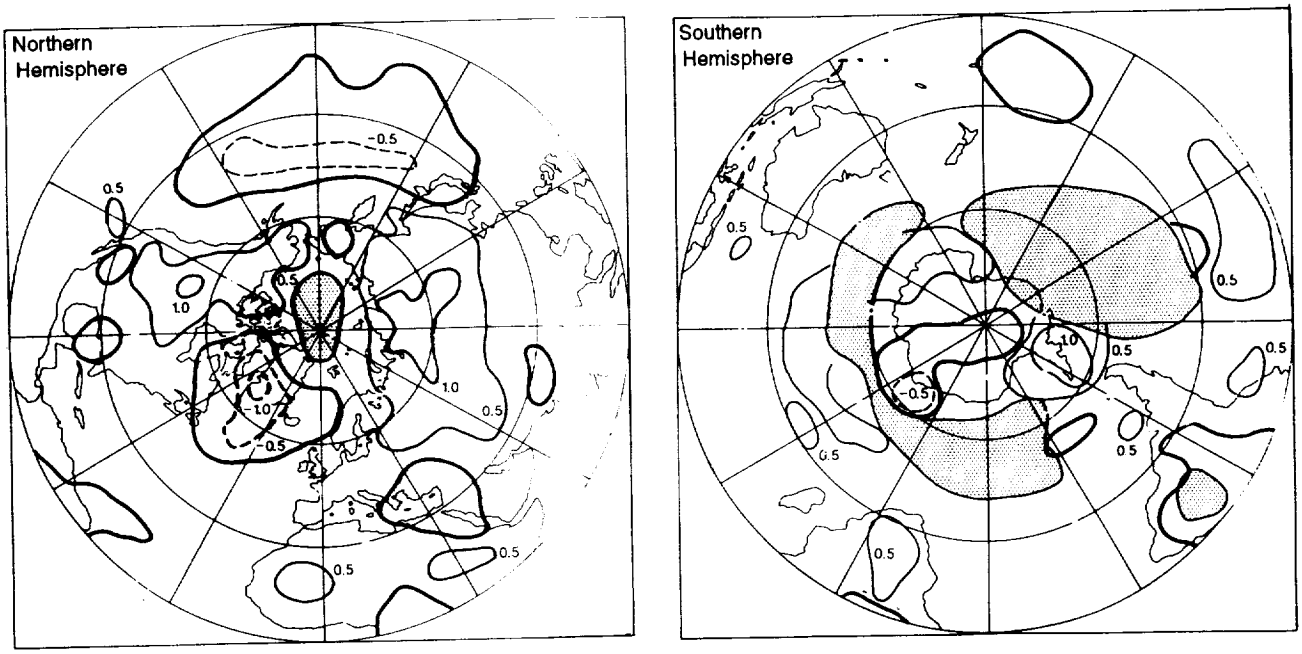


*Figure 25.–Annual mean temperature anomalies for the period 1981-1990. The basic data set used is described in Figure 3 (i.e., land air and SST from CRU and UKMO, respectively). Source: P. D. Jones, 1991.*

little to no regional long-term trend (K. Vinnikov) in high latitudes in contradiction to model predictions; the NOAA/NCDC data also show little regional (USA) change. Perhaps the regions selected were too large, or geopolitical boundaries may not provide the best delineation of climatic or eco-climate zones.

Concurrently with temperature, changes in precipitation, winds, and surface cover and state must be analyzed, as well as the statistical stability or variability of the weather systems and their characteristics. This requires daily data. Space-based observations show great promise but, with few exceptions, they have inherent problems with time continuity, long-term stability (both sensor and algorithms), and calibration.

Since the existing observational record is short, the extraction of meaningful information, requires the use of multiple data sets and data types to at least partly compensate for deficiencies in any one measuring system, measurement type, and the length of the time series.

## *4.3 Detection of the Enhanced Greenhouse Gas Effect*

To unambiguously detect an enhanced greenhouse gas effect (i.e., considering only the rapidly increasing anthropogenically injected radiatively active trace gases such as $CO_2$, $CH_4$, $N_2O$, and CFCs), an accurate quantification is required of all other external forcings, internal variability and feedbacks, and other man-made effects (e.g., albedo changes). That is, it is necessary to know which portion of the warming signal is attributable to the GHG effect and which to other competing causes. This is apparently not possible, unambiguously, at the present time. However, the common assumption is that the GHG signal will soon emerge out of the range of uncertainty, given the exponential increase in atmospheric concentration of GHGs. Currently, speculation abounds as to whether the planet is already seeing enhanced GHG effects.

Several novel approaches have emerged recently to address this issue of GHG effect and to explain the observed temperature record by using climate models (J. Hansen et al.), statistical techniques (K. Vinnikov), and combinations of these (T. Wigley). Factors leading to the $\Delta T_{2x}$ GHG uncertainty that have been discussed earlier are:

- Factors of model structure or parameters such as ocean heat capacity and ocean heat penetration.
- Climate sensitivity factors i.e., the temperature sensitivity of the physical climate systems to changes in various forcings and feedbacks.
- Natural variability of factors other than GHGs external forcings with uncertain histories; active internal variability (unknown history), passive internal variability (unknowable history but may be statistically tractable).
- Other manmade effects such as albedo changes (currently considered minor on a global scale but could lead to regional climate change), $SO_2$ emissions and sulfate aerosol effects, ozone.
- Data factors, i.e., 0.1°C uncertainty in the global mean temperature change.

The net effect of these uncertainties is that the observed warming over the past 100 years cannot yet be attributed to a GHG effect. Despite what some might term a rather nasty setback in our understanding current science displays an array of modeling exercises and newly developed model-data fingerprint techniques to make the GHG effect plausible, even if it is modulated for 2 - 7 or more years at a time on account of ENSO (warming effect), volcanic eruptions (cooling effect), etc.

### 4.3.1 Estimating Climate Sensitivity

The basic method for estimating climate sensitivity (T. Wigley) is as follows:

- Run climate models with observed GHG forcing to simulate global mean temperature changes for various $\Delta T_{2x}$ values;
- Choose a $\Delta T_{2x}$ value that gives the best fit between model and observations;
- Repeat the above allowing for model, data, and natural variability uncertainties;
- Obtain, as a result, a range of possible $\Delta T_{2x}$ values.

The conclusions obtained from the above exercise are encapsulated in Figure 26, which shows the observed vs. modeled temperature changes with a $\Delta T_{2x}$ of 4.0°C, together with the response for other $\Delta T_{2x}$ values. Figure 27 shows the comparison with ENSO factored out (1990 is included) and a best fit $\Delta T_{2x}$ value of 1.43°C. Indeed the modeled change fits the observational record with decadal variability superimposed.

The NASA/GISS climate model has a global mean surface air temperature equilibrium sensitivity of 4.2°C for a doubled $CO_2$ (J. Hansen; other GCMs yield equilibrium sensitivities of 2.5°C to 5.5°C. Reviews by the National Academy of Sciences recommend the range of 1.5°C to 4.5°C, while R. Dickinson (NCAR) recommended 1.5°C to 5.5°C. Extraction of empirical information on climate sensitivity will

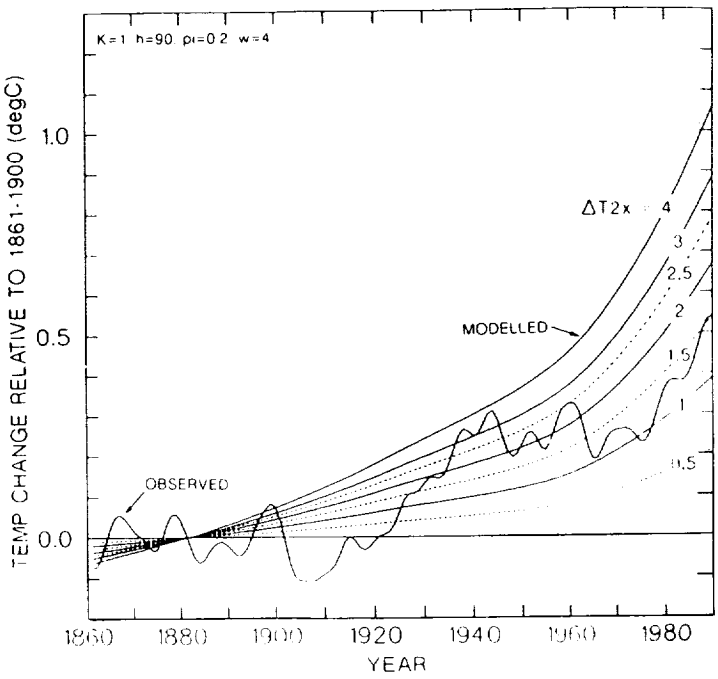


*Figure 26.–Comparison of observed global mean temperature changes with modeled changes due to GHG forcing only. Observed data, from our own data set have had ENSO effects removed, have been smoothed with a 10-year Gaussian filter, and use 1861-1900 as a reference period. Modeled changes use the parameters shown at the top of the figure and span $\Delta T_{2x}$ values from 0.5 to 4.0°C. The least-squares best fit for $\Delta T_{2x}$ = 1.4°C. Source: T. Wigley, 1991.*

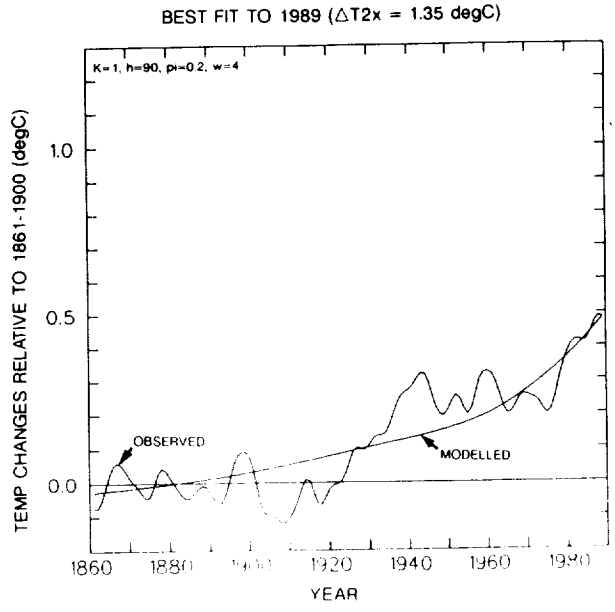


*Figure 27.–Data as in Figure 26, with ENSO effects removed and 1980 included. The least-squares best fit is for $\Delta T_{2x}$ = 1.43. Source: T. Wigley, 1991.*

require observations to reduce the uncertainties related to other (than GHG) forcings and key climate processes such as the rate of heat storage in the ocean. It was also recognized that paleoclimatic evidence would have to be used, extensively, in order to resolve the issue of climate sensitivity, since the available instrumental observational record being too short.

### 4.3.2 Temperature Fingerprint Approach

The basic temperature fingerprint concept (T.Wigley) refers to a multivariate (not multivariable) analysis of temperature change in which the changes simulated by climate models at each grid point (the grid field covering the global surface) are compared with the observational record where data are available. The model-produced change is defined (in this analysis) as the signal and a pattern correlation analysis is carried out between the model grid field and areas that have observations in an observational grid field.

Several models (OSU, GFDL, UKMO, LLNL, and GISS) were used to substantiate the validity of the GHG signals; the first four were equilibrium response experiments and the last (GISS) was a transient response experiment. Table 5 compares the signal from various models. Spatial correlation patterns were calculated using both the raw changes (i.e., nonnormalized) and the normalized patterns over regions of observed data available for the period 1900-1939. Table 6 compares the model vs. observed normalized pattern

TABLE 5.—Model-to-model spatial pattern correlations in annual mean surface for regions of observed data available for 1900-39, temperature calculated using both the raw (i.e., nonnormalized) changes and the normalized patterns (in parentheses; normalization is by the observed local variance; results were interpolated from the different model horizontal resolutions to a standard 5° x 5° latitude/longitude grid)

| Model | OSU | LLNL | GFDL | GISS |
|---|---|---|---|---|
| UKMO | 0.71 (0.89) | 0.72 (0.90) | 0.79 (0.93) | 0.63 (0.83) |
| OSU | 1.00 (1.00) | 0.75 (0.94) | 0.77 (0.90) | 0.44 (0.85) |
| LLNL | | 1.00 (1.00) | 0.79 (0.92) | 0.59 (0.84) |
| GFDL | | 1.00 (1.00) | 0.64 (0.81) | |
| GISS | | | | 1.00 (1.00) |

TABLE 6.—Trend analysis for time series of model vs. observed normalized pattern correlations for five models, calculated for 71 overlapping decades relative to the reference decade 1900-09 and expressed as results for the full grid-point fields and for the zonal means (in parentheses); trends are expressed as the trend/year x 71

| | Trends | | | |
|---|---|---|---|---|
| Model | NORM 1 | NORM 2 | NORM 3 | NORM 4 |
| OSU | 0.478 (1.238) | 0.604 (1.495) | 0.700 (1.569) | 0.305 (0.654) |
| LLNL | 0.475 (1.119) | 0.586 (1.382) | 0.640 (1.408) | 0.276 (0.826) |
| UKMO | 0.415 (1.267) | 0.510 (1.518) | 0.584 (1.431) | 0.327 (1.028) |
| GISS | 0.493 (1.097) | 0.618 (1.348) | 0.697 (1.487) | 0.123 (0.406) |
| GFDL | 0.380 (0.994) | 0.462 (1.359) | 0.589 (1.318) | 0.097 (0.646) |

correlations, normalized in four different ways. When the comparison was done with nonnormalized data (Figure 28) no trend was discernible, but a definite trend emerged with normalized data (Figure 29).

The results of the fingerprint exercise may be viewed as follows (Wigley):

| | |
|---|---|
| (1) Have we detected an enhanced GHG effect signal? | Yes |
| (2) Is the signal detected unique to the enhanced GHG effect? | No |
| (3) Are the results an artifact of the method used? | Probably not |
| (4) Is there any other possible internal or external agent that could cause a steady R(t) trend? | Unlikely, but not impossible |
| (5) Can we improve on this? | Doubtful |

Items 1 and 2 appear at first to be contradictory. In regard to item 1, since the GHG effect signal is defined as the temperature change signal produced by climate models, specifically that forced by GHG climate forcing, the pattern correlation analysis indicated that the signal was detected.

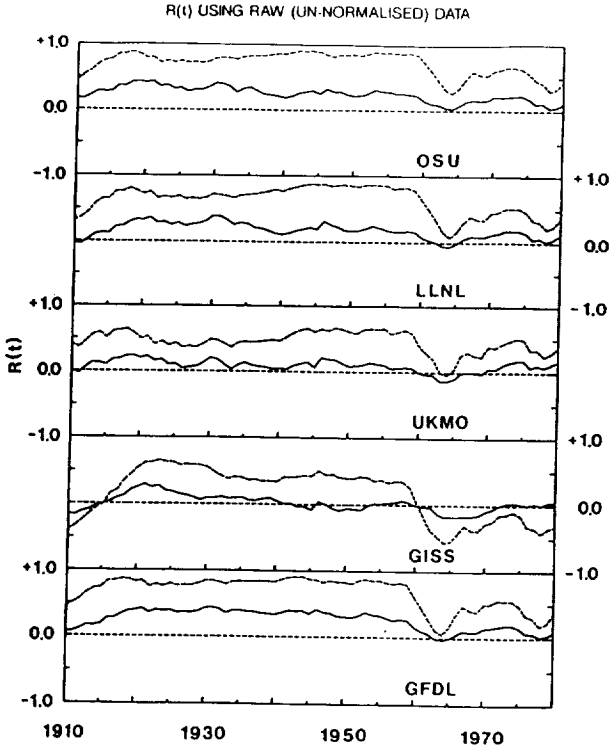


*Figure 28.–Time series of model vs. observed pattern correlations for five models. Model results are annual mean changes from equilibrium experiments performed with OSU, GFDL, UKMO, and LLNL models and from a transient experiment performed with the GISS model. Source: T. Wigley, 1991.*

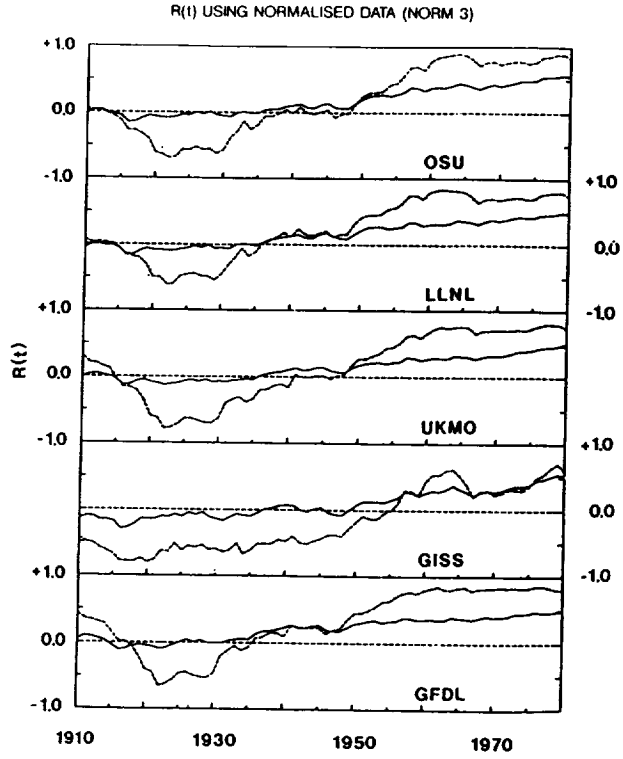


*Figure 29.–Data as in Figure 28 for model vs. observed normalized pattern. Source: T. Wigley, 1991.*

That the detected signal is not unique to the GHG effect (item 2) should be clear from the various uncertainties associated with competing forcing feedback and internal variability, especially in the long time-scale dynamics of the climate system. Given these deficiencies, the conclusion for item 4 is probably correct within the constraints of the best educated guess of present-day science but this does not anoint the conclusion with any absolute validity; time will tell.

There is little question, however, that the methodology used represents the best we can do currently. We need multivariate, multivariable analyses with the necessary supporting data to put the matter to rest, and preferably (but impossibly) an infinite time series in which all of the rather complex physics of the climate system have quantifiably gone through changes with one or more aspect, agent, or factor dominating at different times. Since we do not have the luxury of such a time series, it may be necessary to infer much more (than at present) from pre-instrumental proxy sources of information.

For the future, it becomes paramount to develop new observing systems to monitor precisely those multivariables that are required to detect climate change and GHG effects, while noting that the socioeconomic impact of potential change will require simultaneous observation of a variety of other parameters and variables. A first attempt at a multivariable fingerprint approach is presented in the next

multivariable fingerprint approach is presented in the next section.

### 4.3.3 Water Vapor and Cloud Fingerprint Detection

Attempts have been made to explore the GHG effect through its secondary (via feedback) effect in water vapor and clouds by comparing observational evidence with the change predicted by climate models (M. Chahine).

Temperature change has been the dominant focus of GHG effect primarily because present climate models can better handle the temperature change due increased downward infrared radiation (GHG effect) than elements of, for example, the hydrologic cycle, such as precipitation. The predicted signals are relatively small and local—both good reasons for caution in interpreting model results in this area. However, atmospheric moisture (water vapor and clouds) should plausibly change in response to a temperature change and could be good signals to detect GHG effects.

The basic approach is similar to that for the fingerprint concept for the detection of temperature change in section 4.3.2, namely to use the climate-model-predicted changes in atmospheric moisture and the cloud field as the signal and to analyze available data to check whether, the predicted signal is indeed, observed. The strategy adopted in this investigation, however, looks at more than one physical variable. The model output used was the transient $CO_2$ business-as-usual scenario run from the NASA/GISS ocean-atmosphere GCM described in Hansen et al. 1988. Model-predicted-changes indicate the following:

- For moisture, the largest changes in specific humidity (at 850 mb) are in the tropical strip—about a 35-45% increase for a GHG doubling (Figure 30). The change is more or less independent of longitude. Preliminary analysis using both data and atmospheric model (ECMWF) output in data-sparse areas indicates that there has been an increase in specific humidity of about 10% between 1972 and 1985 (most occurring between 1976 and 1978) at the 850 mb level of the tropical atmosphere; Figures 31 and 32. This change, however, appears to have been an abrupt regime shift, as opposed to a gradual increase. The spatial pattern of the change shows distinct maxima over the tropical Indian Ocean and the eastern Pacific, unlike the general increase over the entire tropics in the 2x GHG model-prediction in Figure 30. Nevertheless, the model-predicted change signal is large and is distributed spatially in a unique pattern. Thus, moisture is inferred to be a good signal for the purposes of detecting a GHG effect .

- Model-predicted cloud changes are shown in Figure 33. At the lowest level, stratus decreases over virtually all latitudes below 50°N; the signal is again strongest in the tropics, particularly along the equator in the central and eastern Pacific. At middle levels, there is a sharp increase predicted over the cold tongue region of the eastern Pacific, but it is confined to close to the equator. Over most of the tropics and subtropics, however, mid-level clouds decrease. Changes in high cirrus clouds indicate an increase over most of the tropical strip, particularly over the equatorial cold tongue and the Indian Ocean and a decrease at around 50°N. The maximum signal associated with the patterns appears to

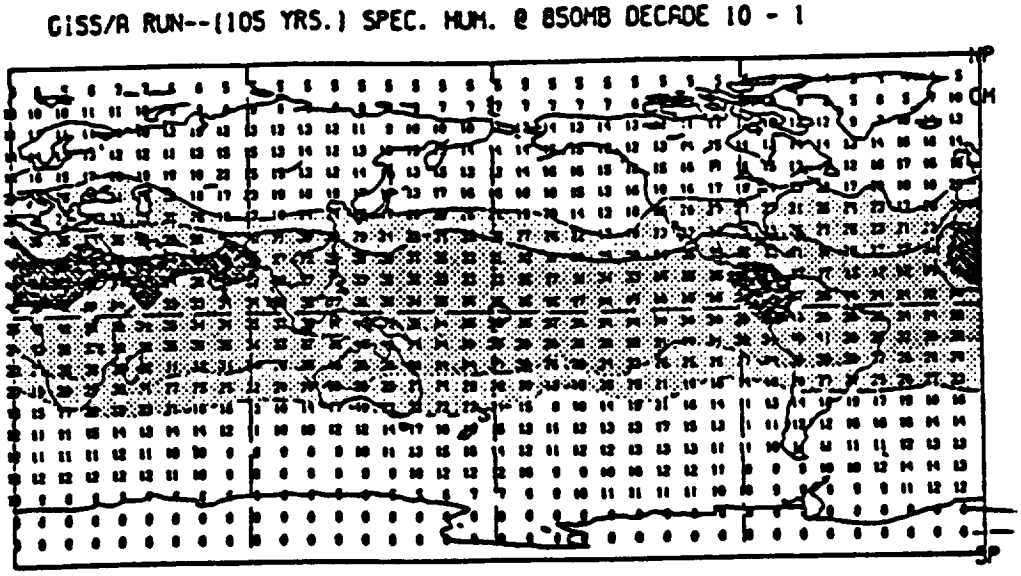


*Figure 30.–Changes in specific humidity at 850 mb from the GISS-A run. The average specific humidity over the first decade of the model integration was subtracted from that obtained from the tenth decade of model integration. This difference was normalized by the mean value for the first decade. The results show the percentage change between decades 1 and 10. Light stippling represents changes of 20-29%, medium stippling 30-39%, and dense stippling >40%. Source: T.P. Barnett et al., 1991.*

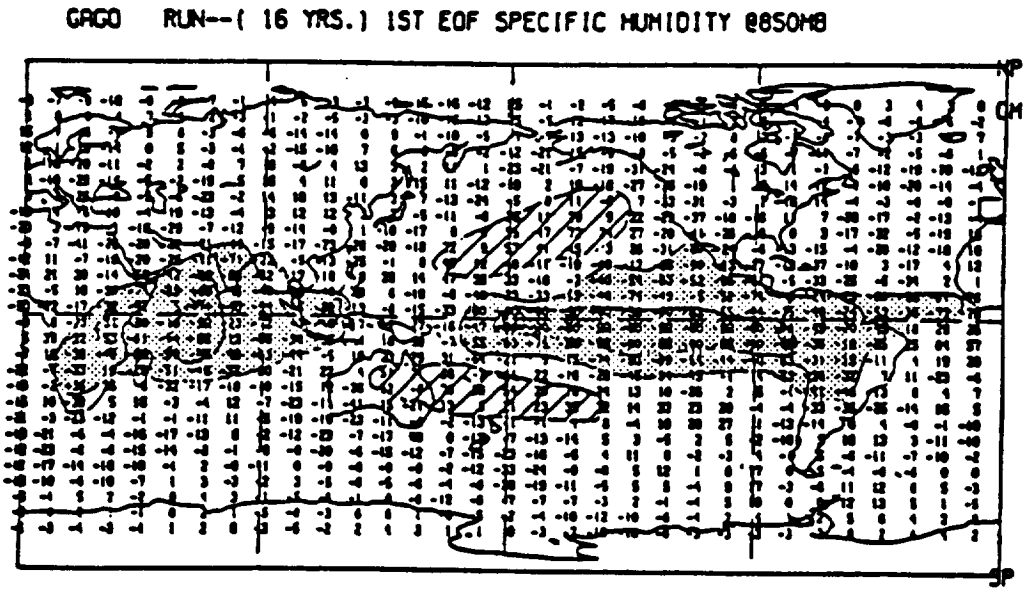


*Figure 31.–First empirical orthogonal function of the ECMWF-T21 model run for the period 1970-1985. The regions of maximum variability are over the equatorial Indian and central/eastern Pacific oceans. This represents a pattern of natural variability and can be compared with the GHG signal shown in Figure 30. Source: T.P. Barnett et al., 1991.*

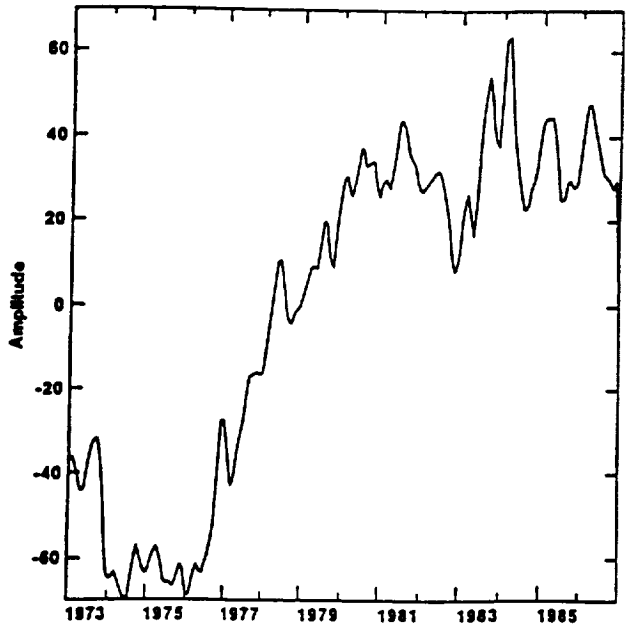


*Figure 32.–Principal component that accompanies Figure 31. Note the abrupt shift in the moisture field of the tropical atmosphere between 1976 and 1978. This change represents roughly a 10% increase in the mean specific humidity. Source: T.P. Barnett, et al., 1991.*

represent changes in cloud cover of about -10% which is not large. However, the change in cloud pattern has a spatially distinctive character—low-level clouds decrease while upper-level clouds increase. This pattern may therefore be used for the detection of the GHG signal.

The basic conclusions of this attempt to develop a moisture-cloud fingerprint application are that (a) the climate models predict a distinct and large (in the case of moisture) change in these variables and (b) the "signal" should be supported by observational evidence. In fact, much of the predicted warming due to the enhanced GHG effect is a result of the model's built-in moisture and cloud feedback, which is a result of the way models handle the hydrologic cycle. The direct radiative effect of doubling of GHGs is about 1.2°C. The associated increase in water vapor (~33%) produces an additional GHG effect of about 1.0°C. Changes in net cloud amount (a decrease) add 0.8°C, and changes in sea ice and snow cover (also a decrease) add another 0.4°C . In the model climate system, all of the above are positive feedbacks to the initial radiative (change) GHG climate forcing. The total change of about 4°C, is substantially larger than the direct climate forcing effect of 1.2°C and will critically affect the final GHG effect. Thus, it becomes vital to observe or detect changes in water vapor and clouds in order to verify and validate climate model physics and parameterizations.

Note also that the various versions of the UKMO climate model, which use different cloud algorithms and produce vastly different warming effects for a doubling of equivalent $CO_2$, range from 5.2°C to 1.9°C (R. Tenue).

### 4.4 Change in Variability

While global mean temperature has been widely used as a measure of enhanced GHG effect (and many believe this to be the best parameter), other parameters

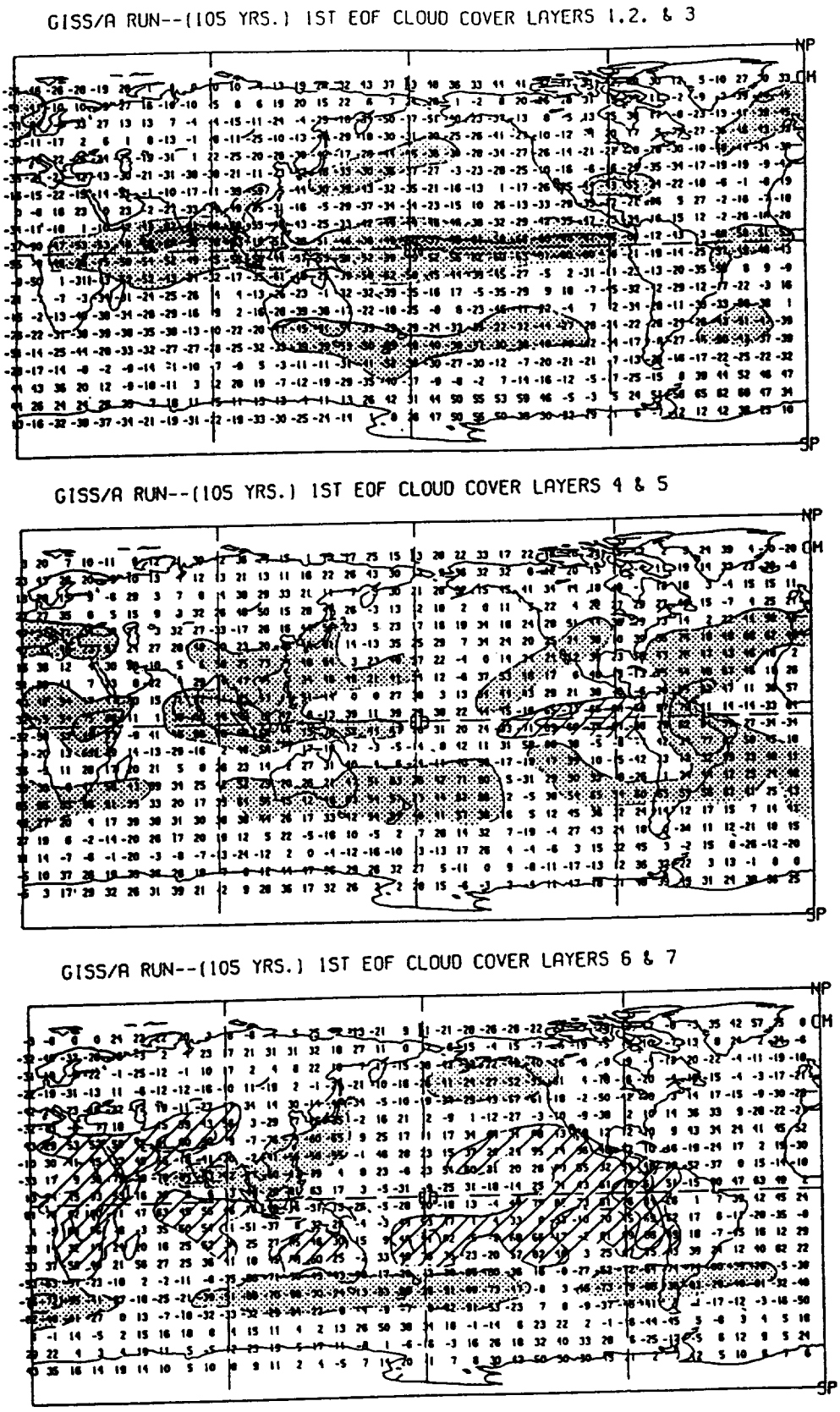


*Figure 33.–Empirical orthogonal functions of the changes in multilevel clouds simulated by the GISS-A run: (a) changes in low-level clouds in the first three model layers, (b) for middle-level clouds, (c) for clouds in layers 6 and 7 of the model. The hatched areas indicate regions where the cloud cover is predicted to increase; stippling represents a predicted decrease in cloud cover. Source: T.P. Barnett et al., 1991.*

are equally if not more important in terms of impact on agriculture, water supply, energy production/distribution, etc.; among these are extreme values of temperature and the frequency of hot or cold spells. As GHGs increase, models predict (J. Hansen) a 60-70% increase in warm spells. However, if there is a volcanic eruption of the magnitude of El Chichon, this number decreases by a factor of 2 to about 30% and, with two El Chichons in succession, the number is down to 20%—a barely perceptible change from the present climate. For the design and construction of large engineering structures (e.g., dams, bridges, harbors), extreme value statistics for wind, snow/ice, precipitation, run-off, storm surges, etc., must be known, as must changes to these statistics for a 2x GHG scenario.

For agricultural and water resources applications, cumulative changes are important. For example, runoff after a storm depends on the antecedent soil moisture conditions. Furthermore, climate change signal may be more clearly defined by analyzing cumulative deviations (A. Nicks). An example illustrating this point is depicted in Figure 34, which shows a time series of annual accumulated precipitation at the center of the Little Washita River Watershed, Oklahoma. No particularly significant climate fluctuations over the period 1901-1989 are evident. However, the corresponding series of cumulative deviations of annual precipitation about the long-term mean (Figure 35) shows pronounced fluctuations with extended periods of above- or below-average water availability.

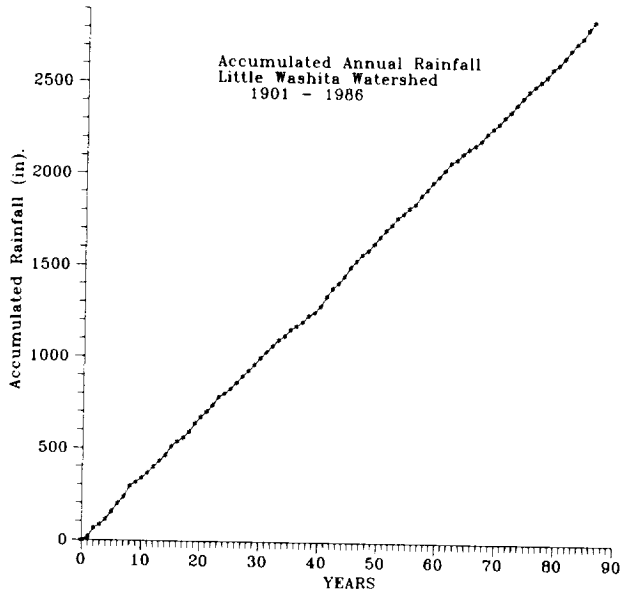


*Figure 34.–Annual accumulated precipitation at the center of the Little Washita River Watershed, Oklahoma. Source: A. Nicks, 1991. 1991.*

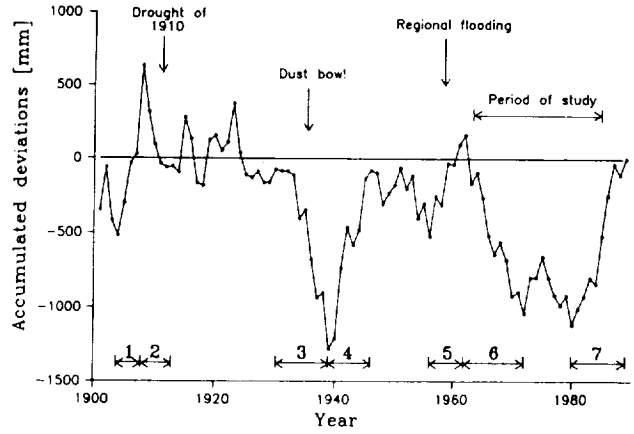


*Figure 35.–Accumulated deviations of annual precipitation for 1901-1989 at the center of the Little Washita River Watershed, Oklahoma. Source: A. Nicks, 1991.*

## 4.5 Change in Second and Higher Order Parameters

The distinction between first, second and higher order variables and parameters is somewhat arbitrary and is largely defined either by existing observational systems (and observations) or by the manner in which current science mathematically describes the physical world through differential, integral, and empirical equations. In principle, momentum flux, evaporation, heat flux, etc., could be independent variables if they were directly measured, but instead they are treated as derived and dependent variables, dependent on wind velocity, temperature, precipitation, etc. (all measured variables). In fact, one of the problems associated with satellite and remote-sensed observations is that the measured quantities are not directly used; they are instead converted through algorithms to conventionally measured variables around which the present system of mathematics has evolved (or perhaps vice versa). These structural or social (scientific) definitions could change over the next 100 years—the time scale of change for enhanced GHG effect.

The change in second order parameters such as evaporation, runoff, and groundwater (i.e., parameters that are dependent on more than one variable) could be substantial in response to rather subtle changes in the mean values of first order parameters such as temperature and precipitation (A. Nicks). For example computed runoff and associated sediment transport increased by a factor of 2 or 3 because of a change in the frequency (and intensity duration statistics) of storm events over the Washita catchment areas in the southern United States. This occurred despite negligible change in annual mean rainfall and temperature.

In regard to the impact on nonirrigated agriculture, the shifts in the statistical timing of rain (wet and dry spells) in relation to crop phenology would be of critical importance. Further, such shifts would invalidate the direct application of present agro-climatic knowledge, and several years of conceivably inappropriate farming practices would result until the characteristics of a new climatic regime were felt and understood. Such predictions are presumably beyond the scope of present generation climate models, even though some information has been obtained by imposing a change in the mean to the present distribution of the variability of a parameter (e.g., temperature or precipitation) about its mean value.

A comparison (A. Nicks) between the dry (1963-1969, evident in Figure 35 as a steadily decreasing cumulative deviation) and the wet (1981-1985 evident as a steadily increasing cumulative deviation) indicated that there was a substantial change in the frequency of occurrence of mean daily discharge (Figure 36) associated with which water yield tripled, sediment yield doubled, and peak flows above 500 cm

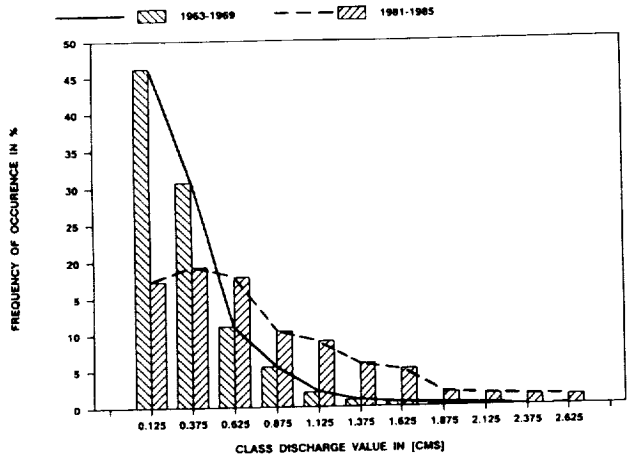


*Figure 36.–Frequency of occurrence of mean daily discharge under 25 cm for the pre- and post-construction periods of the Little Washita River Watershed, Oklahoma. Source: A. Nicks, 1991.*

increased fourfold in spite of the construction of floodwater retardation structures. The above example points to the various types of analyses that need to be carried out in order to detect climate change and to obtain information on real-world applications.

In the example cited above, precipitation was measured rather accurately with a dense and well-calibrated local network of precipitation stations. Regional and national networks may also permit reasonable estimates of area-averaged precipitation but not the data exchanged globally via the GTS communications and data exchange system of WMO. In addition, for estimates of global diabatic heating, ocean precipitation data are required, for which there is little option but to use satellite-derived estimates.

Even with high-density land-surface-based precipitation measurements, there could be problems, and corrections need to be applied (P.Y. Groisman). Usually, existing national rain gauges undercatch the "ground truth" precipitation (i.e., the real amount of water or water equivalent of snow that fell at ground level), especially during periods of solid precipitation. There also are time-dependent biases in many countries when inhomogeneities in precipitation records are scrutinized. These are associated with changes of rain gauges (type or construction) and techniques of measurement, observing practices, and time averaging.

Changes in precipitation, despite the above problems, must be measured since precipitation is a direct index of the hydrologic cycle and must inevitably respond to enhanced greenhouse effects. Cross parameter investigations conducted in the USSR (P.V. Groisman) show definite changes in regional precipitation that are associated with regional temperature changes (Figure 37). These two parameters need to be considered together before any impact calculations can be made without arbitrary assumptions. Given the many uncertainties in the present generation of climate models, particularly in regard to regional cloud-precipitation processes, it is unclear whether model-predicted precipitation changes can be relied on.

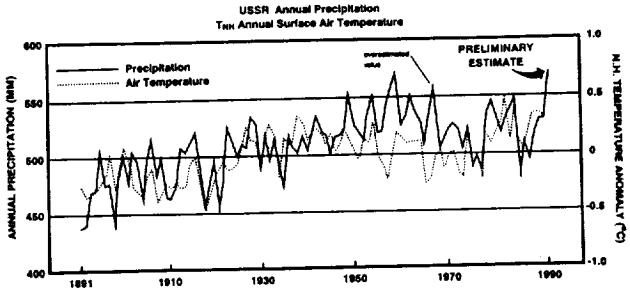


*Figure 37.–Spatially averaged corrected precipitation time series (solid line) compared with mean annual Northern Hemisphere temperature. Source: P. Groisman, 1991.*

## 4.6 Changes in the Upper Stratosphere and Mesosphere

Recent studies (R. Roble and R. Dickinson) suggest that the projected increase in anthropogenic $CO_2$ and $CH_4$, while warming the troposphere, will cool parts of the mesosphere by 10-20°K in the global mean and the thermosphere by as much as 50K. Figure 38 depicts the globally averaged temperature changes in the mesosphere and thermosphere predicted by global circulation models in response to a doubling or halving of $CO_2$ and $CH_4$ concentrations near the stratosphere. Though long-term observational information is lacking, the

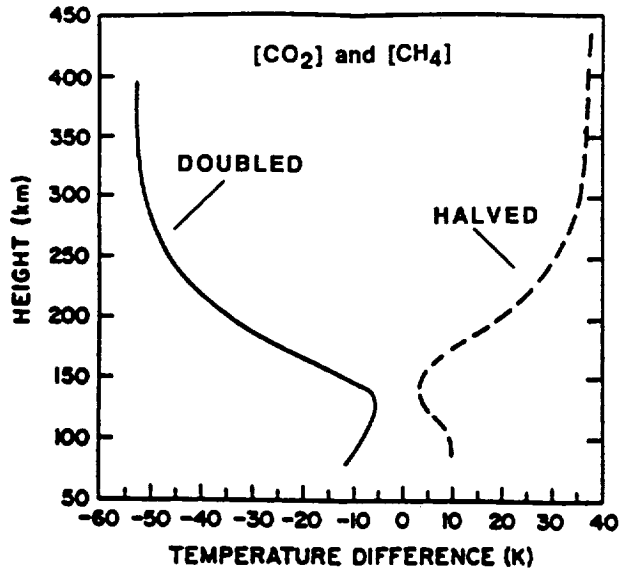


*Figure 38.–At the current rates of increase, atmospheric $CO_2$ and $CH_4$ concentrations are predicted to double within the next century. Plotted here are the calculated temperature changes in the mesosphere and stratosphere for the cases in which $CO_2$ and $CH_4$ concentrations at 60 km are doubled (solid curve) and halved (dashed curve). Source: R. Roble and R. Dickinson, 1989.*

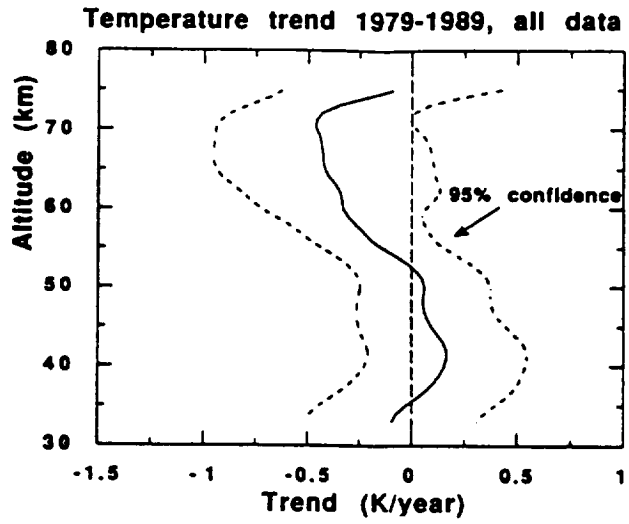


*Figure 39.–During the past decade, Rayleigh lidar measurements of stratospheric and mesospheric temperatures above southern France have exhibited cooling trends approaching -0.4 K per year at 60-70 km altitude. Source: A. Hauchecorne et al., 1991.*

analysis of Rayleigh lidar data collected since 1979 in southern France suggests that parts of the mesosphere may, indeed, be cooling at a remarkably fast rate, perhaps as high as -0.4K per year at 60-70 km in altitude (A. Hauchecorne; see Figure 39). Consequent changes in the thermospheric circulation are expected to alter the electrodynamic structure of the upper atmosphere and, through dynamo action, the magnetosphere-ionosphere coupling processes.

Increasing concentrations of the greenhouse gas $CH_4$, coupled with decreasing temperatures, may also be related to the increased formation of noctilucent clouds (NLC) near 82 km (the highest clouds on Earth) over the cold summertime polarcaps. Historical records contain no reports of NLC sightings before about 1885, even though skilled observers were monitoring auroral and twilight phenomena at high latitudes for many decades by then (R. Thomas et al.). Since the discovery of NLCs more than 100 years ago, the brightness and frequency of NLC displays have been increasing. It is believed that $CH_4$ may facilitate NLC formation because of its ability to transport hydrogen through the stratosphere. Once methane reaches the mesosphere, photo-chemical reactions in the presence of atomic oxygen produce water vapor that is essential for NLC formation.

The above are, conceivably, two other greenhouse gas effects which need to be observationally monitored on a long-term basis for a more comprehensive understanding of climate system changes.

# 5. Future Observations, Research and Analysis Required

## 5.1 Observational requirements

Observational requirements for the detection of climate change and GHG effects are substantially more stringent in terms of accuracy, precision, spatial coverage, and time series than are the requirements for real-time or near-real-time operational applications. This is partly because change signals are subtle, i.e., 0.5°C per 100 years as observed, or even the predicted temperature change of 1.5° to 4.5°C in 50 years, amounting to a maximum annual rate of change of 0.09°C per year. None of the existing observational systems were designed, implemented, or operated to directly and automatically provide this sort of long-term decadal time-scale accuracy. Problems that inhibit such accuracy derive from a variety of causes, not all of which are instrumentation- or sensor-related; examples are

- Changes in instrumentation (sensor and/or calibration)
- Changes in location and exposure of sensors (e.g., surface stations)
- Changes in the methods of observation (e.g., ship measurements of sea surface temperature),
- Changes in computational procedures (e.g., for mean daily temperature)
- Changes in satellite algorithms that derive physical or geophysical parameters from spectral information
- Changes in data assimilation models (physics) used to compute variables or parameters that are not directly measured (e.g., fluxes of heat, momentum, water vapor).

Several areas of deficiencies and weaknesses were identified at the First GEDEX Workshop. It was recognized that achieving the observational capability and corresponding data sets necessary to monitor all the parameters and variables would take some years, and possibly decades.

Furthermore, even if observing capability is substantially improved, there is still the need for long time series. It was felt that a concurrent effort is required by all agencies (national and international) to provide retrospective data collection and analysis, improve present observational procedures and data exchange, and developing new instrumentation capabilities for future monitoring.

Given the present deficiencies, the use and improvement of climate model parameters was considered very important, since no other tool is available to conduct experiments with the global system, barring the occurrence of natural events. The Pinatubo (Philippines) volcanic eruption, if adequately monitored (i.e., for sulfate- and dust aerosol clouds) could provide such an opportunity to investigate climate system sensitivity to aerosol forcing.

Some variables were considered more important than others, namely, those for which climate model results appear to differ substantially from observations, such as stratospheric and tropospheric moisture and temperature, aerosols, and atmospheric ozone (J. Hansen). Improving the estimation of climate sensitivity to GHG and other forcings was also felt to be very important. For the monitoring and detection of change and GHG effects it was considered important to select parameters and variables that have a high signal-to-noise ratio; temperature and moisture were considered good candidates, while precipitation and pressure (for example) were considered poor. The signal should not be model-specific but it should be unique to the process or effect being sought (T. Wigley). No particularly good candidate is known at the present time; the vertical temperature structure and spatial-horizontal temperature patterns were considered poor candidates even though they are widely used.

Low-frequency noise (i.e., variability of >40 years' time scale) needs to be understood and modeled from available data sets. In this regard, more precise evaluations of the paleoclimatic ice core, ocean sediment, lake varve, and proxies (e.g., tree rings, coral cores, etc.) are needed, including expanded global spatial coverage.

In addition to long-term calibrated data with global coverage for climate change studies (usually monthly data), workshop participants also thought it necessary to obtain high-frequency sampling, preferably several times per day, to gather meaningful statistics on rapid atmospheric processes, particularly those affecting clouds, radiation, and precipitation (J. Hansen). Measurements are planned as a part of the proposed EOS platforms and Earth probe satellites (e.g., TRMM).

Other areas in which research data collection and analysis are considered necessary include: expanded global station network data exchange, together with time series and metadata (i.e., station history information); analysis of other parameters, such as precipitation; collection and distribution of instrumentation intercomparison information; and comparison of climate-model-derived radiation budgets and fluxes, together with observations.

## 5.2 Data Sets for GEDEX Research

The capabilities of NASA's Climate Data System were demonstrated in real time at the workshop with a remote terminal linked to on-line computers at the Goddard Space Flight Center (L.Olsen). Various features such as data

catalogue and data set browsing, subsetting, and analysis (e.g., time-series plots, contouring, changing coordinate systems, and display) were considered to be tools necessary for users to access the system and carry out simple data set manipulations. Similar capabilities are planned as a part of the software package to accompany the CD-ROM being prepared under the auspices of the GEDEX project.

In order to cover the breadth of research and analysis needed to address the objectives of GEDEX, workshop participants concurred that it would be desirable to have the following data sets (with complete documentation) on the GEDEX CD-ROM:

- Surface temperature (land, ocean surface);
- Upper air temperature;
- Satellite;
- GHGS; and
- Surface radiation.
- Dobson Network - ozone
- SOI, QBO

These data sets will also be available with on-line access through NASA's NCDS. On-line access capability will enable scientists to obtain updates when they become available. The periodic distribution of updates on CD-ROM is also being considered, e.g., once every two years. All GEDEX data on CD-ROM or on-line from NCDS would be carefully checked and documented prior to release in a consistent standard format to spared the user the painful task of having to decipher various formats before carrying out data intercomparison or multivariable studies. A detailed list is in Appendix 5.

## *5.3 A Framework for GEDEX Research*

There are several ongoing or planned international activities dealing with the detection and prediction of climate change and greenhouse gas effects. In particular, the activities of the WMO/UNEP Intergovernmental Panel on Climate Change (IPCC) and WMO/WCDP's Climate Change Detection Project ICSU/WMO-WCRP (M. Crowe). Complementing these programs is the International Geosphere-Biosphere Programme (IGBP)—the study of Global Change. Under the IPCC or one or more of the programs and projects of the WMO (WCRP, WCDP), UNEP (GEMS) etc., there were several scientific and technical activities covering scientific assessments of climate change, GHG effects, monitoring and detection analysis, future observing systems, and climate modelling. Other international programs are also being formulated to investigate climate system interaction and feedback processes (e.g., TOGA - COARE). Several other projects are directed at investigating the longer term climatological structures and climate system variations (e.g., WOCE, EOS, TRMM, ISLSCP, GEWEX). There are international plans to integrate the observational components of such projects and develop a Global Climate Observing System (GCOS). Given this situation, the workshop thought it, unnecessary for GEDEX to initiate a new infrastructure and program to cover the field of enhanced GHG detection. However, it was felt that GEDEX could serve a useful purpose by providing an umbrella for channeling resources and expertise on specific timely climate change issues. For example, the Pinatubo volcanic eruption was cited as an example—the injection of aerosols into the stratosphere measured by SAGE-II and ground based lidar (e.g., at the MaunaLoa observatory) providing an opportunity to investigate a variety of climate system sensitivities, radiation feedback processes etc. thru model simulation and verification.

The workshop was of the opinion that GEDEX should identify, and as the opportunity arises, provide an impetus to observational, analytical and modeling research experiments and studies to resolve one or more of the issues dealing with the detection and prediction of enhanced GHG effects on climate. Possible candidate subject areas are: Climate sensitivity; Aerosol - Radiation Feedback (Pinatubo case study); Water Vapor Feedback; Cloud - Radiation Feedback; Surface cover, albedo-climate feedback; Climate-atmosphere/ocean circulation interaction; Ozone and Water Vapor Measurements; Atmosphere - Ocean Coupling on long-time scales; Climate Change Monitoring and Detection Specification; and Analysis of precipitation, river flow/run-off, wind, surface radiation budget, evaporation and soil moisture changes.

The planned NASA production and distribution of a CD-ROM containing all (to the extent possible) documented data sets relevant to investigations of climate change and greenhouse effect, was endorsed. It was recommended that this activity be continued under GEDEX through (a) maintaining an updated on-line database at the NASA Goddard Distributed Active Archive Center (DAAC) which incorporates the NCDS and (b) issuing CD-ROMS periodically, approximately once in two years or more frequently if the database expands rapidly. A subset for international distribution on diskettes under the ICSU/IGBP (Global Change Data Diskette Project) and WMO (Climate Change Detection Project) containing at least the basic global and selected regional temperature records was considered useful to encourage international participation. [Note: the diskette version would be for a large number of countries presently equipped with WMO-CLICOM microcomputer systems, but not CD-ROM readers.] Internationally, GEDEX was viewed as a significant activity which could centrally support the objectives of, for example, WMO's CCDP project, the follow up to the IPCC, and ICSU's IGBP. The GEDEX-CDROM is considered to be a test-bed for future CD-ROMs containing EOS and other climate system related databases for international scientific research.

## *Appendix 1*

## *GEDEX Atmospheric Temperature Workshop*

## *Participants List*
## *July 1991*


David Adamec
Earth Science and Applications Division
NASA Headquarters, Code SED
600 Independence Avenue, SW
Washington, DC 20546
USA
202-453-1725 (TEL)
202-755-2552 (FAX)

Arthur C. Aikin
Chemistry and Dynamics Branch
NASA/GSFC
Code 916
Greenbelt, MD 20771
USA
301-286-8913 (TEL)
301-286-3460 (FAX)

James K. Angell
NOAA/Air Resources Laboratory
1325 East West Hwy.
Room 9358
Silver Spring, MD 20910
USA
301-427-7684 (TEL)
301-427-8119 (FAX)

Albert Arking
Climate and Radiations Branch
NASA/GSFC
Mail Stop-913
Greenbelt, MD 20771
USA
301-286-7208 (TEL)
301-286-4804 (FAX)

Ghassem Asrar
Earth Science and Applications Division
NASA Headquarters, Code SEP03
Washington, DC 20546
USA
202-453-1720 (TEL)
202-755-2552 (FAX)

Kenneth Bergman
NASA Headquarters, Code SED
600 Independence Avenue, SW
Washington, DC 20546
USA
202-453-8139 (TEL)

Ralph Brecia
NASA Headquarters
400 Maryland Avenue, SW
Washington, DC 20546
USA
202-453-8452 (TEL)

Moustafa T. Chahine
Jet Propulsion Laboratory
M/S 108-904
4800 Oak Grove Drive
Pasadena, CA 91109
USA
818-354-6057 (TEL)
818-393-4218 (FAX)

John R. Christy
University of Alabama, Huntsville
Atmospheric Science & Remote Sensing Laboratory
R.I. A11, Box 212
Huntsville, AL 35899
USA
205-895-6257 (TEL)
205-895-6970 (FAX)

Fong-Chzauehang
STX
7601 Ora Glen Drive
Suite 300
Greenbelt, MD 20770
USA
301-513-1698 (TEL)

James Closs
NASA/Goddard Space Flight Center
Code 934
Greenbelt, Maryland 20771
USA
301-286-5033 (TEL)

Michael Coughlan
NOAA/R/CAR
1335 East West Highway
Silver Spring, MD 20910
USA
301-427-2474 (TEL)
301-608-3979 (FAX)

Michael Crowe
World Climate Data Program
WMO/Geneva
41-22-7308377 (TEL)
41-22-7342326 (FAX)

Prabhakara Cuddapah
NASA/Goddard Space Flight Center
Code 913
Greenbelt, MD 20771
USA
301-286-5390 (TEL)

G. Dalu
CNR-IFA
Piazzale L. Sturzo, 31
Rome, I-00144
Italy
396-5910941 (TEL)

James C. Dodge
NASA Headquarters, Code SED
600 Independence Avenue, SW
Washington, DC 20546
USA
202-453-1680 (TEL)
202-755-5032 (FAX)

Robert Etkins
NOAA/NCPO
Room 518
1825 Connecticut Avenue, NW
Washington, DC 20235
USA
202-673-5360 (TEL)
202-673-5355 (FAX)

Nancy Firestine
Space Technology Group
WT Chen & Company
1745 Jefferson Davis Highway
Suite 500
Arlington, VA 22202
USA
703-769-1800 (TEL)
703-769-1803 (FAX)

Kevin Gallo
NOAA/NESDIS
National Cimate Data Center
Federal Building
Ashville, NC 28801
USA
704-259-0454 (TEL)

Pavel Groisman
NOAA/NESDIS Natl Climate Data Center
Federal Building
Ashville, NC 28801
USA
704-259-0307 (TEL)
704-259-0246 (FAX)

James E. Hansen
NASA Goddard Institute for Space Studies
2880 Broadway
New York, NY 10025
USA
212-678-5619 (TEL)
212-678-5622 (FAX)

Pat Hrubiak
NASA/Goddard Space Flight Center
Code 913
Greenbelt, MD 20771
USA
301-286-7208 (TEL)

James Hurrell
Natl Ctr for Atmospheric Research
P.O. Box 3000
Boulder, CO 80307
USA
303-497-1383 (TEL)
303-497-1137 (FAX)

Roy Jenne
Scientific Computing Division
National Center for Atmospheric Research
P.O. Box 3000
Boulder, CO 80307
USA
303-497-1215 (TEL)
303-497-1137 (FAX)

Greg Johnson
USDA-ARS
Northwest Watershed Research Center
Plaza IV
800 Park Blvd./Suite 105
Boise ID 837 12-7716
USA
208 334-1363 (TEL)
208 334-1502 (FAX)

Phil D. Jones
Climatic Research Unit
University of East Anglia
Norwich, NR4-7TJ
United Kingdom
44-603-592-090 (TEL)
44-603-507-784 (FAX)

Dale Kaiser
DOE/ORNL/CDIAC
Oak Ridge National Laboratory
P.O. Box 2008
Building 1000, MS-6335
Oak Ridge, TN 37831
USA
615-574-0390 (TEL)

Hyo Sang Lee
SESI
4040 Blackburn Lane
Suite 105
Burtonsville, MD 20866
USA
301-989-1896 (TEL)

Yuhe Liu
University of Maryland
(Student attending w/Alan Robock)

Jianping Mao
University of Maryland
(Student attending w/Alan Robock)

Alan McNab
Climate Perspectives Branch
NOAA/NESDIS National Climate Data Center
Federal Building
Ashville, NC 28801
USA
704-259-0592 (TEL)
704-259-0246 (FAX)

Bernard G. Mendonca
NOAA
Mail Code R-E-CG1
325 Broadway
Boulder, CO 80303
USA
303-497-6650 (TEL)
303-497-6290 (FAX)

Arlin Nicks
USDA/ARS
P.O. Box 1430
Durant, OK 74702
USA
405-924-5066 (TEL)
405-924-5307 (FAX)

George Ohring
NOAA/NESDIS (E/RAI)
Washington, DC 20233
USA
301-763-8078 (TEL)

Lola Olsen
NASA/Goddard Space Flight Center
Code 934.0
Building 26 - Room 110
Greenbelt, MD 20771
USA
301-286-9760 (TEL)
301-286-4952 (FAX)

John S. Perry
N.A.S.
2101 Constitution Avenue, NW
Washington, DC 20418
USA

Alan Robock
Department of Meteorology
University of Maryland
College Park, MD 20742
USA
301-405-5377 (TEL)
301-314-9482 (FAX)

Chester F. Ropelewski
Climate Analysis Center
World Weather Building
Room 605
5200 Auth Road
Camp Springs, MD 20746
301-763-8227 (TEL)
301-763-8395 (FAX)

William B. Rossow
NASA Goddard Institute for Space Studies
2880 Broadway
New York, NY 10025
USA
212-678-5567 (TEL)
212-678-5622 (FAX)

John Sandiland
Canadian Climate Center
4905 Dufferin Street
Donnsview, Ontario Canada M3H5P4
Canada
416-739-4318 (TEL)
416-739-4380 (FAX)

Robert A. Schiffer
Earth Science and Applications Division
NASA Headquarters, Code SED
600 Independence Avenue, SW
Washington, DC 20546
USA
202-453-1680 (TEL)
202-755-5032 (FAX)

Francis J. Schmidlin
NASA Wallops Flight Facility
Building E 106, Code 972
Wallops Island, VA 23337
USA
804-824-1618 (TEL)
804-824-1036 (FAX)

Roy W. Spencer
Marshall Space Flight Center, ES-43
Huntsville, AL 35812
USA
205-544-1686 (TEL)
205-544-5760 (FAX)

Ke-Jun Sun
STX
7601 Ora Glen Drive, Suite 300
Greenbelt, MD 20770
USA
301-531-1681 (TEL)

Joel Susskind
Global Modeling and Simulation Branch
NASA/GSFC
Mail Code 911
Greenbelt, MD 20771
USA
301-286-7210 (TEL)
301-286-2717 (FAX)

Dan Tarpley
NOAA/NESDIS
World Weather Building
Room 712
Washington, DC 20233
USA
301-763-8042 (TEL)

Sushel Unninayar
NASA/ES-GEDEX
600 Maryland Avenue, SW
Suite 230
Washington, DC 20024
USA
202-863-3990 (TEL)
202-863-3995 (FAX)

Konstantin Vinnikov
State Hydrological Institute
State Committee for Hydrometeorology
V.O.2 Ya Liniya 23
Lenningrad 199053
USSR
812-164-6648 (TEL)
812-213-0114 (FAX)

T.M.L. Wigley
Climatic Research Unit
University of East Anglia
Norwich, NR4-7TJ
United Kingdom
44-603-592-721 (TEL)
44-603-507-784 (FAX)

Helene Wilson
Center for the Study of Global Habitability
Columbia University
NASA Goddard Institute for Space Studies
2880 Broadway
New York, NY 10025
USA
212-678-5640 (TEL)
212-678-5552 (FAX)

Martin Yerg
National Climate Program Office
Univeral Building
Room 518
1825 Connecticut Avenue, NW
Washington, DC 20235
USA
202-673-5360 (TEL)
202-673-5355 (FAX)

Jung-Moon Yoo
ARC
Landover, MD 20785
USA
301-286-01024 (TEL)

Joseph M. Zawodny
NASA/Langley Research Center
Mail Stop -475
Hampton, VA 23665
USA
804-864-2681 (TEL)

## *Appendix 2*

## *GEDEX Atmospheric Temperature Workshop*
## *List of Presentations/Presenters*

| | |
|---|---|
| Global Tropospheric and Stratospheric Temperature Through the Spring of 1991 | J. Angell |
| Comparison of Some Temperature Data Records | A. Arking |
| The Role of Water Vapor and Clouds in Climate Change | A. Arking |
| Detection of the Greenhouse Effect from the Cloud and Moisture Observations | M. Chahine |
| Gridpoint Comparisons Between Surface Thermometer and Satellite Microwave Temperature Anomalies | J. Christy |
| WMO Climate Change Detection Project | M. Crowe |
| Climate Forcings and Feedbacks: Implications from Global Temperature Measurements | J. Hansen |
| An Evaluation of MSU and ECMWF Monthly Mean Temperature | J. Hurrell |
| Data for Temperature Trends Studies | R. Jenne |
| Urban Temperature Bias Determination Utilizing Polar Orbiting Satellite Data | G. Johnson |
| Global Temperature Variations Since the 19th Century | P. Jones |
| Impact of Subtle Changes in Climate on Run-Off | A. Nicks |
| Data Content and Format for CD-ROM | L. Olsen |
| The Volcanic Signal in the Global Temperature Record | A. Robock |
| Samplings and Uncertainties in "Global" SST | C. Ropelewski |
| Radiosonde Measurement Accuracy and Precision | F. Schmidlin |
| Global Satellite Temperature Monitoring | R. Spencer |
| Towards the Detection of an Enhanced Greenhouse Effect Fingerprint | T. Wigley |
| Comparison of Surface and Satellite Temperature Maps | H. Wilson |
| SAGE Aerosol, Ozone, and Water Vapor | J. Zawodny |

# *Appendix 3*

## *Selected Bibliography*


Albrecht, B.A., 1989: Aerosols, cloud microphysics, and fractional cloudiness. *Science, 245, 1227-1330.*

Ardanuy, P. E., L.L. Stowe, A. Gruber and M. Weiss, 1991: Shortwave, longwave, and net cloud-radiative forcing as determined from Nimbus-7 observations. *J. Geophys. Res., accepted.*

Angell, J.K., 1990: Variations in global tropospheric temperature after adjustment for El Niño influence. *Geophys. Res. Lett., 17, 1093-1096.*

Angell, J.K. , 1988: Variations and trends in tropospheric and stratospheric global temperatures, 1958-87. *J. Climate, 1, 1296-1313.*

Ardanuy, P.E., L.L. Stowe, A. Gruber, and M. Weiss, 1991: Shortwave, longwave, and net cloud-radiation forcing as determined from Nimbus-7 observations. *J. Geophys. Res., in press.*

Arking, A., 1991: The radiative effects of clouds and their impact on climate. *Bull. Amer. Meteor. Soc., 71, 795-813.*

Arrhenius, S., 1896: On the influence of carbonic acid in the air upon the temperature of the ground. *Philosophical Magazine, 41, 237-271.*

Barnett, T.P., R. Haskins, and M. Chahine, 1991: Detection of the greenhouse gas signal from space: A progress report. *Adv. Space Res., 11, 3(37)-3(44).*

Bolin, B., 1986: How much $CO_2$ will remain in the atmosphere? *In: The Greenhouse Effect, Climate Change, and Ecosystems (Scope 29). Edited by B. Bolin, B.R. Doos, J. Jager, and R. A. Warrick. John Wiley and Sons, Chichester, pp. 93-155.*

Bradley, R.S., 1988: The explosive volcanic eruption signal in Northern Hemisphere: Continental temperature records. *Climate Change, 12, 221-243.*

Broecher, W.S., D. Peteet, and D. Rind, 1985: Does the ocean atmosphere system have more than one stable mode of operation? *Nature, 315, 21-26.*

Budyko, M.I., 1980: *"Climate of the Past and Future"* [in Russian]. Leningrad, Gidrometeorizdat, 352 pp.

Cess, R.D., G.L. Potter, J.P. Blanchet, G.J. Boer, S.J. Ghan, J.T. Kiehl, H. Le Treut, Z. X. Li, X.Z. Liang, J.F.B. Mitchell, J.J. Morcrette, D.A. Randall, M.R. Riches, E. Roeckner, U. Schlese, A. Slingo, K.E. Taylor, W.M. Washington, R.T. Wetherald, and I. Yagai, 1989: Interpretation of cloud-climate feedback as produced by 14 atmospheric generic circulation models. *Science, 245, 513-516.*

Cess, R.D., 1976: Climate change: An appraisal of atmospheric feedback mechanisms employing zonal climatology. *J. Atmos. Sci., 33, 1831-1843.*

Crowley, T.J, 1989: Paleoclimate perspectives on a greenhouse warming. *In: Climate and Geoscience.* Edited by A. Berger et al., Kluwer Academic Publishers, pp. 179-207

Crutzen, P.J., I. Aselmann, and W.S. Seiler, 1986: Methane production by domestic animals, wild ruminants, other herbivorous fauna, and humans. *Tellus, 38B, 271-284.*

Dickinson, R.E., and A. Henderson-Sellers, 1988: Modeling tropical deforestation: A study of GCM land-surface parameterization. *Quart. J. Roy. Meteor. Soc., 114, 439-462.*

Eddy, J.A., 1977: Climate and the changing sun. *Climate Change, 1, 173-190.*

Ellis, J.S., 1978: Cloudiness, the planetary radiation budget and climate. Ph.D. thesis, Colorado State University, Fort Collins, 129 pp.

Friis - Christensen, E., and K. Lassen: Length of solar cycle: An indicator of solar activity closely associated with climate. Science, 254.

Folland C.K., D.E. Parker, and F.E. Kates, 1984: Worldwide marine temperature fluctuations, 1856-1981. *Nature, 310, 670-673.*

Foukal, P., and J. Lean, 1990: An empirical model of total solar irradiance variations between 1874 and 1988. *Science, 247, 556-558.*

Garbrecht, J., A. Nicks, and J. Nancy, 1991: Effect of climate fluctuations on watershed runoff. *Proceedings of the Fifth Interagency Sedimentation Conference, Vol. 2, pp 15(34)-15(41).*

Gordon, A.H., 1991: Global warming as a manifestation of a random walk. *J. Climate, 4, 589-597.*

Grotch, S.L., 1988: *Regional Intercomparisons of General Circulation Model Predictions and Historical Climate Data.* U.S. Dept of Energy, Washington, DC, Report DOE/NBB - 0084 (TR041).

Halley, E., 1715: On the causes of the saltiness of the ocean, and of the several lakes that emit no rivers. *Philos. Trans. Roy. Soc. London, 29, 296-300.*

Halpert, M.S., and C.F. Ropelewski (Editors), 1991: *Climate Assessment: A Decadal Review, 1981-1990.* National Oceanographic and Atmospheric Administration, Washington, DC (DOC/NOAA Technical Report), 109 pp.

Hansen, J.,I. Fung, A. Lacis, D. Rind, S. Lebedeff, R. Ruedy, G. Russell, and P. Stone, 1988: Global climate changes as forecast by Goddard Institute for Space Studies three-dimensional model. *J. Geophys. Res., 93, 9341-9364.*

Hansen, J., and S. Lebedeff, 1987: Global trends of measured surface air temperature. *J. Geophys. Res., 92, 13345-13372.*

Hansen, J., W. Rossow, and I. Fung, 1990: The missing data on global climate change. *Issues in Science and Technology, 7 (1)No.1, 62-69.*

Hartman, D.L., K.J. Kowalewsky, and M.L. Michelsen, 1991: Diurnal variations of outgoing longwave radiation and albedo from ERBE scanner data. *J. Climate, 4, 598-617.*

Houghton, J.T., G.J. Jenkins, and J.J. Ephraums (Editors), 1990: *Climate Change: The IPCC Scientific Assessment* (Report prepared for the Intergovernmental Panel on Climate Change). Cambridge University Press, Cambridge, 362 pp.
Idso, S.B., 1991: The aerial fertilization effect of $CO_2$ and its implications for global carbon cycling and maximum greenhouse warming. *Bull. Amer. Meteor. Soc., 72, 962-965.*

Idso, S.B., B.A. Kimball, and S.G. Allen, 1991: Net photosynthesis of sour orange trees maintained in atmospheres of ambient and elevated $CO_2$ concentrations. *Agric. For. Meteor., 54, 95-101.*

Jenne, R.L., 1991: Climate trends, the U.S. drought of 1988, and access to data. *In: Greenhouse-Gas-Induced Climatic Change: A Critical Appraisal of Simulations and Observations.* Edited by M.E. Schlesinger. Elsevier Science Publishers, Amsterdam, pp. 195-209.

Jones, P.D., and T.M.L. Wigley, 1990: Global warming trends. *Scientific American, 263, 84-91.*

Karl, T.R., and P.D. Jones, 1989: Urban bias in area-averaged surface air temperature trends. *Bull. Amer. Meteor. Soc., 70, 265-270.*

Kellogg, W.W., 1991: Response to skeptics of global warming. *Bull. Amer. Meteor. Soc., 74, 499-511.*

Kutzbach, J.E., and P.J. Guetter, 1986: The influence of changing orbital parameters and surface boundary conditions on climate simulations for the past 18,000 years. *J. Atmos. Sci., 43, 1726-1759.*

Lacis, A.A., J. Hansen, P. Lee, T. Mitchell, and S. Lebedeff, 1981: Greenhouse effect of trace gases, 1970-1980. *Geophys. Res. Lett., 8, 1035-1038.*

Lindzen, R.S., 1990: Some coolness concerning global warming. *Bull. Amer. Meteor. Soc., 71, 288-299.*

Lovelock, J.E., 1988: *The Ages of Gaia: A Biography of Our Living Earth.* W.W. Norton and Co., New York, 252 pp.

Manabe, S., and K. Bryan, Jr., 1985: $CO_2$-induced change in a coupled ocean-atmosphere model and its paleoclimatic implications. *J. Geophys. Res., 90, 11689-11707.*

Manabe, S., K. Bryan, and M.D. Spelman, 1990: Transient response of a global ocean-atmosphere model to a doubling of atmospheric carbon dioxide. *J. Phys. Oceanogr. 120, 722-749.*

Mass, C.F., and D.A. Portman, 1989: Major volcanic eruptions and climate: A critical evaluation. *J. Climate, 2, 566-593.*

Meehl, G.A., and W.M. Washington, 1990: $CO_2$ climate sensitivity and snow-sea-ice albedo parameterization in an atmospheric GCM coupled to a mixed-layer ocean model. *Climatic Change, 16, 283-306.*

Mitchell, J.F.B., 1989: The "greenhouse effect" and climate change. *Rev. Geophys. 2, 115-139.*

National Academy of Sciences , 1991: *Policy Implications of Greenhouse Warming.* National Academy Press, Washington, DC, 127 pp.

Ohring, G., and P.F. Clapp, 1980: The effect of changes in cloud amount on the net radiation at the top of the atmosphere, *J. Atmos. Sci., 37 447-454.*

Ramanathan, V., and W. Collins, 1991: Thermodynamic regulation of ocean warming by cirrus clouds deduced from observations of the 1987 El Niño. *Nature, 351, 27-32.*

Ramanathan, V., R.D. Cess, E.F. Harrison, P. Minnis, B.R. Barkstrom, E. Ahmad, and D. Hartmann, 1989: Cloud-radiative forcing and climate: Results from the earth radiation budget experiment. *Science, 243, 57-63.*

Ramanathan, V., R.J. Cicerone, H.B. Singh, and J.T. Kiehl, 1985: Trace gas trends and their potential role in climate change. *J. Geophys. Res., 90, 5547-5566.*

Raval, A., and V. Ramanathan, 1989: Observational determination of the greenhouse effect. *Nature, 342, 758-761.*

Reynolds, R.W., 1988: A real-time global sea surface temperature analysis. *J. Climate, 1, 75-86.*

Reynolds, R.W., and C.F. Ropelewski, 1991: RMS errors in global sea surface temperature estimates due to historical changes in the distribution of in situ data. Presented at the 16th NOAA Climate Diagnostic Workshop, 28 Oct.-1 Nov. 1991, Lake Arrowhead, California.

Robock, A. 1979: The "Little Ice Age": Northern Hemisphere average observations and model calculations. *Science, 26, 1402-1404.*

Ropelewski, C.F., and M.S. Halpert, 1987: Global and regional scale precipitation patterns associated with the Ei Nino/Southern Oscillation. Mon. Weath, Rev., 115, 1606-1626.

Rosenberg, N., *1986: Climate Change*: *A Primer* Resources for the Future, Washington, DC.

Santer, B.D., T.M.L. Wigley, and P.D. Jones, 1991: Toward the detection of an enhanced greenhouse effect fingerprint. *Submitted to Nature.*

Schlesinger, M.E., T.P. Barnett, and X-J. Jiang, 1991: On greenhouse gas signal detection strategies. *In: Greenhouse-Gas-Induced Climatic Change: A Critical Appraisal of Simulations and Observations.*

Schneider, S.H., 1972 Cloudiness as a global feedback mechanism: The effects of the radiation balance and surface temperature of variations in cloudiness. *J. Atmos, Sci., 29, 1413-1422.*

Schneider, S.H., 1990: The global warming debate heats up: An analysis and perspective. *Bull. Amer. Meteor. Soc., 71, 1291-1304.*

Spencer, R.W., and J.R. Christy, 1990: Precise monitoring of global temperature trends from satellites. *Science, 247, 1558-1562.*

Tsonis, A.A., and J.B. Elsner, 1989: Testing the global warming hypothesis. *Geophys. Res. Lett., 16, 795-797.*

Van Loon, H., and K. Labitzke, 1990: Association between the 11-year solar cycle and the atmosphere, Part IV: The stratosphere, not grouped by the phase of the QBO. *J. Climate, 3, 827-837.*

Vinnikov, K.Y., P.Y. Groisman, and K.M. Lugina, 1990: Empirical data on contemporary global climate changes (temperature and precipitation). *J. Climate, 3, 662-677.*

Washington, W.M., and G.A. Meehl, 1989: Climate sensitivity due to increased $CO_2$: Experiments with a coupled atmosphere and ocean general circulation model. *Climate Dynamics, 4, 1-38.*

Wigley, T.M.L., and S.C.B. Raper, 1990: Future changes in global-mean temperature and thermal-expansion-related sea level rise. In: *Climate and Sea Level Change: Observations, Projections & Implications*, Edited by R.A. Warrick & T.M.L. Wigley. Cambridge University Press, Cambridge.

Wigley, T.M.L, P.D. Jones, and P.M. Kelly, 1986: Warm world scenarios and the detection of climate change induced by radiatively active gases. *In : The Greenhouse Effect, Climate Change, and Ecosystems (SCOPE 29).* Edited by B. Bolin, B.R. Doos, J. Jager, and R.A. Warrick. John Wiley and Sons, Chichester.

WMO, 1990: *Report of Meeting of Experts on Climate Change Detection Project.* (WCDP No. 13, WMO TD No. 418). World Meteorological Organization, Geneva.

## *Appendix 4*

## *List of Abbreviations and Acronyms*

| | |
|---|---|
| ACRIM | Active Cavity Radiometer Irradiance Monitor |
| AVHRR | Advanced Very High Resolution Radiometer |
| CAC | Climate Analysis Center (NOAA) |
| CCDP | Climate Change Detection Project (WMO) |
| CD-ROM | Compact disc—read-only memory |
| CDIAC | Carbon Dioxide Information and Analysis Center |
| CFC | Chlorofluorocarbon |
| COADS | Comprehensive Ocean-Air Data Set (USA) |
| COARE | Coupled Ocean-Atmosphere Research Experiment |
| CRU | Climate Research Unit (University of East Anglia, UK) |
| DAAC | Distributed Active Archive Center (EOS) |
| DMS | Dimethylsulfide |
| DMSP | Defense Meteorological Satellite Program |
| ECMWF | European Centre for Medium-Range Weather Forecasting |
| ENSO | El Niño/Southern Oscillation |
| EOS | Earth Observing System |
| ERBE | Earth Radiation Budget Experiment |
| ERL | Environmental Research Laboratory (NOAA) |
| GCM | General Circulation Model |
| GCOS | Global Climate Observing Experiment |
| GEDEX | Greenhouse Effect Detection Experiment |
| GEMS | Global Environmental Monitoring System |
| GEWEX | Global Energy and Water Cycle Experiment |
| GFDL | Geophysical Fluid Dynamics Laboratory |
| GHG | Greenhouse gas |
| GISS | Goddard Institute for Space Studies (NASA, USA) |
| GLA | Goddard Laboratory for Atmospheres (NASA, USA) |
| GMCC | Global Monitoring for Climate Change |
| GTS | Global Telecommunications System |

| | |
|---|---|
| HIRS | High-Resolution Infrared Radiation Sounder |
| ICSU | International Council of Scientific Unions |
| IGBP | International Geosphere-Biosphere Programme |
| IPCC | Intergovernmental Panel on Climate Change |
| ISCCP | International Satellite Cloud Climatology Project |
| ISLSCP | International Satellite Land Surface Climatology Project |
| ISY | International Space Year |
| LLNL | Lawrence Livermore National Laboratory |
| MSU | Microwave Sounder Unit |
| NASA | National Aeronautics and Space Administration |
| NCAR | National Center for Atmospheric Research |
| NCDC | National Climate Data Center (NOAA) |
| NCDS | NASA Climate Data System |
| NOAA | National Oceanographic and Atmospheric Administration |
| OSU | Oregon State University |
| QBO | Quasi-Biennial Oscillation |
| SAFISY | Space Agency Forum on the International Space Year |
| SAGE | Stratospheric Aerosol and Gas Experiment |
| SAM | Stratospheric Aerosol Measurement Experiment |
| SHI | State Hydrological Institute (USSR) |
| SOI | Southern Oscillation Index |
| SST | Sea surface temperature |
| TIROS | Television Infrared Operations Satellite |
| TOGA | Tropical Ocean and Global Atmosphere |
| TOMS | Total Ozone Mapping Spectrometer |
| TOVS | TIROS Operational Vertical Sounder |
| TRMM | Tropical Rainfall Measuring Mission (joint US-Japan) |
| UKMO | United Kingdom Meteorological Office |
| UNEP | United Nations Environment Programme |
| WCDP | World Climate Data Programme |
| WCRP | World Climate Research Programme |
| WMO | World Meteorological Organization |
| WOCE | World Ocean Circulation Experiment |

# *Appendix 5*

## *GEDEX CD-ROM Data Sets*

| Contributor | CDF Name | Data Type | Description |
|---|---|---|---|
| Angell | ANGELL-SONDE | TMP-DEV | Monthly radiosonde temperature deviations |
| Jones | CLIM-RSRCH-U | TMP-DEV | Climate Research Unit's monthly global temperature deviations |
| Hansen | GISS-TMP-DEV | MON-ZONE | Monthly zonal temperature deviations |
| Hansen | GISS-TMP-DEV | MON-SH | Monthly Southern Hemisphere temperature deviations |
| Hansen | GISS-TMP-DEV | MON-NH | Monthly Northern Hemisphere temperature deviations |
| Hansen | GISS-TMP-DEV | MON-GRD | Monthly gridded temperature deviations |
| Hansen | GISS-TMP-DEV | MON-GLB | Monthly global temperature deviation means |
| Hansen | GISS-TMP-DEV | MON-BIN | Monthly binned temperature deviations |
| Spencer | MSUTMP | MONTHLY | TOVS MSU low tropospheric temperature and anomalies |
| Spencer | MSUTMP | CLIMATOLOGY | TOVS MSU low tropospheric temperature/anomalies climatology |
| Vinnikov | VGLTMP-MONTHLY | MONTHLY | Vinnikov, Groisman, Lugina monthly zonal temperature deviations |
| Vinnikov | VGLTMP-SEASONAL | SEASONAL | Vinnikov, Groisman, Lugina seasonal zonal temperature deviations |
| NOAA/NCAR | SSCLIMATE | 10YR-GLOBAL | Surface Station Climatology - global ten-year means |
| NOAA/NCAR | SSCLIMATE | AFRICA-MONTH | Surface Station Climatology - monthly means for Africa |
| NOAA/NCAR | SSCLIMATE | ARCTIC-MONTH | Surface Station Climatology - monthly means for the Arctic |
| NOAA/NCAR | SSCLIMATE | AUSTRL-MONTH | Surface Station Climatology - monthly means for Australia |
| NOAA/NCAR | SSCLIMATE | GLB-ANNUAL | Surface Station Climatology - global annual means |
| NOAA/NCAR | SSCLIMATE | NAMER-MONTH | Surface Station Climatology - monthly means for North America |
| NOAA/NCAR | SSCLIMATE | 30YR-GLOBAL | Surface Station Climatology - global thirty-year means |
| NOAA/NCAR | SSCLIMATE | ANTARC-MONTH | Surface Station Climatology - monthly means for Antarctica |
| NOAA/NCAR | SSCLIMATE | ASIA-MONTH | Surface Station Climatology - monthly means for Asia |
| NOAA/NCAR | SSCLIMATE | EUROPE-MONTH | Surface Station Climatology - monthly means for Europe |
| NOAA/NCAR | SSCLIMATE | GLB-YR-PST61 | Surface Station Climatology - annual means for additional Me |
| NOAA/NCAR | SSCLIMATE | SAMER-MONTH | Surface Station Climatology - monthly means for South America |
| Labitzke/van Loon | BERLIN-STRAT | MONTH-TMP | Monthly stratospheric temperature |

| | | | |
|---|---|---|---|
| CDIAC | GRNHS-GASES | $CO_2$-HISTORIC | Atmospheric $CO_2$ levels from ice cores |
| CDIAC | GRNHS-GASES | $CO_2$-MONITOR | Atmospheric $CO_2$ levels from continuous monitoring |
| CDIAC | GRNHS-GASES | $CO_2$-FLASK | Atmospheric $CO_2$ levels from flask measurements |
| CDIAC | GRNHS-GASES | METHANE-HIST | Atmospheric methane level from ice cores |
| CDIAC | GRNHS-GASES | MEHTANE-FLAS | Atmospheric methane levels from flask measurements |
| Kyle | N7-ERB | SOLIRR | Nimbus-7 global level-1 radiation budget |
| Willson | SMM-ACRIM | SOLIRR | SMM active cavity radiometer irradiance monitor - full solar |
| ERBE-S2 | ERBE-S2 | SAT-COMB | Solar radiometric data from NOAA-9, NOAA-10, and ERBS |
| Reynolds | CAC-SST | BLENDED | Global in situ/AVHRR-derived sea surface temperature |
| Rossow | ISCCP-C2 | MONTHLY | International Satellite Coud Climatology monthly cloud products |
| Barkstrom | ERBE-S4 | WFVSF-DY | WFOV daily radiation budget from ERBE using shape factor algorithm |
| Barkstrom | ERBE-S4 | WFVSF-HR | WFOV hourly monthly radiation budget from ERBE using shape factor algorithm |
| Barkstrom | ERBE-S4 | WFVSF-MN | WFOV monthly radiation budget from ERBE using shape factor algorithm |
| Kyle | ERB-MATRIX | MONTHLY | Global monthly earth radiation budget from Nimbus-7 |
| McCormick | SAGEII-PROF | AEROSOLS | Aerosol profiles from SAGE II on ERBS |
| McCormick | SAGEII-PROF | $H_2O$VAPOR | Water vapor profiles from SAGE II on ERBS |
| McCormick | SAGEII-PROF | $NO_2$ | Nitrogen dioxide profiles from SAGE II on ERBS |
| McCormick | SAGEII-PROF | OZONE | Ozone profiles from SAGE II on ERBS |
| NOAA/NCAR | RAOB-STATION | MONTHLY | Monthly radiosonde station data |
| Susskind | SUSSKIND-TOVS | MONTHLY | Monthly TIROS-N series TOVS/HIRS meterological retrieval |
| Dutton | CMDL-MLOA | SOLTRN-DAILY | Atmospheric solar transmission index at Mauna Loa |
| Dutton | CMDL-SFC | SOLIRR-HOUR | Surface solar irradiance at NOAA/CMDL baseline sites |
| Angell | ANGELL-TOTO3 | SEASON-DEV | Angell's total ozone seasonal deviations for selected regions |
| Angell | ANGELL-LYRO3 | SONDE-SEASON | Angell's sonde layer seasonal deviations for selected zones |
| Angell | ANGELL-LYRO3 | UMKEHR-SEASN | Angell's Umkehr layer seasonal deviations for selected zones |
| CAC | CAC-SOI | S-OSCIL-IND | Climate Analysis Center's Southern Oscillation index |
| NMC | Q-BI-OSCIL | MONTHLY | Quasi-biennial oscillations monthly temperature and wind |
| Tapping | PENTICTON | SOLIRR | Penticton (BC) 2800 MHz solar radio flux |